AMERICAN UNIVERSITY OF BEIRUT

ESTIMATION OF TRANSIT TIMES IN KARST AQUIFERS USING ENVIRONMENTAL TRACERS (TRITIUM, HELIUM, CHLOROFLUOROCARBONS, AND SULFUR HEXAFLUORIDE): APPLICATION ON THE JEITA AQUIFER SYSTEM-LEBANON

by
AHMAD ZOUHEIR HAMDAN

A thesis
submitted in partial fulfillment of the requirements
for the degree of Master of Science
to the Department of Geology
of the Faculty of Arts and Sciences
at the American University of Beirut

Beirut, Lebanon
February 2018

AMERICAN UNIVERSITY OF BEIRUT

ESTIMATION OF TRANSIT TIMES IN KARST AQUIFERS USING ENVIRONMENTAL TRACERS (TRITIUM, HELIUM, CHLOROFLUOROCARBONS, AND SULFUR HEXAFLUORIDE): APPLICATION ON THE JEITA AQUIFER SYSTEM-LEBANON

by

AHMAD ZOUHEIR HAMDAN

Approved by:

Joanna Doummar

Dr. Joanna Doummar, Assistant Professor — Advisor
Geology

A. Abdel-Rahm

Dr. Abed-Fattah M. Abdel-Rahman, Professor — Member of Committee
Geology

M. Salah

Dr. Mohamad Salah, Associate Professor — Member of Committee
Geology

Mutasem Fadel

Dr. Mutasem Fadel, Professor — Member of Committee
Civil and Environmental Engineering

Date of thesis defense: January 18, 2018

AMERICAN UNIVERSITY OF BEIRUT

THESIS, DISSERTATION, PROJECT RELEASE FORM

Student Name: Hamdan (Last) Ahmad (First) Zouheir (Middle)

☑ Master's Thesis ○ Master's Project ○ Doctoral Dissertation

☐ I authorize the American University of Beirut to: (a) reproduce hard or electronic copies of my thesis, dissertation, or project; (b) include such copies in the archives and digital repositories of the University; and (c) make freely available such copies to third parties for research or educational purposes.

☑ I authorize the American University of Beirut, to: (a) reproduce hard or electronic copies of it; (b) include such copies in the archives and digital repositories of the University; and (c) make freely available such copies to third parties for research or educational purposes after :

One ---- year from the date of submission of my thesis, dissertation, or project.

Two ☑ years from the date of submission of my thesis, dissertation, or project.

Three ---- years from the date of submission of my thesis, dissertation, or project.

Ahmad Hamdan — Signature

February 8, 2018 — Date

ACKNOWLEDGMENTS

I wish to express my sincere gratitude to my advisor Dr. Joanna Doummar for her continuous supervision, grateful support, and immense advice and help for completing my thesis and making it possible.

I would like to thank Dr. Abdel-Rahman for his continuous supervision, advice, encouragement, and for his guidance to insure my successful graduation.

I wish to thank Dr. Mohamad salah and Dr. Mutasem Fadel for the examination of the thesis and for their valuable suggestions and improvements.

Special thanks are for Mr. Maroun Ijreiss, Mrs. Nesrine Lababidi-Hawi, and to my colleagues in the Hydro-Geo group Assad Kassem, Michel Aoun, Reda Ghawi, Eliane Shwairi and Fouad Andari, for their help and support in the field and lab work.

Many thanks to Ayman Ibrahim and especially Najib Najib from the Jeita Grotto staff for their help and assistance during the sampling campaigns.

I would like to thank the University Research Board for funding this research (URB grant 2015-2017).

Special thanks go to the Institute of Environmental Physics/Section of Oceanography at the University of Bremen especially Dr. Jürgen Sültenfuß, and to the Centre for Stable Isotope Research and Analysis Büsgen-Institute in Goettingen.

Last but not least my best thanks goes to my family for their care, support, and encouragement.

AN ABSTRACT OF THE THESIS OF

Ahmad Zouheir Hamdan for Master of Science
Major: Geology

Title: Estimation of transit times in karst aquifers using environmental tracers (Tritium, Helium, Chlorofluorocarbons, and Sulfur Hexafluoride): Application on the Jeita aquifer system-Lebanon

In this study, groundwater residence times in the Jeita spring aquifer (Lebanon) were estimated using several environmental tracers such as Tritium (^3H), Tritium-Helium (^3H- ^3He) Chlorofluorocarbons (CFCs), and Sulfur Hexafluoride (SF_6). Additional stable isotope and major ion analyses were performed to characterize water types and recharge elevations. Groundwater samples were collected in two sampling campaigns under different flow periods, from six different wells in the Jeita catchment area (Jurassic Kesrouane aquifer) as well as from the cave itself and its new branch, and three samples from wells outside the Jeita catchment area.

Tritium in all groundwater samples shows nearly the same concentration with slight variations (2.12 TU to 2.97 TU). The latter makes the Tritium method not accurate to provide reliable age results, thus it was complemented by the Helium method. The results are reproducible for the Tritium-Helium method giving absolute mean residence times that ranged from 7 to 24 years except for the Jeita cave sample where a zero age was determined due to the re-equilibration and degassing of light noble gas with the atmosphere. The youngest age is attributed to a newly discovered branch in the Jeita system (JN) while the oldest ages were obtained in wells tapping the fissured matrix (Ain delbe (AD), Ouata el Joz (OJ), and Ain errihane (AR)). Some samples showed extreme excess air (ΔNe is greater than 70 %) while the remaining samples have ΔNe in the expected range between (10-35%). Moreover Tritium-Helium analysis has showed some radiogenic Helium ($^4He_{rad}$) in some samples implying a mixture with old groundwater (older than 50 years).

Correlations between CFC, SF_6 and Tritium indicate that none of the samples fit to a piston flow model except for Ain errihane (AR) well, however the latter is highly dependent on the accuracy and variability of the input concentration of Tritium, CFCs, and SF_6 in air in the region for the last 20 years, especially in the case of CFCs and SF_6 atmospheric concentrations are highly affected by local anthropogenic contamination. Chahtoul (CL) well and Jeita New cave (JN) fit on a Binary Mixing model, indicating their substantial new water component (reaching 54% and 69% respectively). Stable isotope results showed a high mixing of fractionated water in Jeita new cave sample, Ain errihane, and Qachqouch wells while the Ain delbe (AD) and Ouata el Joz (OJ) wells showed very minimal fractionation with higher isotopic depletion indicating higher altitude for their recharge infiltration area. In Lebanon this type of spatial groundwater age dating using environmental tracers was not applied to date, to the exception of grab sample analysis in the cave.

CONTENTS

ILLUSTRATIONS

Figure Page

TABLES

Table Page

CHAPTER 1

INTRODUCTION

Groundwater is considered to be the main and largest source of fresh water accessible for human use. Sea water or saline water covers two thirds of the surface area of planet Earth, while fresh water represents 2.5% (Caron, 2014). Most of the fresh water (69%) is bound in ice and permanent snow cover in the Antarctic, Arctic, and in continental mountains, thirty percent (30%) is present as fresh groundwater (0.75% of all water on earth) such as in lakes, rivers, and groundwater aquifers, and the remaining one percent (1%) is estimated to occur as soil moisture, swamp water and permafrost (Caron, 2014). Aquifers in both types, renewable and non-renewable, make up ninety five (95%) of accessible fresh water (0.7% of all water on the earth surface) providing more than half of all domestic and irrigation water used around the world (Caron, 2014).

The major problem facing groundwater in most places in the world is the rapid decrease of groundwater levels as water abstraction is exceeding natural recharge. Moreover, groundwater contamination and degradation of water quality have become major alarming issues (Kurwadkar, 2017). Sustainable use and management of aquifers require an understanding of aquifer hydrogeology and its dynamics. The latter can be accomplished by observations and continuous measurements of precipitation, groundwater and river flows, water table level etc. Achievements in groundwater hydrology were concentrated on means to estimate aquifer hydraulic properties; namely

hydraulic conductivity needed for the development of transient groundwater flow models.

Isotope and tracer methods that are being used to estimate the age of groundwater is helping build up a conceptual framework of aquifer hydrogeology and flow systems. Since the discovery of the natural radioactivity of Tritium (^{3}H) and Carbon-14 (^{14}C) sixty years ago (Caron, 2014), many studies relied on radioactive isotopes along with anthropogenic tracers [Chlorofluorocarbons (CFCs) and Sulfur Hexafluoride (SF_6)] to estimate average groundwater age, as these methods have revealed successful in providing insights into the rate of groundwater renewal, flow velocity, and aquifer storage. Moreover, the estimation of groundwater age helps improve and validate groundwater flow numerical models in major aquifers where water level data is poor.

1.1 Transit Time and Vulnerability

Groundwater ages range from less than a month to millions of years depending on the regional setting and types of aquifers (unconsolidated versus fractured; Kazemi et al., 2006). Nowadays, the constantly increasing demand for fresh water for various purposes, along with the drastic increase of population, improper waste disposal, and potential changes in the current climate, groundwater investigations require considerate attention. The estimation of groundwater age reveals to be very important in order to understand the nature of recharge, rates of renewal, and groundwater flow in aquifers, especially in highly fractured and karstic aquifers as they are more complex and thus highly vulnerable to contamination (Polemio et al., 2009).

The assessment of vulnerability of karst systems consists of the delineation of zones within a catchment area having varying degree of sensitivity to contamination; e.g., a highly vulnerable zone will be defined by a zone contributing highly to recharge of a water point (well or spring; Doummar et al., 2012). This process is important in order to recommend restrictions on land use within the various delineated protection zones (Polemio et al., 2009). Preventive protection measures must be strict in highly sensitive areas, and more flexible in the least sensitive ones. Source protection zones (SPZs) are assigned to areas that are at a high risk of polluting factors and release pollutants to the groundwater mainly from industrial and agricultural areas (Mull, 1981; Lo Russo and Taddia, 2012).

SPZs have been delineated for nearly 2,000 groundwater sources that are public and private water wells and springs used for drinking water supply in England and Wales (Carey et al., 2009). Generally porous and fractured aquifers have three protection zones defined as follows:

1) SPZ1 – Inner Protection Zone is defined by a minimum radius of 50 m from the source and a 50-day travel time from any point below the water table to the source (Mull, 1981). This designed zone is protected against hazardous activities that may rapidly transmit degrading toxic chemicals and some water-borne disease. Thus, building, pesticides or liquid manure, and roads are prohibited (Carey et al., 2009, Mull 1981).

2) SPZ2 – Outer Protection Zone is defined by a minimum radius of 250 or 500 m or a 400-day travel time. This zone is designed where hazardous activities such as

industry, waste deposits, wastewater treatment plants, and others are prohibited (Carey et al., 2009).

3) SPZ3 – Source Catchment Protection Zone is defined as the total protected area in order to provide a protected groundwater from a long term groundwater recharge (Carey et al., 2009).

In the case of karst aquifers, the delineation of SPZs is based on methods that estimate travel times supported by field investigations such as tracer tests and a conceptual understanding of the groundwater flow (Carey et al., 2009). These SPZs in karst systems are delineated after the generation of vulnerability assessment maps using developed methods such as COP, GLA, DRASTIC, EPIK, and PI (Weatherington-Rice et al., 2006; Christoph et al., 2008) that are based on hydrogeological characterization; type of aquifer (karst, fractured, or porous), type and degree of karstification, local conditions, etc..

For that reason, any vulnerability map especially for complex aquifers such as karst (refer to Section 1.2) should be designed based on a detailed hydrogeologic map, karst features, estimated travel times, and groundwater flow (Carey et al., 2009). All of the latter parameters require an extensive field investigation and may be very challenging to characterize.

1.2 Karst Aquifers

Karst aquifers are one type of fractured rock aquifers that could be made up of limestone, dolomite, or magnesite prone to dissolution by carbonation (Harmon et al., 2006). Karst aquifers are continuously changing; they evolve with time as water

percolating in the fractures that is enriched in Carbon dioxide (CO_2) dissolves the relatively soft rock and enlarges the size of the initial fractures into solution cavities and conduits that can reach tens of meters wide forming underground cave systems (White, 1988). Hence, the orientation of the flow system in a karst aquifer may undergo changes in time as many conduits collapse or get filled up with sediments and convert for instance saturated (phreatic) conduits into unsaturated (vadose) conduits. Therefore, karst aquifers are characterized by mazes of groundwater flow paths and drainage discharge points due to their temporal variation (Goldscheider and Drew, 2007).

A karst aquifer drains sinkholes and sinking streams that are present in its groundwater basin resembling a watershed on the surface in addition to diffuse recharge (Goldscheider and Drew, 2007). Precipitated water gets carried directly through sinkholes, large fractures, and dolines to larger underground conduits joining together and forming larger passages with higher flow, and eventually discharging at a spring. A karst groundwater catchment may not be related to or has little connection with surface watershed boundaries (Williams, 2008). A cave stream, as a surface stream, erodes headward (upstream), however, it can extend beneath a ridge without modifying the surface above in order to capture flow from the adjacent watershed (Williams, 2008). Therefore, delineating the actual watershed area of a karst spring is a difficult task as the watershed could be much larger or smaller as apparent on topographic maps. On the other hand, sinkholes and dolines shown on maps may belong to one watershed, but actually drain to a far-away spring.

Aquifers are known to have a certain degree of anisotropy and heterogeneity. On one hand, in the case of unconsolidated porous aquifers (such as sand and gravel),

prediction of water heads distribution and well siting can be readily performed. In such a medium, the application of Darcy's equation can provide an estimate on the travel time of water in the aquifer (Fig. 1). This can be determined by a series of calculated parameters and equations as follows (Fetter, 2001):

$$Q = kA\frac{dh}{dl}$$

(Equation 1)

Where Q is the water discharge (L^3/T), k is the hydraulic conductivity (L/T), A is the area (L^2) and $\frac{dh}{dl}$ is hydraulic gradient (Fetter, 2001).

By replacing into the equation, the hydraulic conductivity, the hydraulic gradient and the porosity of the aquifer, one can determine the transport velocity according to the following equation (Fetter, 2001):

$$v = k\frac{dh}{n_e dl}$$

(Equation 2)

Where v is the velocity in L/T, and n_e is porosity.

By knowing the traveled distance (d; L) and velocity (v; L/T) of groundwater, we can have an estimate of the travel time (t) of the groundwater in the aquifer (Fetter, 2001).

$$v = \frac{d}{t}$$

(Equation 3)

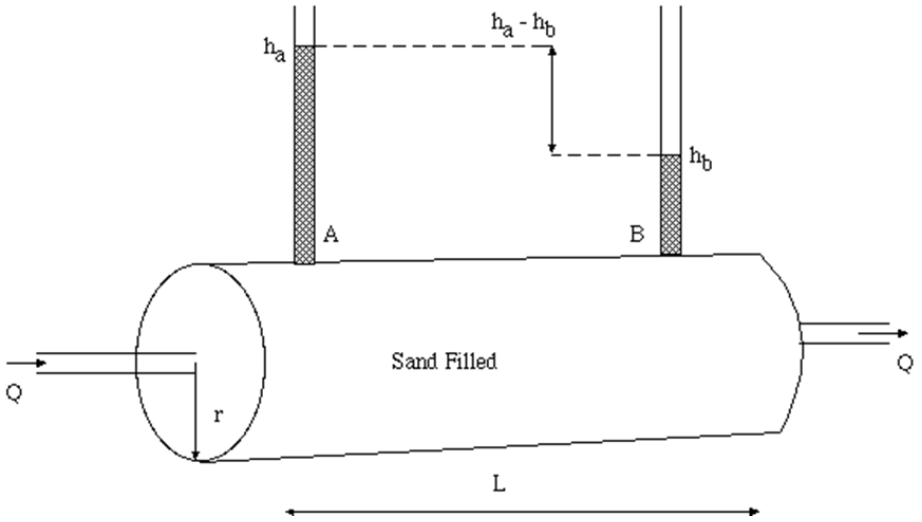

Fig. 1. Horizontal pipe filled with sand demonstrating Darcy's experiment and equation (Fetter, 2001).

On contrary, in the case of a highly heterogeneous karst aquifer i.e., the absence of a homogenously distributed water table, and the duality of flow and infiltration any prediction of groundwater flow reveals to be challenging. As a matter of fact, groundwater might be present in large volumes in conduits and caves. Few meters away, massive bedrocks might turn out to be unproductive.

In a karst system, the latter cannot be directly applied as porosity varies (double versus triple porosity). Even for large fractures and conduits, the effective porosity can be taken equal to 1 (n_e=1; Fetter, 2001), and only fast transit times (a few days to a month) could be calculated for conduits and shafts. Various karst aquifers are characterized by a layer called "epikarst"; it consists of a compartment where a portion of groundwater is suspended and stored above the main part of the aquifer between the

top soil and mostly unaltered bedrock The water in the epikarst is stored in enlarged joints and bedding planes (Goldscheider and Drew, 2007).

Karst systems in general are well known to have complex flow initiating high mixing effect of new and old water in the groundwater system (Einsiedl, 2005). This mixing is mainly due to their duality of recharge as the infiltrated water could originate from the karstic area (autogenic recharge) or from adjacent non-karstic areas (allogenic recharge) In addition to that, karst systems exhibit differential pathways for infiltration (duality of infiltration; Geyer, 2008).

Fig. 2 illustrates the fast preferential flow of water through sinkholes and dry valleys (point infiltration), slow diffusive flow through fissured matrix karst system (Goldscheider and Drew 2007), and the water stored in the rock matrix, conduits, and in the epikarst below the soil layer. All contribute to this heterogeneity and variability in karst system (Williams, 2008). Variability in karstic systems is shown in the high water table fluctuations throughout the year and in the rapid variations in discharge and water quality (Goldscheider and Drew, 2007).

Heterogeneity and anisotropic conditions in karstic aquifers make them highly vulnerable to contaminations and cause uneven distribution of pollutants in the groundwater system. The term ‘vulnerability’ is divided into intrinsic and specific vulnerability (Leibundgut, 1998). Intrinsic vulnerability is defined as the degree of natural protection along with the contaminant degradation capacity of the unsaturated zone or semi-confining layers above a karst aquifer as a result of physicochemical processes such as filtration, dispersion, diffusion, adsorption, and biodegradation

(Leibundgut, 1998). Specific vulnerability is defined as the degree of risk due to actual threats from human impact such as land use, spills, industry, etc. (Leibundgut, 1998).

Thus, contamination management and groundwater protection applications are highly recommended in karstic aquifers. This can be accomplished by selecting appropriate hydrogeologic methods for investigation. Mainly isotopic techniques and tracer tests, such as stable and radioactive isotopes are used. They can provide information about the origin of groundwater, its transit times, and the mixing processes it went through before discharge (Goldscheider and Drew, 2007). Artificial tracer experiments are used to detect hydrological connection between springs and sinkholes or dolines, to delineate catchments areas, and to identify transport parameters such as flow velocities or transit times in fast flow pathways (Goldscheider and Drew, 2007).

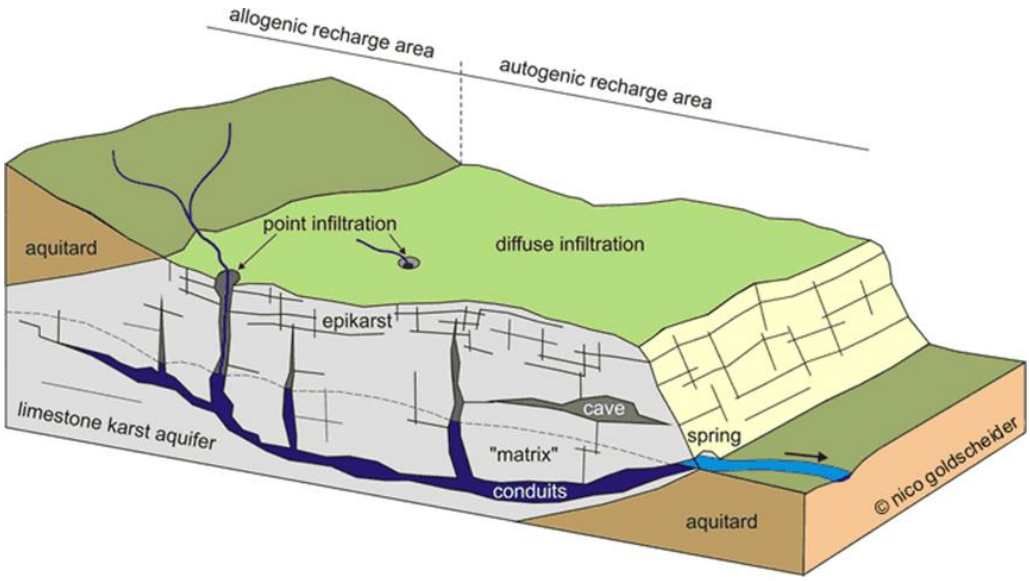

Fig. 2. Block diagram of a heterogeneous karst aquifer showing the duality of recharge (allogenic vs. autogenic), duality of infiltration (point vs. diffuse) and porosity/flow (conduits vs. matrix); (Goldscheider and Drew, 2007).

1.3 Background Studies on Groundwater Age Dating

Isotope and tracer methods are being used in hydrological studies frequently to help in building up a conceptual framework of aquifer hydrogeology and flow systems. Stable isotopes are being integrated in hydrological studies to have an insight on the origin of groundwater (Aouad-Rizk et al., 2005; Al-Ameri et al., 2014). The water molecule itself possesses stable and radioactive isotopes. For instance, the Hydrogen atom has three isotopes. Two are stable and one is radioactive. The first stable major one is Protium (^{1}H), with a mass number of one and an abundance of 99.985 % (HYDROISOTOP GMBH, 2005). The second stable one is Deuterium (^{2}H), with a mass number of two and abundance up to approximately 0.015 % (HYDROISOTOP GMBH, 2005). Tritium (^{3}H) is the radioactive isotope of Hydrogen, and it is mainly used in groundwater age dating. The Oxygen atom also has two stable isotopes: Oxygen-17 (^{17}O) and Oxygen-18 (^{18}O). The latter is of great relevance in hydrological studies. In normal water composition, out of 10^{6} water molecules only 2000 molecules contain heavy Oxygen (^{18}O), and 160 molecules of Deuterium isotope replaces Protium (^{1}H); (HYDROISOTOP GMBH, 2005). However, this ratio may vary due to physical, biological, and chemical processes (isotopic effect). Isotopic effect causes variation in isotopic composition in precipitated water and simultaneously in different water bodies. The distribution of isotopic content is influenced by several factors. The temperature effect is based on the fact that during evaporation of water, fractionation is more significant at low temperatures. For that reason cold environment rainfall are more depleted than warmer environments. The altitude effect is based on the fact that with increasing altitude, rainfall tends to be more depleted. Typical gradients are -0.15 to -0.5

‰ per 100m for ^{18}O, and -1.5 to -4 ‰ per 100m for Deuterium (Leibundgut et al., 2009). Depletion of $\delta^{18}O$ and $\delta^{2}H$ values occur with increasing latitude because of the increasing degree of rainfall since with increasing amount of rainfall heavier isotopes has lower concentration however this effect is not seen in snow, also isotopic ratios show a decline from the coast toward inland areas (continental effect); (Leibundgut et al., 2009).

Recently, hydrogeologists started tackling the concept of groundwater age in a different way; the new approach comprises understanding the nature of subsurface flow regimes. Concerns about groundwater age is not novel idea, however the concept of groundwater age is a complex one and has long been central to a hydrologist's work (e.g., Mazor, 1997; Kendall and McDonnell, 1998; Phillips and Castro, 2003; Kazemi et al., 2006). **Groundwater age or residence time** is defined as the time interval that has elapsed between the time groundwater reached the subsurface at a location in a flow regime and the time it came out from the system through an outlet (Bethke and Johnson, 2008). Groundwater age cannot be determined directly from collected samples; it often requires numerical simulation of hydrological models or by comparing measured concentration of specific tracers in the sample with specific input concentration function while assuming flow and transport conditions.

Previous studies on groundwater age were concentrated mostly on direct applications and estimation of transit times using different artificial and environmental tracers (Helium, Tritium, Chlorofluorocarbons, and Sulfur Hexafluoride), and assess the suitability of each method in estimating transit times in different types of aquifers (e.g., unconsolidated: Szabo et al., 1996; or karst aquifers: Delbart et al., 2014). Other

research focused on the refinement of methods for the sampling and analysis of environmental tracers and decrease of analytical uncertainty (Kazemi et al., 2006; Cornaton and Perrochet, 2006). Moreover, there was an increasing interest in developing the analytical transport models used in the interpretation of groundwater ages, such as age distribution functions (Sültenfuβ et al., 2011; Jurgens et al., 2012; Visser et al., 2013). Groundwater age distribution in an aquifer gives insights on the nature of flow regime and mean velocity in an aquifer (e.g. Visser et al., 2013). For instance, old groundwater may indicate upwelling of ancient fluids to the aquifer from below; on the other hand the presence of young groundwater reflects fast and active infiltration from the surface (Bethke and Johnson, 2008).

The concept of groundwater age can be addressed and studied by physical or chemical means. Physical hydrologists make use of Darcy's law to determine flow velocities in an aquifer in order to predict the corresponding age gradient through particle tracking or direct age simulation (e.g. Cornaton, 2011), although these models are valuable, they are prone to uncertainties due to the limitations in measurements (Zuber et al., 2011).

Environmental tracers have been used by hydrochemists to determine groundwater age, many have used the radioactive decay of radiogenic isotopes (e.g. Clark and Fritz, 1997; Phillips and Castro, 2003; Kazemi et al., 2006; Caron, 2014) or of an isotope or particle that marks an anthropic event (e.g. nuclear weapons testing). Lumped Parameter Models (LPMs) treat a flow system as an entity, ignoring spatial variations and assuming constant flow pattern (Geyer, 2008). In the case of high

availability of tracer data, age distribution can be determined without groundwater mixing assumptions (e.g. Fienen et al., 2006), however the limitations in data availability and collection make it impossible to overcome the large degree of freedom using a "shape free" or "non-parametric" approach of Lumped Parameter Models (LPM; e.g., McGuire and McDonnell, 2006). Another approach to LPMs is a simplified parametric one that takes into consideration groundwater mixing based on aquifer geometry and well construction, this approach is used in cases of insufficient tracer data availability and the low possibility of "non-parametric" or more complex models to be applied (e.g. Turnadge and Smerdon, 2014).

The parametric LPMs are function of mean residence time along with one or more mixing parameter. They mainly include the Piston flow Model (PM), the Exponential Piston flow Model (EPM), the Binary mixing model (BM) the Exponential Mixing Model (EMM), and the Dispersion Model (DM; Geyer, 2008)

The Piston flow Model (PM) is based on the assumption that a packet of groundwater has been migrated in the subsurface along a flow line having the same velocity with negligible dispersion and diffusion to the sampling or discharge point position (Fig. 3). In other words it resembles a closed system where water molecules neither exchange nor leave the system (Bethke and Johnson, 2008).

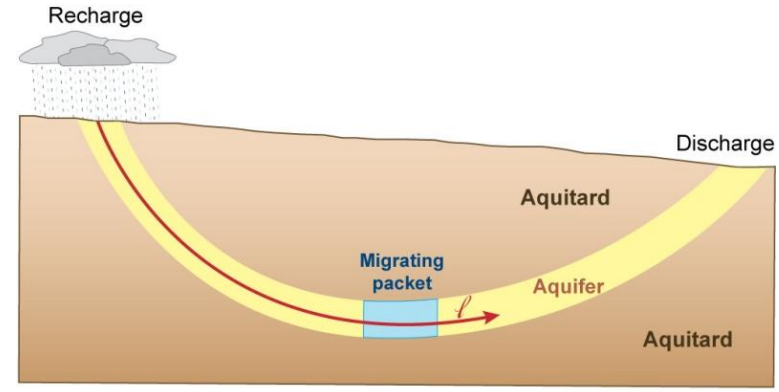

Fig. 3. Piston flow model of groundwater age, as applied in groundwater age dating studies (Bethke and Johnson, 2008).

However, this closed system is not physically existing as groundwater molecules do not move in a packet (Fontes 1983), as they may diffuse into the adjacent aquitards or the water stored in aquitards may diffuse into the aquifer through cross-Formational flow (Bethke and Johnson, 2008). Moreover water molecules have the tendency to flow in several different pathways through the aquifer sediments. Hence, they are prone to mixing in different direction along a flow path (owing to hydrodynamic dispersion). Therefore, hydrogeologists are abandoning the closed system assumption (Bethke and Johnson, 2008) and considering that a groundwater sample is a pool of water molecules each having a specific age. Any estimated age is a mean age of all water molecules. The determined mean age could have several age distributions scenarios as shown in Fig. 4.

To the opposite extreme, a Binary mixing model can be assumed, this model is based on the mixing of waters of different origins and chemistries, depending on the type of solute some will behave conservatively, and mix proportionally according to

their end-member concentrations while others type of solutes tend to react in the mixed solution and modify the water chemistry.

Binary mixing is a simple conservative mixing between two end-members, for instance mixing of cold young shallow ground waters with old rising geothermal water (Fig. 4; c and d) with different range in geochemistry and temperature (Han et al., 2012). Calculating the portion of each requires a water-based mass balance equation and a solute-weighted mass balance (Han et al., 2012).

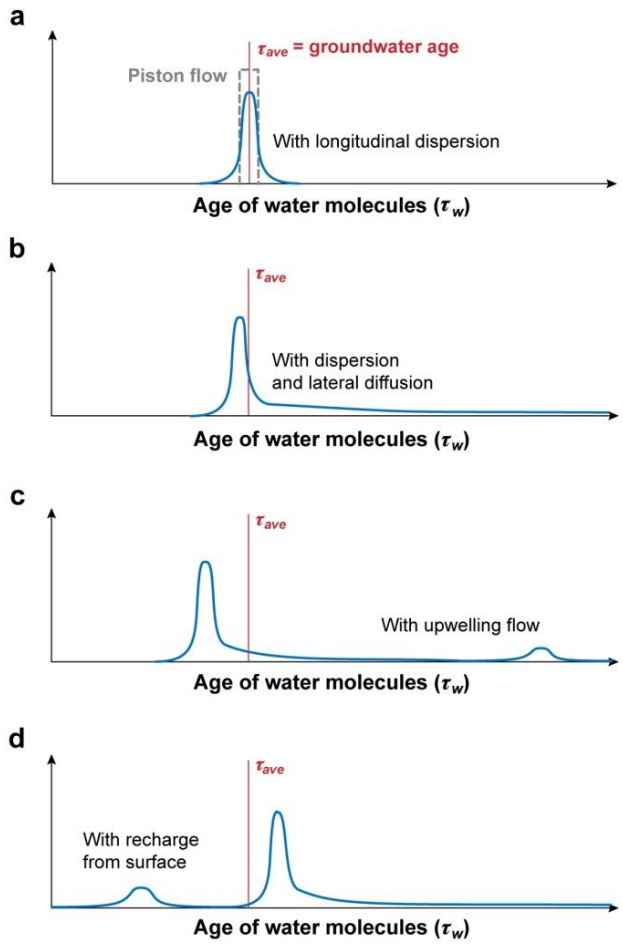

Fig. 4. Various scenarios according to which transport processes may affect groundwater age interpretation (Bethke and Johnson, 2008).

The exponential models (EM) assume exponential distribution of transit times of flow lines with mixing occurring at the outlet or sampling site (Fig. 5a). An example of exponential piston (EPM) flow model is demonstrated in Jurgens et al., (2012) at well X with a mean age of 25 years with an age distribution expected at Well X assuming an EPM ratio (n) of 1 (Fig. 5 b). Einsiedl (2005) has proposed a dispersion model in order to account for the diffusion between mobile water in fissures and conduits and stagnant water stored in the porous matrix of a karst aquifer.

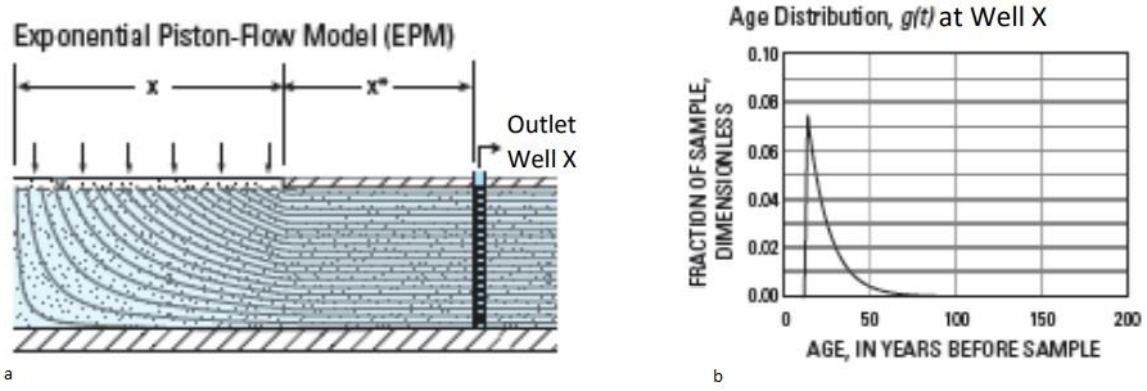

Fig. 5. (a) Schematic diagram of an idealized aquifer in which the exponential piston flow model. (b) Example of an age distribution with exponential piston flow model (Jurgens et al., 2012).

Tritium-Helium (^{3}H-^{3}He) isotopes and Chlorofluorocarbons (CFCs) techniques have been used to determine shallow groundwater age by Szabo et al (1996) in a porous unconfined Kirkwood-Cohansey aquifer system (unconsolidated medium to coarse grain sediments). The groundwater travel time along flow paths was determined by means of particle-tracking flow path analysis from simulated water levels and intercell flows. The flow path analysis gave insight on the vertical flow velocity of the shallow

groundwater aquifer system (~ 1 m/yr), giving Helium (^{3}He) confinement between 90 and 100% along with only a small source of error in the Tritium-Helium (^{3}H-^{3}He), since the tritiogenic Helium is confined in the groundwater as a function of the vertical advection velocity, the higher the advection velocities the higher the Helium (^{3}He) confinement. The apparent groundwater ages based on Tritium-Helium (^{3}H-^{3}He) and Chlorofluorocarbons (CFC) dating methods and flow model-based travel times could not be statistically separated and were strongly correlated with depth. Moreover a good correspondence between the Tritium-Helium (^{3}H-^{3}He) and Chlorofluorocarbons (CFCs) ages implies a minimal effect of dispersion on the tracer-based ages of groundwater in this aquifer. This study has found that the minor differences between flow model-simulated travel times and Chlorofluorocarbons (CFCs) and Tritium-Helium ($^{3}H^{3}He$)-based groundwater ages is mainly due to enrichment of local air in Chlorofluorcarbons-11 (CFC-11) and Chlorofluorcarbons-12 (CFC-12) from urban and industrial sources and by minor contamination from sampling equipment and due to uncertainties in model input parameters.

On the other hand, in a recent study conducted by Delbart et al (2014) on a carbonated fractured hill in Burgundy (France); groundwater samples were collected from boreholes and springs for the analysis of Oxygen-18 (^{18}O), Deuterium (^{2}H), major ions, Tritium (^{3}H), Helium (^{3}He), Chlorofluorocarbons (CFCs), Sulfur Hexafluoride (SF_6), Krypton-85 (^{85}Kr) Argon (^{39}Ar), Carbon-13 (^{13}C) content of Total Dissolved Inorganic Carbon (TDIC), and Carbon-14 (^{14}C) content of Total Dissolved Inorganic Carbon (TDIC),. A Lumped Parameter Model was applied using the entire set of geochemical tracers that characterize the recharge event, CFC-SF_6 results show that the

direct recharge water has several weeks residence time, while the base flow has apparent ages of 29 years along with presence of excess air in water samples which is expected scenario in karst systems (Delbart et al., 2014). Tritium-Helium results in spring samples showed re-equilibration with air within the 1 year period prior to sampling and failed in providing accurate age estimations. A similar result of Tritium-Helium method was obtained from cave drip samples (Kluge et al., 2010). Most of the samples showed no excess air indicating high degassing. It is believed that equilibration with cave ambient air eventually occurred during sampling (Kluge et al., 2010). Some samples showed no partial re-equilibration as excess air was present. In that case, excess air Formation in these samples should have required the presence of trapped and pressurized air, in a perched layer with quasi-saturated conditions in some places in the cave. Similar to Delbart et al (2014), the ages using the Tritium-Helium method in Kluge et al (2010) were nil or underestimated.

In Lebanon this type of groundwater age dating was not applied previously. An analysis of Chlorofluorocarbons (CFCs), Sulfur Hexafluoride (SF_6), Helium (^3He) and Tritium (^3H) in four springs from different catchment areas was done as part of the Jeita Project (Geyer and Doummar, 2013). The obtained results show that water is relatively young ranging between 1-10 years. However the collected samples did not account for the atmosphere interaction with the spring water which resulted in this age variation, as spring water equilibrates with ambient air in the cave.

Artificial tracer experiments were performed in the Jeita karst system (Doummar, 2012) to investigate fast flow transit times (< 1 month). Fast transit times

calculated from tracer experiments ranged between 3 and 300 hours (12 days). The shortest transit times were recorded in the Jeita subsurface conduit (3 to 19 hours under various flow conditions) while injections in sinkholes yielded fast to moderate transit times ranging between 25 and 90 hours. On the other hand, the fissured matrix and fissured unsaturated zone resulted in a wider range of relatively long transit times (69 to 292 hours).

1.4 Objectives of this Study

This study focuses on the characterization of relatively young groundwater of the Jeita aquifer system. Tracer experiments only allow the estimation of relatively fast transit times (not greater than a month) as the likelihood of tracer recovery after one month from the injection is very low with a highly damped breakthrough curve if any. Therefore, this particular study aims at estimating longer water transit times (1 to 60 years); (fissured matrix and storage base flow) in the Jeita aquifer using environmental tracers Tritium-Helium (^3H-^3He) and Chlorofluorocarbons (CFCs) and Sulfur Hexafluoride (SF_6); (karstic aquifer-Kesrouanne Formation). The groundwater age can be determined with the help of simplified Lumped Parameter Models (LPMs). Results are compared and contrasted to assess the efficiency of the used methods and to identify the main limitations for this type of application in Lebanon. Moreover, the outcome of this study allows a more detailed characterization of the water in the Jeita system (including water chemistry types and potential origin, total phreatic volumes etc.). This

work aims ultimately at refining the concept of vulnerability of a karst system in relation to transit times in such a complex system like that of Jeita spring.

1.5 Structure of the Thesis

The thesis is arranged in eight chapters. Chapter 1 gives a general overview of the groundwater along with different models and previous work on groundwater age dating, and objectives of the study. In Chapter 2, a review of the methods and techniques in groundwater age dating in young and old water is presented including Tritium (^{3}H), Tritium–Helium (^{3}H-^{3}He), Helium-4 (^{4}He), Krypton-85 (^{85}Kr), Chlorofluorocarbons (CFCs), Sulfur Hexafluoride (SF_6), Chlorine-36 ($^{36}Cl/Cl$) , and Carbon-14 (^{14}C). In Chapter 3, the field site is described, including the topography, lithology, hydrogeology, geological structures, and karstic features of the study area. Chapter 4 provides information about the sampling campaigns and field methods used in the study. In chapter 5 the analytical methods of Tritium–Helium (^{3}H-^{3}He), Chlorofluorocarbons (CFCs), and Sulfur Hexafluoride (SF_6) for groundwater age determination along with event analytical method are detailed. Chapter 6 presents the results of this work entailing major ions, stable isotopes ($\delta^{18}O$ and $\delta^{2}H$), and environmental tracers (Tritium (^{3}H), Tritium–Helium (^{3}H-^{3}He), Chlorofluorocarbons (CFCs), Sulfur Hexafluoride (SF_6). The discussion in Chapter 7 consists of a comparison of the different applied dating methods. It outlines the limitations and sensitivity of the parameters used in the age calculations. Additionally it provides insights into the spatial vulnerability of the Jeita aquifer system in relation to transit

times. A conclusion is provided in chapter 8, highlighting the main outcomes of this study and recommendations for future research.

CHAPTER 2

METHODS FOR GROUNDWATER AGE-DATING

2.1 Introduction

Several solutes infiltrate along with precipitated water to reach the groundwater table. The analysis of these compounds, known as environmental tracers, provides information on the time the water spent in the aquifer since it has reached the groundwater system (Newman et al., 2010). Environmental tracers include radioactive isotopes or anthropogenic compounds released in the atmosphere at known rates (Newman et al., 2010).

Radioactive isotopes (such as Tritium and Krypton) are naturally found in water and have the ability to decay with time at a certain known decay rate (such as half-life for radioactive isotopes), while other are industrial compounds (such as Chlorofluorocarbon; CFCs) interact with precipitated water during atmospheric gas exchange and are therefore input into infiltrated water (Kazemi et al., 2006) .

Groundwater ages range from a very few years to tens, hundreds, or thousands of years and they may even reach millions of years. In many literatures (Plummer and Friedman, 1999; Phillips and Castro, 2003; Kazemi el al., 2006; Newman et al., 2010), groundwater age is classified into three large groups 1) young, 2) old, and 3) very old groundwater; the boundaries between the age groups are not sharp (e.g. Plummer and Friedman, 1999; Phillips and Castro, 2003; Kazemi el al., 2006; Newman et al., 2010).

Hence, based on the wide range of years of groundwater, environmental tracers are selected according to their application range. Therefore, groundwater age dating requires a contextual understanding of the aquifer type and system, geological configuration, hydrological conditions, and the geochemistry of its waters as these may give some sight on the age range of the investigated groundwater before an appropriate method is applied (Plummer and Friedman, 1999).

Various environmental tracers exist in groundwater and can be a useful tool for groundwater age dating and in determining the rate at which groundwater is replenished over a wide range of time scale, these environmental tracers include Tritium (^{3}H), Helium-3 (^{3}He), Helium-4 (^{4}He), Krypton-85 (^{85}Kr), Chlorofluorocarbons (CFCs), Sulfur Hexafluoride (SF_6), Chorine-36 (^{36}Cl), Argon-35 (^{35}Ar), and Oxygen-18(^{18}O). Young groundwaters are of greater focus than old groundwaters as they refer to a higher flow rate, so recharged water is assumed to reach the aquifer and to flow relatively at faster rates than older waters. Thus, aquifers with young groundwater will be more vulnerable to contaminations; therefore it is more relevant to characterize young waters than old groundwater for the proper management of water contamination (Newman et al., 2010).

2.2 Old and Very Old Groundwater

Groundwater having transit times exceeding 60 years are considered to be old groundwater, yet if it exceeds 50,000 years it is considered to be very old. Moreover, very old groundwater might reach tens of millions of years of age (Kazemi et al., 2006).

This subdivision of old groundwater into old and very old groundwater in many literatures is based on the environmental tracers used, as some environmental tracers have a much greater half-life than others, which can be more suitable for dating very old groundwater (Kazemi et al., 2006).

The Carbon-14 (^{14}C) method was discovered in 1957 as a useful tool for dating old groundwater (Kazemi et al., 2006). Carbon-14 (^{14}C) is a naturally occurring radioactive carbon isotope that is highly present in the atmosphere mainly in the form of carbon dioxide (CO_2) or carbon monoxide (CO). These atmospheric gases (containing carbon-14) will eventually dissolve in the percolating rain water and reach the groundwater system by infiltration. Carbon-14 (^{14}C) after that starts in decaying to Nitrogen with a half-life of 5,730 years (Kazemi et al., 2006). Efforts were made in order to develop isotopic models to estimate the initial amount of carbon-14 (^{14}C) of the dissolved inorganic carbon (Clark, 2015). However, the difficulty of translating Carbon-14 (^{14}C) dates into water ages motivated researchers to search for other environmental tracers that are suitable for dating old groundwater, these isotopes include, Chlorine -36 (^{36}Cl), Helium-4 (^{4}He), Krypton-81 (^{81}Kr), Uranium (^{238}U) isotope ratios, and carbon-14 (^{14}C) in dissolved organic carbon (Kazemi et al., 2006)

Helium-4 (^{4}He) is a stable isotope of Helium that is used along with Helium-3 (^{3}He) in groundwater age dating. It is frequently used in dating very old groundwater and recent studies have used it in dating young groundwater. However its usage in young groundwater is still limited. Helium-4 (^{4}He) in the groundwater originates from several sources including:

1. Inflow from the crust (crustal flux of Helium) or production from aquifer matrix and from sediments grains (radiogenic Helium), through the alpha decay of Uranium and Thorium (Kazemi et al., 2006).
2. Inflow from the mantle (Terrigenic Helium) (Kazemi et al., 2006).
3. Release from the aquifer sediments, as the entrapped Helium-4 (^{4}He) in sediments' crystal lattices is released into the groundwater through the process of solid-state diffusion (Kazemi et al., 2006).
4. Atmosphere: As atmospheric Helium is dissolved in rain and percolates into the groundwater, the ratio $^{3}He/^{4}He$ in air is 1.384×10^{-6} however due to slight fractionation it is decreased to 1.36×10^{-6} when Helium is dissolved in rain water (Clark, 2015). Moreover, some atmospheric ^{4}He present in groundwater is caused by excess air during recharge leading to higher concentration of ^{4}He in the recharged water. In groundwater dating excess ^{4}He in groundwater must be separated from dissolved ^{4}He, this can be done by measuring Neon (Ne) concentration in groundwater and comparing Helium/Neon ratio in groundwater to those in the atmosphere (Kazemi et al., 2006); (refer to section 5.1.1 for details about Neon and excess air).

Therefore, these sources lead to an increase in the ^{4}He content in the groundwater, knowing the rate of in situ production and crustal flux of ^{4}He into the groundwater can provide an estimate of the age of known ^{4}He content in a groundwater sample (Kazemi et al., 2006).

2.3 Young Groundwater

Young groundwater is mainly a shallow groundwater found at a depth that ranges from 0 to 30 m in unconsolidated sediments and can reach depths up to 300 m in fractured-rock systems (Plummer and Friedman, 1999). Shallow ground water has a relatively young age given that it recently recharged. Moreover, it contributes largely to the base flow in rivers and lakes. For this reason it is mostly used for drinking and irrigation (Plummer and Friedman, 1999). However shallow ground water is more vulnerable to a wide variety of pollutants and contaminants produced recently than deeper groundwater. Groundwater age dating is a recent tool that provides substantial information about recharge rates and improves hydrologic models of groundwater systems. Hence, it can allow predicting the time needed for contaminates to be flushed out of the groundwater system (Plummer and Friedman, 1999).

Young groundwater has an age that range from 0 to 60 years (Kazemi et al., 2006); it is worth noting that 0 years implies an age that is less than one hydrological year, characteristic of fast infiltration and flow. Recently many methods related to the use of different environmental tracers were discovered and adopted in dating young groundwater that has been recharged in the late 60 years. Tritium (^{3}H) method was previously used frequently in many studies and provided encouraging results as it relied on the input of ^{3}H into the atmosphere post- nuclear atomic bomb testing in 1955 (refer to section 2.3.1). However recently due to the low concentration of Tritium in the atmosphere, this method is being abandoned or coupled with other higher resolution methods. These new methods for dating young groundwater include Tritium-Helium ($^{3}H/ ^{3}He$), CFCs, SF_6, Krypton-(^{85}Kr) and Chlorine-36 ($^{36}Cl/Cl$); (Clarke, 2015).

2.3.1 *Tritium Method (^{3}H)*

The Hydrogen atom is the lightest and most abundant atom in the universe; it has been believed to be generated during the Big Bang by proton-electron combinations (Newman et al., 2010). The Hydrogen atom is present in water, organic compounds, and living things. As previously mentioned three different isotopes exist for the Hydrogen atom, while ^{1}H, the most abundant Hydrogen atom (Protium), and ^{2}H is Deuterium are stable isotopes, ^{3}H Tritium is radioactive (Kazemi et al., 2006).

Tritium isotope constitutes part of the water molecule, and it is subjected to decay into Helium with a half-life of 12.32 years (Kazemi et al., 2006). Tritium concentrations are measured in Tritium units (TU) where 1 TU is one Tritium in 10^{18} atoms of Hydrogen (Kazemi et al., 2006). Tritium can be produced naturally by several ways either by alpha α decay of lithium-7 or by secondary neutron cosmic ray bombardment of Nitrogen and Deuterium in the upper atmosphere producing Carbon-12 and Tritium (Kazemi et al., 2006).

The Tritium average concentration in the atmosphere before the atmospheric nuclear bomb testing in the 1950s was approximately between 2 and 8 TU (Kazemi et al., 2006). After the nuclear bomb testing about 1.13×10^{9} TU of Tritium were added in the northern hemisphere with a maximum concentration detected in 1963 (Kazemi et al.,2006). Hence after the peak of Tritium in 1963 (Fig. 6), Tritium method started to be widely used for groundwater age dating, as the Tritium in the atmosphere eventually enters the hydrological cycle through the processes of precipitation and infiltration reaching the groundwater systems and aquifers. It was however, suitable to date waters that are 50 years old or younger.

Therefore, groundwater Tritium concentration reflects the atmospheric Tritium level at the time when the water has reached the groundwater system and lost the contact with the atmosphere (Newman et al., 2010). So, the Tritium method is based on the detailed estimated input function of Tritium concentration variations in the atmosphere throughout the years (Fig. 6), in order to establish an approximate groundwater recharge rates and travel times (Clark, 2015).

After the cessation of thermonuclear tests, Tritium concentrations started to decrease varying between 12 and 15 TU (Kazemi et al., 2006) in the early 1990, although nuclear power plants still produce Tritium but their contribution is considered very minimal. Hence as no atmospheric nuclear weapons testing is planned to occur in the future, Tritium concentration in the atmosphere will descend reaching a constant background levels (Fig. 6). Therefore, Tritium method for dating young water is getting closer to its expiry date (Harvey et al., 2006).

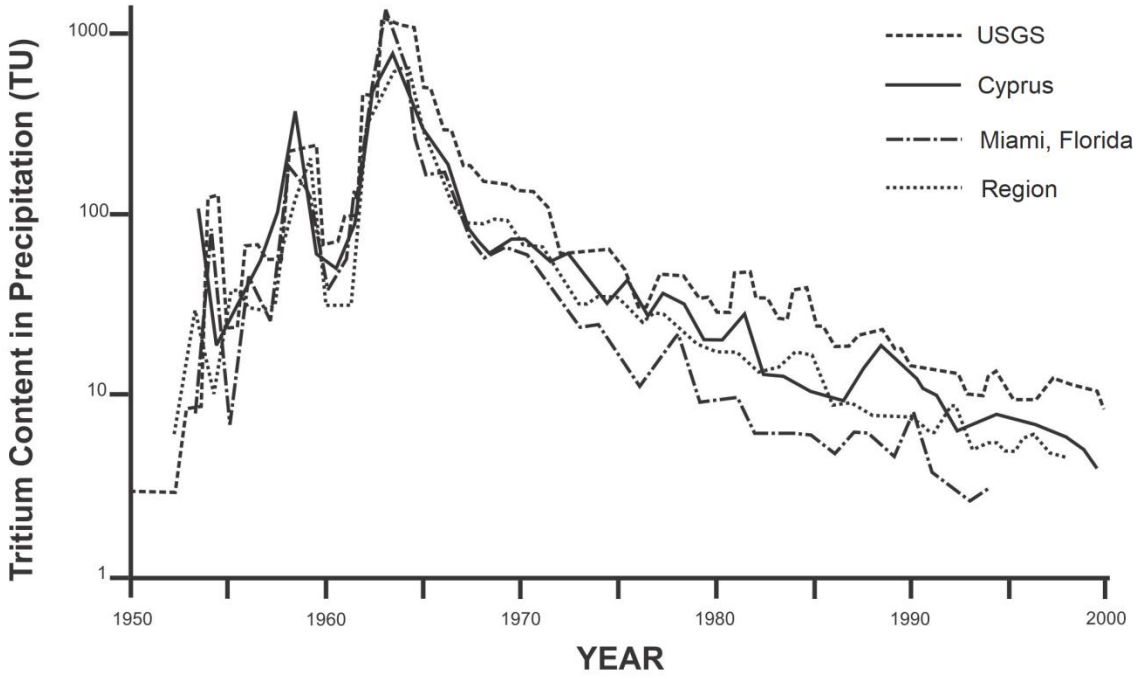

Fig. 6. Compiled Tritium concentrations in precipitation through time 1950-2000 in the region (Palestine); (Kaufman et al., 2002), Cyprus (Boronina et al., 2005), Miami, Florida (Harvey et al., 2006), and from USGS data.

2.3.2 *Tritium-Helium Method (^{3}H-^{3}He)*

Tritium-Helium method for dating young groundwater was previously proposed in 1969 by Tolstikhin and Kamensky (Kazemi et al., 2006), but at that time it was not highly recommended due to the difficulties in sampling and analysis of the Helium-3 (^{3}He) in the collected samples. However, starting 1990, the method started to be widely used in groundwater age dating, substituting the Tritium method as the use of Tritium method was fading (Kazemi et al., 2006).

The Tritium-Helium method is based on the ability of Tritium (^{3}H) to decay into Helium-3 (^{3}He) by beta (β) particle emission with a well-known decay rate (Fig. 7).

This method is useful for groundwater ages ranging from several months to about 30 years without exceeding 50 years (Kazemi et al., 2006).

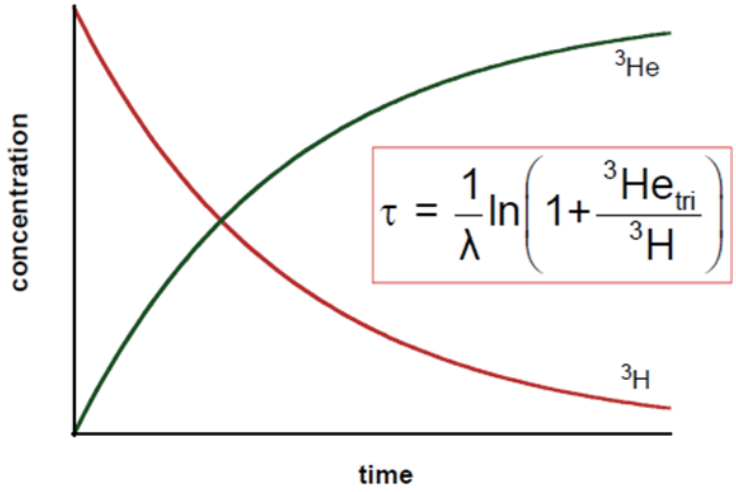

Fig. 7. The decay of Tritium (^3H) to Helium-3 (^3He); (Kazemi et al., 2006).

In the groundwater there are four main sources for Helium-3. These are as follows:

1. The first source is atmospheric, where the rain or snow water will be in a direct contact with the air that contains Helium (He_{atm}); the water will absorb and dissolve the Helium ($^3He_{eq}$) molecules from the air and then infiltrate to the subsurface.
2. The second source is from the fission of ^6Li (Lithium) by neutrons, where ^6Li will produce ^3H that will eventually decay to ^3He, this is called nucleogenic Helium (^3He_n).
3. The third source is the decay of Tritium to Helium; this is called tritiogenic Helium ($^3He_{trit}$); (Kazemi et al., 2006).

4. The fourth source is the release of ^{3}He to the groundwater from the mantle ($^{3}He_{prim}$). Each of the above sources has their own specific $^{3}He/^{4}He$ ratio that eventually leads to a particular ratio in groundwater; this can help in differentiating Helium of different sources. In young groundwater, mantle and nucleogenic sources are insignificant, but still differentiating atmospheric Helium form tritiogenic Helium reveals to be a difficult task. This exercise becomes extremely difficult if nucleogenic and mantle sources were to be considered significant (Kazemi et al., 2006).

2.3.3 *Chlorofluorocarbons (CFCs) Method*

Chlorofluorocarbons (CFCs) are synthetic organic compounds that have been produced in the early 1930 for their use as a refrigerant as they are safer (Leibundgut et al., 2009), replacing several refrigerants that were highly toxic and flammable. In addition CFCs started to be used since 1950 as blowing agents for foams and plastics, solvents for cleaning delicate electronic equipment, also as sterilizers for surgical instruments (Leibundgut et al., 2009). The production of Chlorofluorocarbons (CFCs) has increased considerably reaching about one million tons in the global atmosphere by the year 1974 (Kazemi et al., 2006). As a consequence this tracer had marked out in the hydrological cycle. For that reason CFCs are used to trace the flow of young water (below 50 years), by acquiring their concentration in water (Han et al., 2014).

There are three atmospheric trace gases of CFCs produced in the atmosphere and leaked into the environment reaching the groundwater systems in a high content; these are CFC-11, CFC-12, and CFC-113. The high production of CFC-12 took place in

the early 1940s, it was followed in the 1950s by CFC-12, and by CFC-113 in the 1960s. CFCs generally have a long atmospheric life; CFC-11, CFC-12 and CFC-113 have lifetimes of 45 years, 100 years, and 85 years respectively. CFC-11 and CFC-12 uses were restricted as working fluids in refrigerators and air-conditioning systems, while CFC-113 was used as a solvent. CFCs concentration continued to rise until the 1990s, when production was reduced to protect the ozone layer and they were replaced with Hydrochlorofluorocarbons (HCFCs), their concentration started to decrease in the atmosphere (Kazemi et al., 2006). The variations in concentrations of CFC-11, CFC-12, and CFC-113 from 1940 to 2010 are shown in Fig. 8.

The CFC method is used to estimate groundwater age based on precisely knowing their input in atmospheric concentrations over the past 60 years. It is highly reflected in the CFC content that was present in the infiltrated water during recharge of groundwater system, with assumptions that the initial concentration of CFC in water must be known, and that the CFC is stable and not altered by geochemical, biological, and hydrogeological processes.

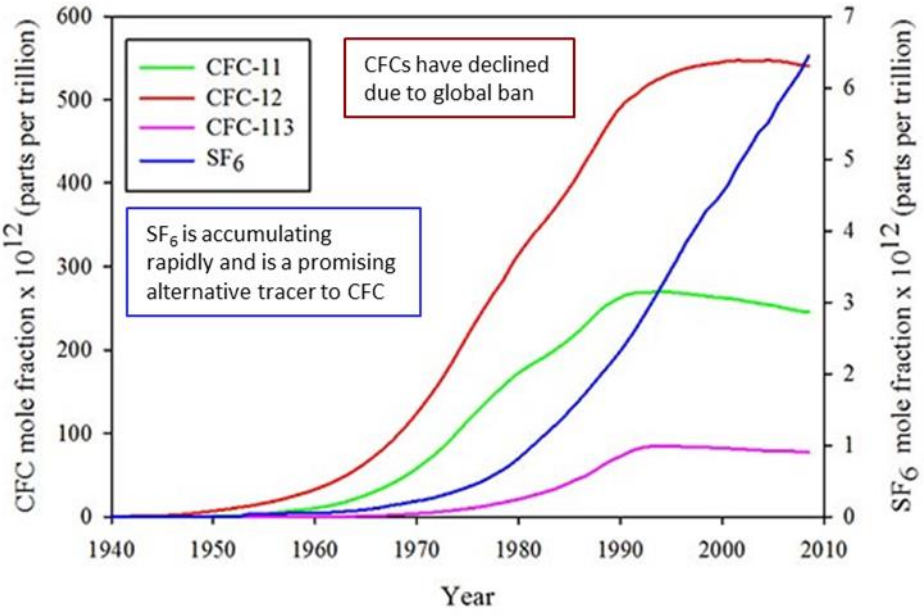

Fig. 8. Chlorofluorocarbons (CFCs) and Sulfur Hexafluoride (SF_6) concentrations in the Northern Hemisphere Atmosphere air (pptv) during the last 70 years (RSMAS).

2.3.4 *Sulfur Hexafluoride (SF_6) Method*

Sulfur Hexafluoride (SF_6) is predominantly of anthropogenic origin but occurs naturally and can be found in many minerals, rocks, igneous and volcanic fluids. SF_6 is a colorless, odorless, stable, nontoxic, and nonflammable gas; it has several applications mainly in electric power industry due to its excellent electrical insulating property, in the semiconductor industry, in the melting operations of reactive metals such as magnesium and aluminum, in blood products, and many others. The industrial production of SF_6 began in 1953 with the introduction of SF_6-filled high voltage electrical switches. Since 1953 the annual production of SF_6 has increased from approximately zero to about 85,700 t of SF_6 in 1995 (Busenberg and Plummer, 2000).

During the last 40 years the SF_6 concentrations in the air have increased promptly from steady-state level of about 0.02 to about 6 parts per trillion (pptv; Busenberg and Plummer, 2000). However SF_6 has the lowest solubility with respect to other environmental tracers.

Recently the SF_6 has received a great global recognition due to its long life time that has been estimated to range between 1935 to about 3,200 years (Busenberg and Plummer, 2000), in addition to its high greenhouse-warming potential making it one of the most powerful greenhouse gas of all those stated under the Kyoto protocol (1997); (Breidenich et al., 1998). SF_6 is mainly used for dating young groundwater, however it is used in other applications such as determining the longitudinal dispersion coefficients in rivers, gas exchange rate in streams, and air-sea gas exchange and dispersion (Kazemi et al., 2006).

The SF_6 concentration in the atmosphere is predicted to continue in increasing into the 21st century, and along with its known atmospheric concentrations throughout the history, SF_6 are being recently widely used in dating young groundwater. Hence, similarly to the CFCs the precise knowledge of the SF_6 concentration in the atmosphere throughout the years, along with knowledge the recharge air temperature, we can estimate the recharge year of the tested groundwater samples. However unlike the CFCs, SF_6 is resistant to biodegradation and it does not sorb into organic matter, rubber, and polymers, so contamination during sampling is less likely to occur. However excess air during sampling and the presence of natural SF_6 background source, may complicate the process of dating groundwater using SF_6 (Kazemi et al., 2006).

2.3.5 *Krypton-85 Method*

Krypton-85 is a colorless and an inert radioactive noble gas that is highly soluble in water, with a half-life of 10.76 years (Kazemi et al., 2006). Krypton-85 is produced naturally in minimal amounts in the atmosphere by spallation and neutron activation of stable Krypton-84. Krypton-85 is artificially created by fission of Uranium and Plutonium. However other sources also exist for Krypton-85 production. These include, nuclear-bomb testing, nuclear reactors, and to nuclear fuel reprocessing plants (Newman et al., 2010). These factors have led to a major increase of Krypton-85 in the atmosphere, increasing to a 85 dpm/cc (decays per minute per cm^3 STP) of Krypton in the northern hemisphere and 15% less in southern hemisphere over the last 45 years (Delbart et al., 2014).

Dating using this method is based on isotope ratios ($^{85}Kr/Kr$). This method has advantages on other methods as infiltration temperature and height are not required for the dating procedure, moreover the risk of excess air and degassing is not present, however this method requires large sample volume and relatively high analytical cost (Delbart et al., 2014).

2.3.6 *$^{36}Cl/Cl$ Method*

Chlorine-36 is a radioactive isotope with a half-life of 301,000 years (Davis et al., 2000); it is produced naturally by cosmic-ray splitting of Argon-40 (^{40}Ar) in the atmosphere and by neutron activation of Chlorine-35 in the atmosphere and in the shallow and deep subsurface. In addition Anthropogenic Chlorine-36 is produced from

nuclear weapon testing in the Pacific between 1952 and 1958 and from nuclear power and nuclear fuel reprocessing facilities (Davis et al., 2000).

$^{36}Cl/Cl$ method is used for dating recently charged groundwater by using the ^{36}Cl pulse produced from nuclear weapon testing moreover it can be used to date old groundwater ranging between 50,000 years and two million years by the slow radioactive decay of Chlorine-36.

Hence, this method provides the residence time of the groundwater since it has entered the groundwater system (Davis et al., 2000). However in both cases for dating young and old groundwater using this method, the initial concentration of ^{36}Cl and the history of chlorine in the groundwater must be known. Usually the measured ^{36}Cl is reported as ratio $^{36}Cl/Cl \times 10^{15}$ (Davis et al., 2000).

CHAPTER 3

FIELD SITE

3.1 Overview

Lebanon is characterized by its mountainous chains that mainly consist of carbonate rocks with large amount of springs and caves (Edgell, 1997). The Jeita cave is one of the most renowned caves in Lebanon as it is the longest one with an underground river 6 km upstream of the spring (Hahne, 2011). The location of its entrance is at N32°56.616′; E035°38.516′ and about 90 m above sea level on the western flank of central Mount Lebanon (Doummar et al., 2014), approximately 5 km east of the Mediterranean coastline and about 18 km north of Beirut (Doummar et al., 2014), in the Nahr el Kalb Valley. The Nahr el Kalb River is the dividing line between the Metn area to the south and the Kesrouane area to the north (Hahne, 2011).

The Jeita groundwater catchment area approximately extends 150 km^2 east to the Lebanese Mountains (Fig. 9), and it ranges in altitude from 90 to 2000 m above sea level (Doummar et al., 2014) this is mainly based on geological mapping, tracer experiments, and monitoring of chemical and physical parameters from several springs. The groundwater catchment area of Jeita was not well delineated before the hydrological investigation done by the BGR project (Hahne, 2011; Abi Rizk and Margane, 2011; Königer and Margane, 2014).

The southern part of the Nahr el Kalb Valley is excluded from the Jeita catchment (Fig. 10 A), since geological dip is mostly towards the south and tracer tests done in this area yielded negative results as no tracer has arrived to Jeita spring from these injections (Hahne, 2011).

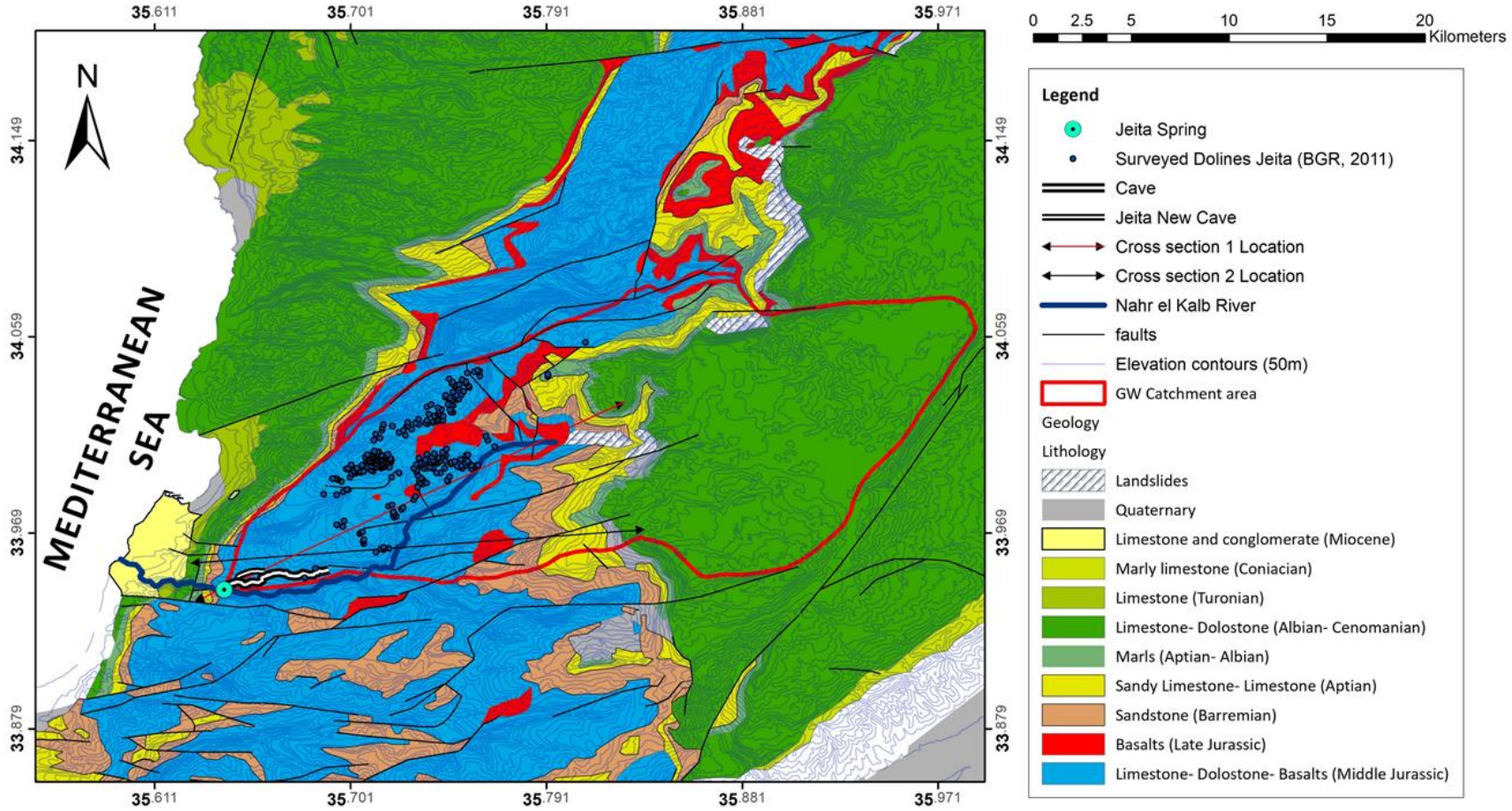

Fig. 9. Geologic map of the tentative Jeita Catchment area. The dolines in the Jeita catchment area has been surveyed and mapped in the BGR project (Abi Rizk and Margane, 2011).

A

B

Fig. 10. (A) Lower part of the Jeita Catchment and (B) Nahr El Kalb River (Photo courtesy of Emmanuel Dubois).

The topography of this area extends from 90-2000 m, above sea level and is characterized by deeply incised relatively structurally controlled young rivers. The direct catchment is composed of massive micritic limestone of Jurassic age locally dolomitized (Verheyden et al., 2008). Parts of the catchments especially the middle area display an intense karstification, as portrayed by the presence of multiple dolines, lapiaz, pinnacles. In these areas, soil cover is almost absent. Furthermore, the catchment is lacking drainage patterns, to the exception of Nahr el Kalb River that dries during summer time, as it is mostly fed by seeping groundwater and feeding springs (Fig. 10 B).

3.2 Climate

The Jeita catchment area is characterized by a Mediterranean and semiarid climate. The mean annual precipitation in the Jeita catchment area is 1200 mm/yr on average (Doummar et al., 2014). Precipitation mainly varies from above 900 mm/yr at Jeita to about 2,100 mm/yr near Mount Sannine (Königer and Margane, 2014). Mainly October to April are the raining months in this site, however during the period between December and March in the mountainous region at elevations greater than 1,800 mostly snow rainfall dominates (Königer and Margane, 2014). Hence groundwater recharge is greatly influenced by the type and distribution of precipitation.

3.3 Lithology and Hydrogeology

The direct Jeita groundwater catchment (75 % of the total catchment) consists of micritic limestone locally dolomitized, known as the Kesrouane Formation (Hahne,

2011). The catchment is extended towards the upper area consisting of upper Jurassic and middle Cretaceous Formations. It is assumed that overland flow over these areas might infiltrate downslope into the direct catchment and contribute to the water balance of the Jeita spring. However this phenomenon has been not investigated yet.

The Jeita catchment area is 75% covered by four different carbonatic units acting as karstic aquifers cropping out in the study area as shown in the geologic cross section 1 (Fig. 11 A) and cross section 2 (Fig. 11 B).

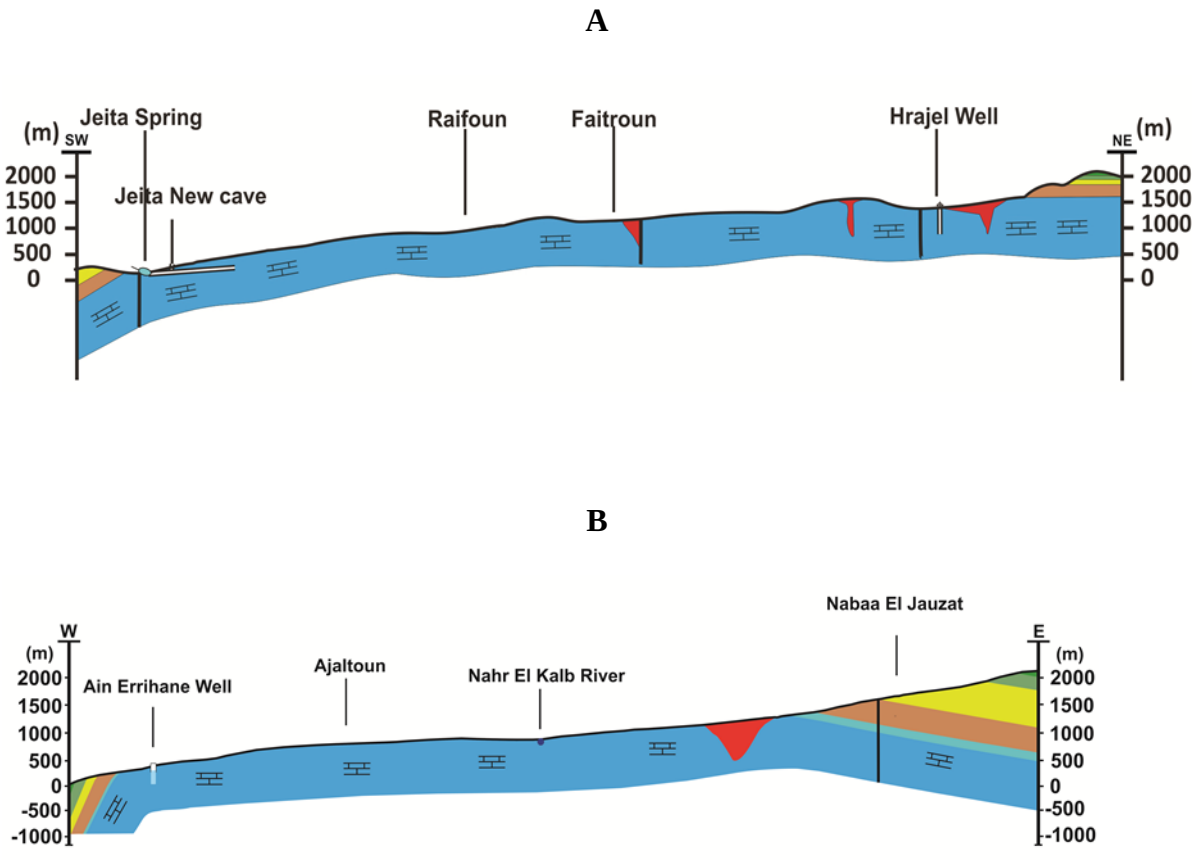

Fig. 11. Two geologic cross sections: (A) cross section 1 through the Jeita spring and Hrajel well in the Jeita Catchment area and (B) cross section 2 through the Ain errrihane well in the Jeita Catchment area.

The Formations and series of Formations mainly 1) Kesrouane, 2) Upper Jurassic complex, and 3) Middle Cretaceous complex are detailed below.

3.3.1 *The Kesrouane Formation (J4)*

The Kesrouane Formation is subdivided into units the lowest units can be recognized near the dam of Chouane with a typical dark and approximately one hundred meters thick dolomite that consist of developed microbial laminites, collapse breccias and tepees (Walley, 1997). These beds might be dated to Late Triassic or more likely a Liassic age, as evaporates in the region have been deposited toward the end of Triassic. This basal component of the Kesrouane Formation is termed Chouane Dolomite Member (Walley, 1997). The overlying units, which form the bulk of the Kesrouane Formation, are mainly thick, massive and poorly fossiliferous limestones with thin clay units. The highest beds of the Kesrouane Formation comprise different fauna including abundant stromatoporoids (Walley, 1997).

The Kesrouane Limestone is characterized by a thick sequence of shallow inner to middle shelf carbonates and may represent deposition under a combination of local post rift thermal subsidence and global sea level rise (Walley, 1997).

In the Jeita catchment area this Kesrouane Formation is a cliff-forming covering 88 km² of the total catchment area with a light grey to white color (Hahne, 2011). It has an age ranging from lower to upper Jurassic (Liassic to Oxfordian) (Walley, 1997). It is made up of massive micritic to fossiliferous (locally), karstified, thick bedded limestone with horizons of dolomitic limestone and some chert nodules, with an average stratigraphic thickness of about 1000 m in the area (Verheyden et al.,

2008). The differentiation of the Kesrouane Formation from the overlying Bhannes and Bikfaya Formations is not clear in the geologic map but it has the largest outcrop where it occurs given its thickness.

The Kesrouane Limestone has been affected by secondary hydrothermal dolomitization mainly along basaltic intrusions, deep and multi-level Karstification has affected the entire Formation since the beginning of the Mount Lebanon uplift in the upper Cretaceous forming large conduits and caves among them the Jeita cave and Jeita spring, making the Formation one of the most significant aquifers in Lebanon due to its extensive karstification, thickness, exposure, and extent that all enhance the high storage and recharge capacity of the Kesrouane aquifer. In the UNDP 1970 study transmisivity values of the Kesrouane Jurassic Aquifer were mainly calculated using pumping tests ranging between $2x10^{-3}$ and $2x10^{-2}$ m^2/sec. The Kesrouane Juraasic aquifer is part of the Kesrouane Jurassic basin (16) that is hydraulically connected to the overlying Chouf Sandstone Formation close to the Coastal flexure (UNDP, 2014). In the Kesrouane Formation Groundwater preferentially flow along fault zones, fractures, and karst conduits or cavities generally towards the southwest (UNDP, 2014).

3.3.2 *Bhannes Formation (J5)*

The Bhannes Formation ranges in age from Oxfordian to early Kimmeridgian with a thickness of 200m (Walley, 1997). It consists this layers of baslts, marls, clay, siltstones, and limestones acting as an aquiclude (UNDP, 2014).

3.3.3 *Bikfaya Formation (J6)*

The Bikfaya Formation covers 5.3 km² of the total catchment area and it is made up of a massive cliff- forming micrtic limestone with layers of chert nodules with an age ranging from Kimmeridgian to Thitonian (Hahne, 2011). This Formation is 100m thick and highly karstified as J4 however due to its limited extent and thickness this Formation yields limited quantities of groundwater (Hahne, 2011).

The Salima Formation overlying the Bikfaya Formation is considered as a Jurassic-cretaceous disconformity, as it is reported as eroded in the study area (Walley, 1997).

3.3.4 *Chouf Formation (C1)*

This unit, of Neocomian age, is about 80 m thick and consists of brown to white layers of sandstone, argillaceous sandstone, ferruginous sandstone, clay and volcanics (Dubertret, 1955; Walley, 1997). The sandstone is composed of poorly sorted quartz grains, intercalating locally with beds and lenses of clay. The cement bonding the matrix is composed of calcite, oxides and clays. This Formation is considered a fissured aquitard in the study area, i.e., yielding flow rates not exceeding 3 l/s (Hahne, 2011).

3.3.5 *Abieh Formation (C2a)*

The Abeih Formation overlying the Chouf Formation has a total thickness of around 175 m based on the constructed cross sections. It is subdivided into two minor units of Barremian-Aptian ages (Walley, 1997). This unit consists at its base of clays

and marly units, grading into jointed sandy limestone (Peltekian, 1980). The boundary between the underlying Chouf Sandstone Formation and the Abeih is a gradational transitional contact (Walley, 1997). This Formation is considered mostly an aquiclude especially the marly layers found at its base.

3.3.6 *Mdairej Formation (C2b)*

The Mdairej Formation covers 4.2 km² of the total catchment area, consisting of a massive cliff-forming micritic limestone that is strongly karstfied and with an age of early Cretaceous to Aptian and thickness of 50 m (Walley, 1997). The Mdairej Formation is considered a fractured karst aquifer with limited potential because of its thickness (Hahne, 2011).

3.3.7 *Hammana Formation (C3)*

The Hammana Formation has an age ranging from upper Aptian to middle Albian and a thickness 110 to 350 m (Walley, 1997), this thickness is influenced probably by syn-depositional faults. Lithlogically it is made up of claystone and light grey marls with basalt intrusion at the base forming the red soil (Hahne, 2011). This non-karstic Formation is an aquiclude, its boundary with the overlying Sannine Formation is considered a spring line, where important springs emerge (Hahne, 2011).

3.3.8 *Sannine Formation (C4)*

The Sannine Formation in the Jeita catchment area is 1,050m thick with an age of upper Albian to Cenomanian. This Formation is made up mainly of micritic limestone that is strongly karstified (Hahne, 2011) and green and grey marl with bioturbation is present at its base. The Sannine Formation covers 148 km² of the Jeita catchment (Hahne, 2011), forming a gently dipping high plateau of the Mount Lebanon mountainous range (Fig. 11 A). The Sannine Formation has a wide extent in the catchment area and is highly karstified were preferential groundwater can flow through the large fractures and cavities enhancing its high storage and recharge capacity (UNDP, 2014). The hydraulic conductivity values for Sannine aquifer are estimated to vary depending on the degree of karstification (UNDP, 2014).

3.4 Structures

During the Late Jurassic and Early Cretaceous time the area of Lebanon underwent block faulting due to a major uplift (Walley, 1998), giving emergence and erosion of existing rocks that possibly lasted for 10 or more million years, resulting in the deposition of the Lower Cretaceous sandstones of the Chouf Formation lying unconformably upon the Jurassic limestones (Walley, 1998).

Later on several phases have occurred sequentially. First, in the Late Mesozoic/Early Cenozoic the closure of the Tethyan Ocean due collision of Eurasia and the Africa-Arabia plate has developed a coast-parallel (NNE-SSW-trending) mega-structure of a wide spanned asymmetric anticline with steep layer dip (25°-75°) towards

the west and more gentle dip (5°-10°) towards the east (Walley, 1988), forming the syncline of Bekaa Valley and the anticline of Anti-Lebanon mountain range. Second, the Dead Sea Fault System has developed along with left-lateral shear zones approximately ten million years ago where the area began to be dissected by the first motions along this fault system, which caused new tilting,uplift, and major disruption of drainage along with synthetic fault-branches which are linked to the main fault (Yammouneh Fault striking NNE) at angles of approximately 45° affecting the mega-anticline by faulting and to a minor extent also by folding over the last five million years (Walley, 1998).

The Jeita catchment area is part of the zone affected by the Dead Sea Fault System (DSFS). The Dead Sea Fault System (DSFS) has generated a 200 km long restraining bend and compressional forces represented by the Mount Lebanon mountain chain and the development of the coastal flexure (Hahne, 2011). This coastal flexure is an asymmetrical anticline whose western limb has very steeply dipping beds reaching almost 90° degrees in some areas (Fig. 11 B) and gently dipping eastern limbs towards the Yammouneh Fault system (Walley, 1998). This monocline feature acts as a major groundwater hydraulic barrier for the Jurassic core, trapping the water behind it and triggering the development of overflow springs (Hahne, 2011).

Several faults of different types and scale are present in the catchment, the main river valleys and other detectable lineaments are represented by faults. These valleys show vertical fault planes partially with well-developed tear-off-edges and slickensides indicating a left-lateral movement also right-lateral movement can be observed (Hahne, 2011). In addition to the vertical faults and normal faulting also

shallow overthrusting faults are recognized in the catchment area. Shear lenses and thrusts are well developed in the area due to the area's transpressional regime. Many of these faults are filled with fragmented material of the host rock (Hahne, 2011). In some faults of calcareous Formations, a high iron content of pebbly fragmented host rock, iron concretions and highly ferruginous sandstone from other Formations can be observed proving hydrothermal activity which is related to widespread multiphase basaltic intrusions (Hahne, 2011).

A major fault is located at the north end of Jeita catchment area passing by the Chahtoul village (Chahtoul fault) and acting as water divide to the Jeita catchment, this fault cuts Mesozoic Formations, mainly the Jurassic sequence creating preferential groundwater flow pathways along it. This fault is one of the WSW-ENE to WNW-ESE trending faults cutting the Mesozoic sequence due to an extensional event that took place in Lebanon during the Early Cretaceous (Homberg et al., 2009). This extensional phase started during the deposition of the Chouf sandstones (late Valanginian or Hautervivian times) and ceased during the Cenomanian. Hence, this NNE-SSW extension event produced WSW-ENE to WNW-ESE normal faults with a length of several kilometers to several tens of kilometers and with offsets as large as several hundred meters (Homberg et al., 2009).

To the south of the Jeita catchment area a major ENE-WSW trending fault (Dbayeh Fault) stretching from the Yammouneh fault in the east most likely extending to the west offshore from the Mediterranean coastline (Bou Jawdeh, 1999; Gedeon, 1999). This fault is a dextral fault with horizontal displacement reaching 3 km as

determined by the displacement of the coastal flexure and vertical displacement of 300m (Gedeon, 1999; Bou Jaoude, 1999)

The area has been also subjected to an intense volcanism that took place in Lebanon in the Early Cretaceous (Homberg et al., 2009).

3.5 Karst Features

The Jeita catchment area is dominated with highly karstified geological units (more than 80%; Abi Rizk and Margane, 2011). The karstic features developed are either on the surface or underground and they can be of a small scale or large scale (Fig. 12).

Dolines are the most important large scale karstic feature. Collapse cavities are most prominent type of the Jurassic J4 limestone dolines, where at the bottom of these dolines soil is accumulated in a significant amount. In the high plateau of the upper Cretaceous (C4) limestone numerous dolines were recognized, many of them were formed on the Qana plateau (Abi Rizk and Margane, 2011). Moreover, a large number of dolines is encountered in the uppermost part of the Jurassic J4 limestone as in the Raashine, Boqaata, Achkout and Faitroun area at an elevation of 1000 to 1200 m (Abi Rizk and Margane, 2011).

The dolines clusters are oriented mostly along a northeast-southwest direction mimicking major faults with a similar trend extending at the northern boundary of the catchment and within the catchment (Fig. 9).

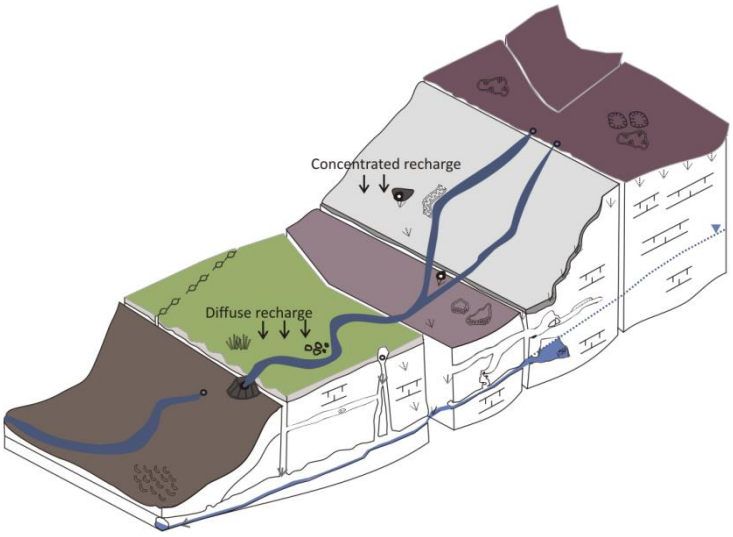

Fig. 12. Schematic representation of the Jeita subsurface channel and recharge area (Doummar, 2012).

3.6 Jeita Spring

In the 1950s, a tunnel was dug into the Jeita cave to make it more easily accessible to tourists. The Jeita cave has a ceiling that is more than 15 m high (Verheyden et al., 2008) and includes a major underground spring making it continuously exposed to numerous hydrogeological studies (Fig. 12). Besides that, the large underground halls in the cave contains many speleothems especially in the upper gallery making the cave center of attention for tourism, most of the speleothems are characterized by a ‘pile d'assiettes’ or ‘dish-stacks’ structure (Verheyden et al., 2008) as shown in Fig. 13.

The Jeita spring (Fig. 13) is one of the major karst springs in Lebanon; it provides for about 2 million inhabitants major potable water resource in the Greater Beirut Area. It has a discharge rate ranging from 1 m^3/s during low flow periods to approximately 20 m^3/s during high flow periods (Doummar et al., 2014).

Fig. 13. Jeita Spring and lower cave.

The Jeita Spring discharges from a lower Jurassic aquifer but this lower aquifer is interconnected and it is recharged with an upper upper aquifer Cretaceous in age (C4) through several springs discharging into the lower aquifer by infiltration such as Afqaa, Assal, Labbane, and Rouaiss (Königer and Margane,2014). The Qachqouch spring was monitored and revealed no connection with Jeita spring (Königer and Margane, 2014).

The Jeita karst system is characterized by a duality of infiltration and flow, where water infiltrates in point source karst features and reaches the spring at relatively high velocities, while diffuse recharge occurs over less karstified areas characterized by a thick soil cover. The fast infiltrated water follows developed secondary porosity and cavernous shafts resulting from extensive karstification. Storage is mostly concentrated in the relatively low permeability porous matrix.

CHAPTER 4

FIELDWORK

4.1 Sampling Campaigns

Two sampling campaigns have been undertaken in 2014 and 2016 to collect a total of 16 samples for groundwater age analysis using environmental tracers. Samples were collected according to Standard Operating Procedures for sampling for Helium, Tritium, CFCs, SF_6, stable isotopes, and major ions. In addition, to in-situ physical parameters were measured onsite to ensure a comprehensive sampling at each of the investigated points.

4.1.1 *First Campaign (October 2014)*

Mean groundwater age dating was achieved by the analysis of environmental tracers (Chlorofluorocarbons, Sulfur Hexafluoride, Tritium, Helium, Neon, Oxygen, Deuterium and major ions) in groundwater samples taken from six wells and one spring (two samples; one from the Jeita main cave and one from the Jeita new cave) belonging to the Jeita spring catchment in the Kesrouane area as shown in Table 1 and Fig. 14.

Table 1. Name and Location of the wells/spring where groundwater samples were collected in the first campaign.

Site Number	Type	Name of site	Altitude (asl)	Well Depth (BG)	Water Level (asl)	Latitude (WGS, 1984)	Longitude (WGS, 1984)
1	Well	Ain delbe	1083 m		783m	N34˚2'43.33'' 34.045369°	E35˚45'50.22'' 35.763950°
2	Well	Ouata el Joz	1082 m	650m	482m	N34˚00'36.4" 34.010111°	E035˚47'22.7" 35.789639°
3	Well	Hrajel	1237 m	-	-	N34˚00'52.4" 34.014556°	E035˚44'49.3" 35.747028°
4	Well	Aintoura	169m	250m	-	33°57'43.60" 33.962111°	35°38'10.78" E35.636328°
5	Well	Harissa	499 m	-	-	N33˚59'00.2" 33.983389°	E035˚39'8.2" 35.652278°
6	Well	Ain errihane	383 m	450m	288m	N33˚57'25.2" 33.957000°	E035˚38'53.4" 35.648167°
7	Spring	Jeita cave & Jeita New cave	90 m	-	-	N33˚56'38.55'' 33.944040°	E35˚38'23.72'' 35.639922°

4.1.2 *Second Campaign (April and May 2016)*

Mean groundwater age dating was achieved by the analysis of environmental tracers (Chlorofluorocarbons, Sulfur Hexafluoride, Tritium, Helium, Neon, Oxygen, Deuterium and major ions) in groundwater samples taken from seven wells and from the Jeita new cave belonging to the Jeita spring catchment in the Kesrouane area as shown in Table 2 and Fig. 15.

Table 2. Name and Location of the wells/spring where groundwater samples were collected in the second campaign.

Site Number	Type	Name of site	Altitude (asl)	Well Depth (BG)	Water Level (asl)	Latitude (WGS1984)	Longitude (WGS1984)
1	Well	Ain delbe	1083m		783m	N34˚2’43.33’’ 34.045369°	E35˚45’50.22’’ 35.763950°
2	Well	Ouata el Joz	1082m	650m	482m	N34˚00’36.4” 34.010111°	E035˚47’22.7” 35.789639°
3	Well	Hrajel	1237m	-	-	N34˚00’52.4” 34.014556°	E035˚44’49.3” 35.747028°
4	Well	Chahtoul	1005	375m	-	N 34° 2' 0.00" 34.033334°	E 35°43'40.21" 35.727835°
5	Well	Quachqouch	64	240m	-160m	N 33°56'39.97" 33.944437°	E35°38'15.05" 35.637515°
6	Well	Ain errihane	383m	450m	288m	N33˚57’25.2” 33.957000°	E035˚38’53.4” 35.648167°
7	Well	Kfar zebian	1127	-	-	N33°58'28.51" 33.974585°	E35°45'6.85" 35.751904°
8	Spring	Jeita New cave	90m	-	-	N33˚56’38.55’’ 33.944040°	E35˚38’23.72’’ 35.639922°

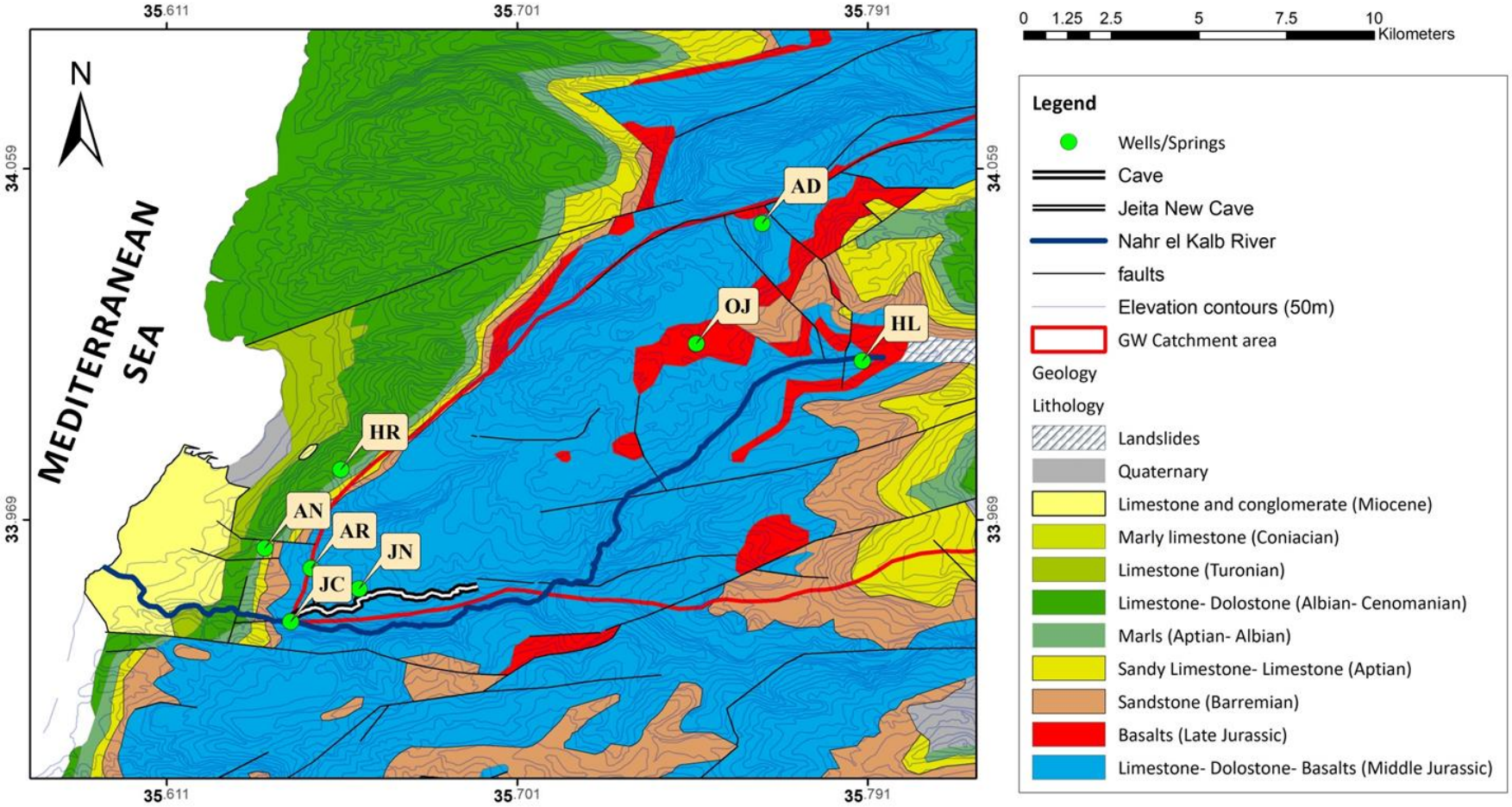

Fig. 14. Geologic map showing the sampled wells and spring in the first campaign.

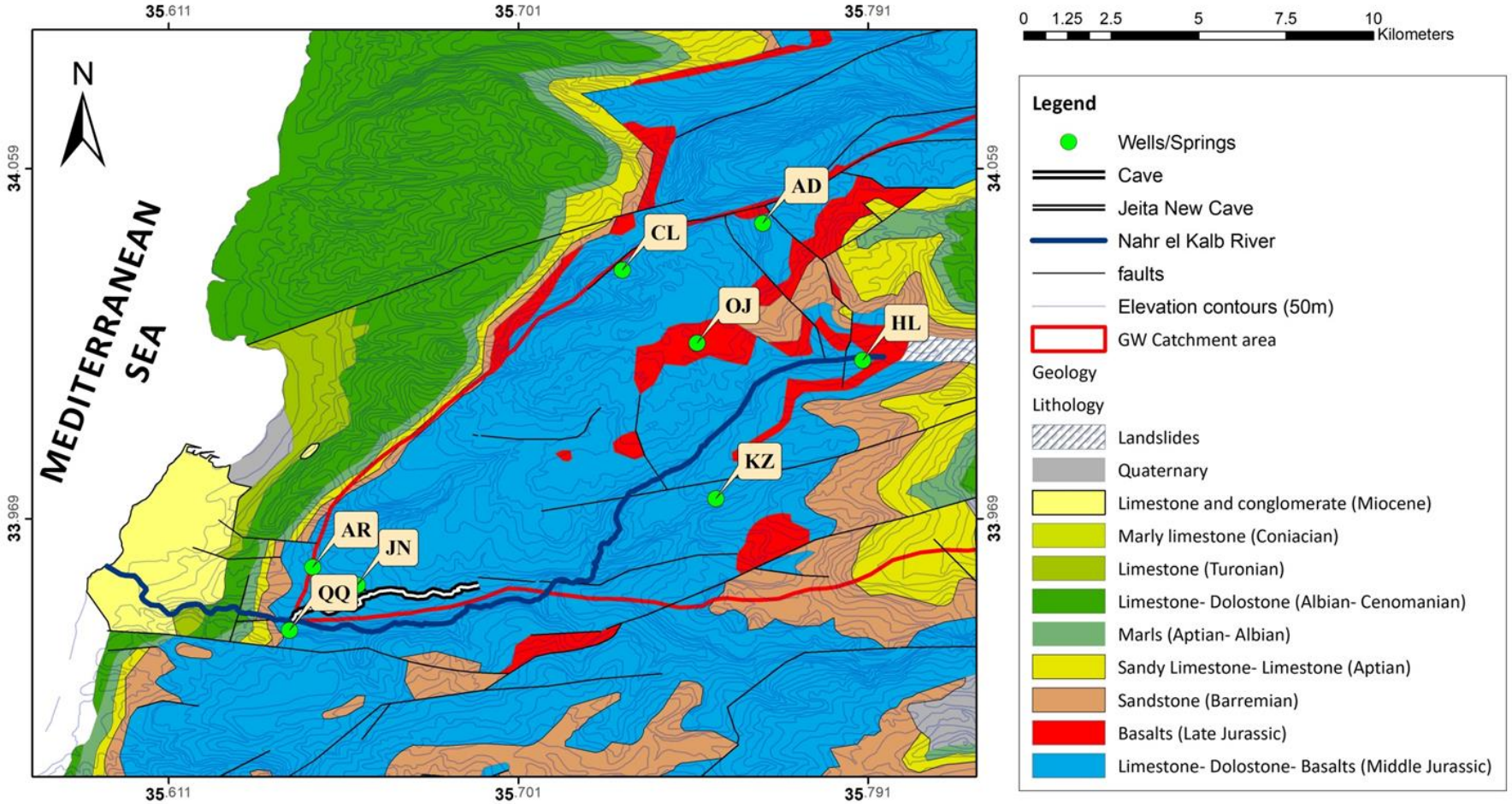

Fig. 15. Geologic map showing the sampled wells and spring in the second campaign.

4.2 Sampling Methods

4.2.1 *Physico-chemical Parameters*

Electrical Conductivity (EC), Temperature, pH, and Dissolved Oxygen (DO) were measured using a multi parameter probe system.

4.2.2 *Tritium (^3H)*

Samples for Tritium analysis were collected using a 1-L plastic (HDPE) bottles (Fig. 16). A few precautions are usually taken such as certain watches and compasses should be avoided during sampling. In addition, samples with high content of radon-222 must be degassed as radon-222 causes interference by emitting beta particles (Kazemi et al., 2006). There are mainly four methods of analysis of Tritium in water samples these are liquid scintillation counting or direct counting (detection limit 8-10 TU), low level counting (detection limit ~1 TU), ultra-low level counting (detection limit ~0.1 TU), and Helium-3 ingrowth method (detection limit 0.1 TU) used in the current study, in this method water samples are degassed in a vacuum line and stored in a sealed glass bottle for few months up to a year then the ^3He atoms produced by the decay of ^3H will be measured using mass spectrometer (Kazemi et al., 2006). The Tritium samples were collected in a two polyethylene plastic bottles, the bottles are filled and closed tightly and labeled according the well name and number.

Fig. 16. Sampling for Tritium using 1 liter HDPE (High Density Polyethylene) bottles.

4.2.3 *Tritium-Helium (^{3}H-^{3}He)*

Helium gas is sampled using a 10 ml copper tube sealed with stainless steel clamps. Extensive care must be taken during sampling of Helium, as any air contamination with the sampled water can severely reduce the efficiency of the dating method (Fig. 17). Before sampling the tube must be flushed about 10 times to remove any air entrapped in the tube, during sampling the copper tube must be raised to about 45˚, and in order to release air bubbles from the inner walls of the tube, the tube must be hit with a stiff tool. Neon and Helium-4 will be also measured along with Helium-3 as they are used to determine the tritiogenic Helium ($^3He_{trit}$) in the age analysis. The Helium and Tritium concentration in water are reported in TU, where one TU of ^{3}He is equivalent to one atom of ^{3}He per 10^{18} Hydrogen atom, and is approximately equal to 2.487 pcm^3 ^{3}He per kg of water (Kazemi et al., 2006).

In our campaigns two Tritium-Helium samples were collected in a two copper tubes, sampling took 30 to 45 minutes, first the copper tubes were flushed for 10 minutes, then the tubes were filled with water by holding the copper tube at 45˚ and continuously hitting the tubes using a wrench in order to force out any gas bubbles in the tube, then the two clamps are closed tightly together using the wrench. Finally the copper tubes are labeled according to the well name and number.

Fig. 17. Copper tubes used in ^{3}H- ^{3}He dating method.

4.2.4 *Chlorofluorocarbons (CFCs) and Sulfur Hexafluoride (SF_6)*

Sampling of groundwater using CFC- SF_6 methods requires extensive care in order to prevent any contamination of air in the sampled groundwater, as the average concentration of CFC in the atmosphere is about 300 times greater than that in groundwater. Several sampling methods are used in CFC- SF_6 sampling. The first

method is to use the apparatus developed by CSIRO (Commonwealth Scientific and industrial research organization), Australia (Kazemi et al., 2006). The apparatus consist of nylon tube connected to a bailer and sent down hole for sampling, an ultrahigh-purity (UHP) Nitrogen source used as excess air removal, tripod, torch, and ampoule are also used (Kazemi et al., 2006). The second method is to use a 500 ml glass bottles, water will be pumped in these bottles mounted in a saturated metal can, and to avoid contact of water with air, the bottles are closed under water. The third method used for the purpose of this study uses stainless steel bottles for sampling (Fig. 18), the bottles will be flushed several times and the bottle is kept upright until the bottle is totally filled with water (Fig. 18); (Kazemi et al., 2006). In our field campaigns the collection of the CFC- SF_6 took 20 minutes on average, the water was flushed for 10 to 15 minutes throughout the stainless steel bottles in order to make sure that no bubbles are present, then the stainless steel bottles were filled up by holding it vertically as shown in Fig. 18. Then the two valves are closed together tightly. Finally samples were labeled according to the well name and number.

Fig. 18. Stainless steel tubes used in CFC and SF_6 dating methods.

The content of CFCs in the sample is measured using purge-and-trap gas chromatography with an electron capture detector. The CFCs are usually reported as pmol/kg (picomole per 1 kg of water), and SF_6 in fmol/kg (femtomole per 1 l kg of water).

The samples for Tritium, Tritium-Helium, Chlorofluorocarbons and Sulfur Hexafluoride were shipped to the Institute of Environmental Physics / Section of Oceanography at the University of Bremen in Germany for analysis. Analysis of collected samples took 6 months for each sampling campaign.

4.2.5 *Major ions*

No specific precautions are needed in sampling for major ions; water samples for major ions are collected in plastic bottles for cation and anion analysis (calcium, magnesium, potassium, sodium, bicarbonates, nitrates, chloride, and sulfate mostly).

4.2.6 *Stable Isotopes*

The groundwater samples for Oxygen-18 and Deuterium isotopes analysis were collected in 50 ml glass bottles from different wells and springs (Fig. 19). The samples were stored in a refrigerator and later shipped and analyzed in the Centre for Stable Isotope Research and Analysis Büsgen-Institute in Goettingen (Germany). The method used for isotope water analysis was High Temperature Conversion Elemental Analyzer, with a precision of 0.2‰ for ^{18}O and 2‰ for Deuterium. The TC/EA method is known as pyrolysis, "it is a technique, in which Oxygen present in a water sample is converted to CO, and Hydrogen contained in a compound is converted to H_2" (Thermofisher), the separation of these reaction gases is done in an isothermal gas chromatograph, which is also part of the TC/EA (Thermofisher). The process is rapid and quantitative in a reducing environment at high temperatures, typically exceeding 1400 ˚C (Thermofisher). The standards used in the laboratory were calibrated in reference to the Vienna Standard Mean Ocean Water (VSMOW) standard, and the analyzed data of $\delta^{18}O$ and $\delta^{2}H$ are reported in the conventional δ-notation relative to the VSMOW standard.

Fig. 19. Sampling for stable isotopes in 50 ml glass bottles immersed in a beaker filled with water.

4.3 Event Sampling

Samples were collected at varying intervals using an automatic sampler deployed in the cave following a precipitation event on March 13 2016. Water level and temperature were measured every 30 minutes using a multi parameter probe mounted with a datalogger. Samples from the rain at 600 m and 900 m above sea level were also collected to obtain the signature of rain water in stable isotopes and calcium. Rain was measured using a climatic station deployed at 900 m asl every 15 min. Calcium analysis was performed in the American University of Beirut core lab (Central Research Science Lab) using the Atomic Absorption Spectrophotometer apparatus, after calibrated with calcium standards and performing appropriate dilution for the collected water samples (Fig. 20). Based on a rating curve, discharge rates were estimated from the water level data measured at the spring.

Fig. 20. Dilution of collected water samples prior to the measurement of calcium using Atomic Absorption Spectrophotometer.

CHAPTER 5

ANALYTICAL METHODS

5.1 Age Determination

5.1.1 *Tritium-Helium (^{3}H-^{3}He)*

The Tritium-Helium method relies on the decay of Tritium to Helium (half-life of 12.4 years); (Delbart et al., 2014) , by measuring the amount of Tritium (^{3}H) present in the sample at the time of sampling and measuring the amount of Helium (^{3}He$_{trit}$) that decayed from ^{3}H. The sum of both is the total amount of Tritium that was present during recharge (Kazemi et al., 2006).

$$^3H_0 = {}^3H + {}^3He_{trit}$$

(Equation 4)

Where ^3H is the amount of measured Tritium (TU) in the sample, $^3He_{trit}$ is the Helium that resulted from the decay of Tritium (TU), and H_0 is the initial amount of Tritium at the time of recharge (TU). TU stands for Tritium unit where one TU of ^{3}He represents one ^{3}He atom per 10^{18} Hydrogen atom (Kazemi et al., 2006).

$$1\ {}^{cc_{STP}}/_{cc_{H_2O}} = 4.02 * 10^{14}\ \ TU \text{ (Kazemi et al., 2006)}$$

($1\ {}^{cc}H_2O$ = 1g of low salinity water)

Thus, by determining the initial amount of Tritium and if groundwater flow is described by piston flow and the transport parameters of both ^{3}He and ^{3}H is the same, the age of the sample can be calculated by the following formula (Schlosser et al., 1988 and Geyer, 2008):

$$^3H/\,^3He\ age = \frac{T_{1/2}}{ln2}\ ln\left(1 + \frac{^3He_{trit}}{^3H}\right)$$

(Equation 5)

Where $T_{1/2}$ is the half life time of ^{3}H, $^3He_{trit}$ is the tritiogenic Helium concentration in sample, and ^3H is the Tritium concentration in sample)

So, in order to assess the date of a groundwater sample, it is enough to know the amount of ^{3}H and the ^{3}He$_{trit}$ present in the sample. In order to determine ^{3}He$_{trit}$ in the sample, it is required to differentiate between the ^{3}He that decayed from ^{3}H and the atmospheric Helium and other sources of ^{3}He in groundwater. Helium (^{3}He) present in a water sample is originating from various sources as per (Geyer et al., 2007)

$$^3He_{sample} = \ ^3He_{eq} + \ ^3He_{excess} + \ ^3He_{trit} + \ ^3He_{rad} + \ ^3He_{prim}$$

(Equation 6)

Where $^3He_{eq}$ is the concentration of Helium at equilibrium with the atmosphere (TU), $^3He_{excess}$ is the component resulting from excess air (TU), $^3He_{trit}$ is the Helium coming from decay of Tritium ^{3}H (TU), $^3He_{rad}$ is the radiogenic component originating from decay of Uranium and Thorium (TU), and $^3He_{prim}$ is the mantle release of ^{3}He (TU).

The He_{sample} is determined by measurement. In this investigation, the mantle-derived sources of Helium are assumed to be insignificant as in many literatures (e.g. Kazemi et al., 2006; Sültenfuβ et al., 2011; Delbart et al., 2014). Therefore mantle sources (He_{prim}) of ^{3}He can be neglected.

The solubility equilibrium with the atmosphere in infiltrated water was estimated from values of Helium for specific altitudes, water temperature, and salinity that have been measured during sampling (Weiss, 1971). Lithium containing minerals are most common in granitic and other igneous rocks (Price et al., 2003) that could be a source for in situ Tritium and Helium-3 (nucleogenic Helium); (Kazemi et al., 2006) or in some literatures it is referred also as geogenic or radiogenic Helium-3 ($^{3}He_{rad}$); (Clark, 2015).

Moreover Neon (Ne) is a noble gas that its concentration in the sample is measured to compute Ne/He ratio and Delta-Ne (ΔNe); (Equation 7) as the dissolved Neon concentrations is used to correct for any excess air, since the atmosphere is considered the sole source of dissolved Neon (McCallum et al., 2015). Excess air is often defined as the volume of dry air (cm^3 at STP) injected per gram of water. Since Neon is a poorly soluble gas the excess air can be expressed as a relative Delta-Ne (ΔNe) using the following formula:

$$\Delta Ne = \frac{Ne_{exc}}{Ne_{eq}} * 100$$

(Equation 7)

Excess air could result from air bubbles trapped within the aquifer or introduced during sampling. Some of the excess air may be lost by diffusive re-equilibration across the water table. This process depends mainly on gas diffusion coefficients, temperature and matrix properties.

The latter is complemented by measuring ^{4}He concentration in the water sample and determining the ^{3}He/^{4}He ratio (McCallum et al., 2015). ^{4}He can be determined using the following equation (Stute and Schlosser, 2001):

$$^4He_{sample} = {}^4He_{eq} + {}^4He_{exc} + {}^4He_{rad}$$

(Equation 8)

$^4He_{sample}$ is measured in the groundwater sample, $^4He_{eq}$ is determined from the solubility equilibrium of Helium with the atmosphere. $^4He_{exc}$ is caused by excess air, $^4He_{rad}$ is considered negligible. However, in some cases radiogenic Helium-4 might be present due to interaction of groundwater and rocks in the order of 1000 years indicating the presence of very old groundwater component.

The equations 6 and 8 can be rearranged as follows:

$$^3He_{trit} = {}^3He_{sample} - {}^3He_{excess} - {}^3He_{eq} - {}^3He_{rad}$$

(Equation 9)

$$^4He_{rad} = {}^4He_{sample} - \left(Ne_{sample} - Ne_{eq}\right)(0.288) - {}^4He_{eq})$$

(Equation 10)

With

$$0.288 = \frac{^4He_{atm}}{Ne_{atm}} \quad (Atmospheric\ ratio)$$

$$Ne_{exc} = Ne_{sample} - Ne_{eq}$$

Ne_{sample} is the measured Neon in the sample, $^4He/Ne$ in the atmosphere is equal 0.288. Helium and Neon concentration in the sample at equilibrium are determined based on their solubility in water for specific temperatures and salinity. These concentrations can be calculated using the following equations (Clark, 2015).

$$He_{dissolved} = 4.07 * 10^{-12}\,T^2 - 2.58 * 10^{-10}\,T + 4.98 * 10^{-8}$$

(Equation 11)

$$Ne_{dissolved} = 2.50 * 10^{-11}\,T^2 - 2.31 * 10^{-9}\,T + 2.28 * 10^{-7}$$

(Equation 12)

Where, $He_{dissolved}$ and $Ne_{dissolved}$ are the concentration of Helium and Neon at equilibrium in $^{CC}STP/^{CC}H_2O$ and T is in ˚C.

By replacing each item into equation 9, Helium coming from Tritium decay He_{trit} can be calculated as follows:

If no radiogenic Helium is found in the sample, then $^3He_{trit}$ can be calculated as follows (Kazemi et al., 2006):

$$^3He_{trit} = {}^4He_{sample}\left(R_{sample} - R_{atm}\right) + {}^4He_{eq}R_{atm}(1-\alpha)$$

(Equation 13)

Where R_{sample}= ^{3}He/^{4}He measured in the sample, R_{atm}= measured ^{3}He/^{4}He ratio of air (1.384 E10^{-6}), α=solubility isotope effect (0.983). The Tritium can be converted from TU to cm^{3}STPg^{-1} (Kazemi et al., 2006).

However if radiogenic Helium is found in the sample $^{3}He_{trit}$ can be calculated as follows (USGS):

$$^{3}He_{trit} = {}^{4}He_{sample}(R_{sample} - R_{atm}) + {}^{4}He_{eq} * R_{atm}(1-\alpha) + {}^{4}He_{rad}(R_{atm} - R_{rad})$$

(Equation 14)

Where $^{4}He_{sample}$ is the concentration of ^{4}He in the sample, $^{4}He_{eq}$ is the concentration of ^{4}He in solubility equilibrium with the atmosphere, $^{4}He_{rad}$ is radiogenic ^{4}He in the sample, R_{atm} is the ratio of atmosphere ($^{3}He_{atm}/^{4}He_{atm}$ = 1.38 x 10^{-6}); R_{rad} is the radiogenic ratio ($^{3}He_{rad}/^{4}He_{rad}$ = 2 x 10^{-8}); (Clark, 2015), R_{sample} is the sample ratio, and α is the effect of fractionation of ^{3}He and ^{4}He during solution and it is about 0.983 (Kazemi et al., 2006).

5.1.2 *Chlorofluorocarbons (CFCs)*

The concentration of the anthropogenic Chlorofluorocarbons (CFCs) gas in the atmosphere provides information about groundwater residence times (up to 50 years) and mixing processes (Delbart et al., 2014). CFCs concentration in groundwater can be interpreted based on the assumption that the water during recharge was in equilibrium with the soil gas before it arrived in the saturated zone. Hence the atmospheric and groundwater concentrations of CFCs can define a groundwater residence time. However

certain parameters such as excess air, air pollution and local sources of CFCs must be well considered in using CFCs as a dating method (Delbart et al., 2014).

Groundwater age dating using CFCs is obtained by determining the CFC content that was present in water during recharge of groundwater system. This can be obtained by three steps procedure.

a. The CFC content is measured in the sampled water (Kazemi et al.,2006).
b. Estimate the recharge air temperature; this can be taken as the mean summer temperature (for areas with summer rainfall), mean winter temperature (for areas with winter rainfall), or mean annual air temperature (for areas where rainfall is over the entire year);(Kazemi et al., 2006). In this study mean winter temperature is considered (10°c).
c. Determining the solubility of CFC in water at the considered recharge air temperature.

After determining these three values we can calculate the equivalent atmospheric concentration (EAC) using the following formula (Kazemi et al., 2006):

$$EAC = \frac{CFC_{gw}}{S*MW}$$

(Equation15)

Where *EAC* is equivalent atmospheric concentration, CFC_{gw} is the concentration of CFC in the sampled water in pg/kg (picograms per 1 kg of water), *S* is the solubility (mol/kg/atm), and *MW* is the molar weight of CFCs (g/mol) (Kazemi et al., 2006).

The air-equilibrated water concentrations of CFCs (Solubility) depend on water temperature and salinity of water. For a low salinity the temperature-dependent values of Henry's constant can be calculated according to the following equations:

$$K_{CFC-11} = -6.22 * 10^{-7}T^3 + 6.15 * 10^{-5}T^2 - 2.27 * 10^{-3}T + 3.85 * 10^{-2}$$

(Equation 16)

$$K_{CFC-12} = -1.28 * 10^{-7}T^3 + 1.30 * 10^{-5}T^2 - 5.03 * 10^{-4}T + 9.37 * 10^{-3}$$

(Equation 17)

$$K_{CFC-13} = -2.28 * 10^{-7}T^3 + 2.21 * 10^{-5}T^2 - 7.95 * 10^{-4}T + 1.25 * 10^{-2}$$

(Equation 18)

Where, K_{CFC} is in mol/L/atm and T is in ˚C

Based on the calculated Henry's coefficient the atmospheric concentration of CFC during recharge can be calculated using the following equation (Clark, 2015):

$$K_{CFC} = \frac{m_{CFC}}{P_{CFC}}$$

(Equation 19)

Where K_{CFC} is the CFC Henry's Coefficient in mol/L/atm, m_{CFC} is the concentration of CFC in sample in mol/L or pptv, and P_{CFC} is the equivalent atmospheric concentration in mol/L or pptv.

The calculated equivalent atmospheric concentration is then compared to the graph of CFCs concentration in the atmosphere deriving the year of recharge of the sampled groundwater, as shown in Fig. 21.

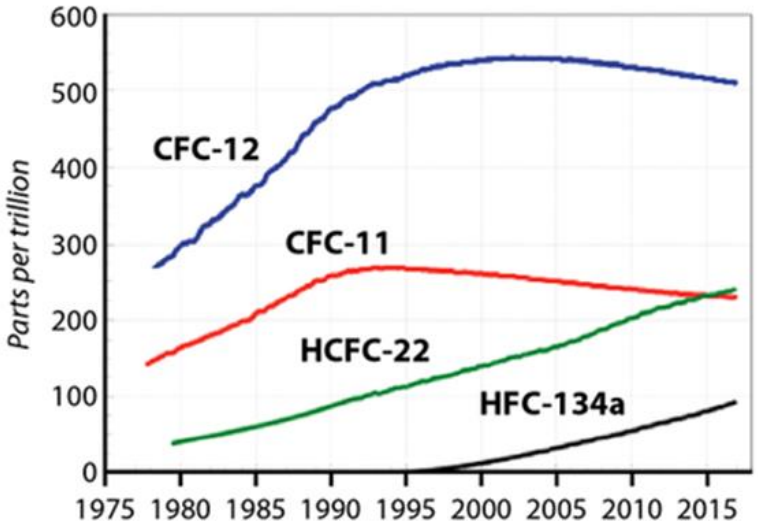

Fig. 21. Global average abundances of CFC-12, CFC-11, HCFC-22 and HFC-134a from the National Oceanic and Atmospheric Administration. Global air sampling network are plotted since the beginning of 1979 (NOAA).

Another method for dating is using ratios of several CFCs substances CCl_3F (CFC-11), CCl_2F_2 (CFC-12), $C_2Cl_3F_3$ (CFC-113), so the concentration of two CFC substances must be measured in the sample to determine their ratio, and then relate the ratio of the groundwater sample to the atmospheric ratio of these two substances at a specific year of recharge (Darling et al., 2012). Moreover ratios of Chlorofluorocarbons (CFCs) with Sulfur Hexafluoride can provide groundwater ages (Darling et al., 2012). However many issues limit the use of this method (Darling et al., 2012).

5.1.3 *Sulfur Hexafluoride (SF_6)*

Similar to CFCs, SF_6 is carried into the groundwater through rain and snow infiltration to the subsurface, the atmospheric SF_6 gas is dissolved in the rain and snow

where the amount of dissolution depends on atmospheric concentration of SF_6 and atmospheric temperature.

Hence, dating groundwater using SF_6 is based on the concentration of SF_6 in water samples, where concentration above background level indicates post 1970 groundwater and the higher the SF_6 content in the sample the younger its age (Delbart et al., 2014).

In some cases inclusion of excess air into groundwater during recharge can be a source of error in age calculation and also the presence of surface or subsurface source of natural or anthropogenic SF_6 can also lead to an error in age determination, but if the contribution of the excess SF_6 in the vadose zone is known then this problem can be resolved (Delbart et al., 2014).

Groundwater age determination using SF_6 requires several steps (Kazemi et al., 2006), in the first step SF_6 concentration in the sample is measured, and the recharge temperature must be known either by using mean annual air temperature, annual average groundwater temperature, or by measuring some noble gases (Neon; Ne, Nitrogen; N_2, and Argon; Ar) concentration in the sample and deriving from them the recharge temperature. Then excess air component in the sample must be measured using recharge temperature and then correcting for this excess air if required. Similar to CFCs, corrected SF_6 concentration is converted to equivalent to air concentration using calculated recharge temperature and computed solubility of SF_6 using the following formula (Kazemi et al., 2006):

$$EAC = \frac{SF_{6gw}}{S*MW}$$

(Equation 20)

Where *EAC* is equivalent atmospheric concentration of SF_6, SF_{6gw} is the concentration of SF_6, in the sampled water fg/kg (femtograms per 1 kg of water), *S* is the solubility (mol/kg/atm), and *MW* is the molar weight of SF_6, (g/mol) (Kazemi et al., 2006).

The air-equilibrated water concentrations of SF_6 (Solubility) depend on water temperature and salinity. For a low salinity the temperature-dependent values of Henry's constant can be calculated according to the following equation:

$$K_{SF_6} = -1.95 * 10^{-9}T^3 + 2.60 * 10^{-7}\,T^2 - 1.57 * 10^{-5}\,T + 5.01 * 10^{-4}$$

(Equation 21)

Where, K_{SF_6} is in mol/L/atm and *T* is in ˚C

Based on the calculated Henry's coefficient the atmospheric concentration of SF_6 during recharge can be calculated using the following equation (Clark, 2015):

$$K_{SF_6} = \frac{m_{SF_6}}{P_{SF_6}}$$

(Equation 22)

Where, K_{SF_6} is the SF_6 Henry's Coefficient in mol/L/atm, m_{SF_6} is the concentration of SF_6 in sample in mol/L or pptv, and P_{SF_6} is the equivalent atmospheric concentration in mol/L or pptv.

Based on the computed SF_6 atmospheric concentration the equivalent year of recharge will be then deduced.

5.2 Stable isotopes: Deuterium (^{2}H) and Oxygen-18 (^{18}O)

Oxygen-18 and Deuterium isotopic ratios have been defined by the international Atomic Energy Agency IAEA in Vienna and are expressed as the standard mean ocean water (V-SMOW) having the following values (Leibundgut et al., 2009):

$$R_{^{18}O/^{16}O} = \left(\frac{^{18}O}{^{16}O}\right)_{VSMOW} = 2005.2 \pm 0.45 * 10^{-6}$$

$$R_{D/H} = \left(\frac{^{2}H}{^{1}H}\right)_{VSMOW} = 155.76 \pm 0.05 * 10^{-6}$$

Sample measurements are denoted as (δ):

$$\delta = \frac{R_{sample} - R_{standard}}{R_{standard}} * 1000$$

(Equation 23)

The values of δ^{18}O and δ^{2}H are not constant throughout the hydrological cycle due to the fractionation of isotopes due to phase changes, evaporation condensation, freezing, melting, and some chemical reactions.

The ocean has δ^{18}O value is close to 0‰ (Leibundgut et al.,2009), Positive values indicate enrichment of heavy Oxygen and Deuterium whereas negative values

indicate depletion of ^{18}O and ^{2}H compared to the standard values. The $\delta^{18}O$ value in water varies from -50‰ and -25 ‰ in ice samples from cold arctic areas to +10‰ in drying water bodies and lakes in arid areas (Leibundgut et al., 2009).

During evaporation process for instance water pressures of the heavier species $^{1}H_2{}^{16}O$ and $^{1}H_2{}^{18}O$ differ by ~ 1% at 20˚C for that reason higher diffusion of $^{1}H_2{}^{16}O$ into the ambient air occurs at a higher rate than $^{1}H_2{}^{18}O$. Similar the case for the heavier species $^{1}H_2{}^{16}O$ and $^{2}H_2{}^{16}O$ that are also affected by fractionation during evaporation. Hence, heavy isotopes of Oxygen and Deuterium tend to be depleted in the gaseous phase (Leibundgut et al.,2009).

A linear correlation of ^{2}H to ^{18}O contents is observed in rainfall by Craig (1961) at a global scale and the following equation has been developed:

$$\delta\ ^{2}H = 8\delta^{18}O + 10‰$$

This equation defines the "Global Meteoric Water Line" (GMWL), where precipitation data are collected from sites around the globe, with an R^2 value of better than 0.95 (USGS). This relation was developed as an average of many local water lines that differ from the GMWL as a result of climatic and geographic factors. Hence at some regional scale precipitation collected from a single site or set of local sites such as the Mediterranean and other coastal areas may reveal a deviation from the GMWL, with a different slope and intercept and this is called "Local Meteoric Water Line" (LMWL); (Königer and Margane, 2014).

5.3 Event Analysis: Simple Mixing Model

Following a precipitation event, the analysis of the spring response (hydrograph and chemograph) helps assess the flow dynamics in the system and estimate the amount of fast recharge into the system. The fast recharge component is a proportion of recharge that bypasses the fissured matrix and flows though fast flow pathways such as conduits. This component yield information about the degree of karstification of an aquifer system, and consequently reflects the distribution of transit times in the aquifer. The volume of water discharged from a spring increases drastically during spring response, it consists of a mixture of new and old water components as karst systems are characterized by a duality infiltration and flow (Doummar et al., 2014).

In order to determine the percentage of new and old stored water, several previous event time series were analyzed based on the electric conductivity that was measured at the spring. At each time series after a rainfall event the beginning of the Jeita spring response was denoted as (t_0) at this time electric conductivity increases along with discharge, the increase in EC is due to the flushing out of conduit old water after a rainfall event. After EC reaching its maximum value (t_1) it starts to decrease gradually indicating new water coming directly from precipitated water (new water has lower EC than stored old water as it has lower ionic activity as they had shorter period of time to react with rocks) reaching a minimum value (t_2), following (t_2) the EC gradually increases returning back to its background level and stabilizing at (t_3) the EC increase is due here to the discharge of phreatic stored water. At each time interval the total volume of discharged water is calculated by:

$$V = Qt$$

(Equation 24)

Where *V* is volume in [L^3], *Q* is discharge in [L^3/T], and *t* is time [T].

By this equation, the different percentages of stored conduit water, new conduit water, and phreatic conduit water can be calculated.

The results of the event were analyzed to determine the portion of fast infiltrated water arriving to the spring through fast flow pathways.

A binary mixing model was used to identify the percentage of the newly fast infiltrated waters as follows:

$$\int C_n Q_n dt + \int C_b Q_b dt = \int C_a Q_a dt$$

(Equation 25)

Where *Qn, Qa,* and *Qb* are discharge from new waters, actual discharge, and discharge from background waters respectively, while *Cn*, *Ca*, and *Cb* are the concentration in the rain, concentration of the spring, and concentration of pre-event water respectively.

5.4 Correlations between Variables

Correlation provides the extent to which two quantitative variables follow similar trend; a positive correlation exists when the two variables have the same trend and a negative one is when the two variables have opposite trend. Many variables do not show any relation towards each other where no correlation might exist. The degree of correlation between the various variables was assessed using the coefficient of correlation R^2 (Equation 26). This statistic quantifies the degree of the variance of one

variable in relation to the other one. It range from zero to 1 the closer to one the stronger the relation between the two tested variables.

$$R^2 = 1 - \frac{\sum(c_i - c)^2}{\sum(c_i - \frac{1}{n}(\sum c_i))^2}$$

(Equation 26)

Where, *n* is the total number of observation data, c_i is the observed value, and *c* is the modelled value.

CHAPTER 6

RESULTS

6.1 Event analysis

6.1.1 *Time Series*

Twenty six (26) spring responses following precipitation events were analyzed using the method detailed in section 5.3 (Fig. 22). The percentage of newly infiltrated waters was calculated from the hydrograph by integrating the discharge over time during the time interval where dilution is observed. Fast infiltrated waters range between 6% and 73%. The amount of newly infiltrated waters characterized by fast transit times is highly dependent on the antecedent saturation in fast point source shafts and conduits (e.g., sinkhole), the location of the point source infiltration, precipitation intensity, ambient temperature and snow cover on the catchment.

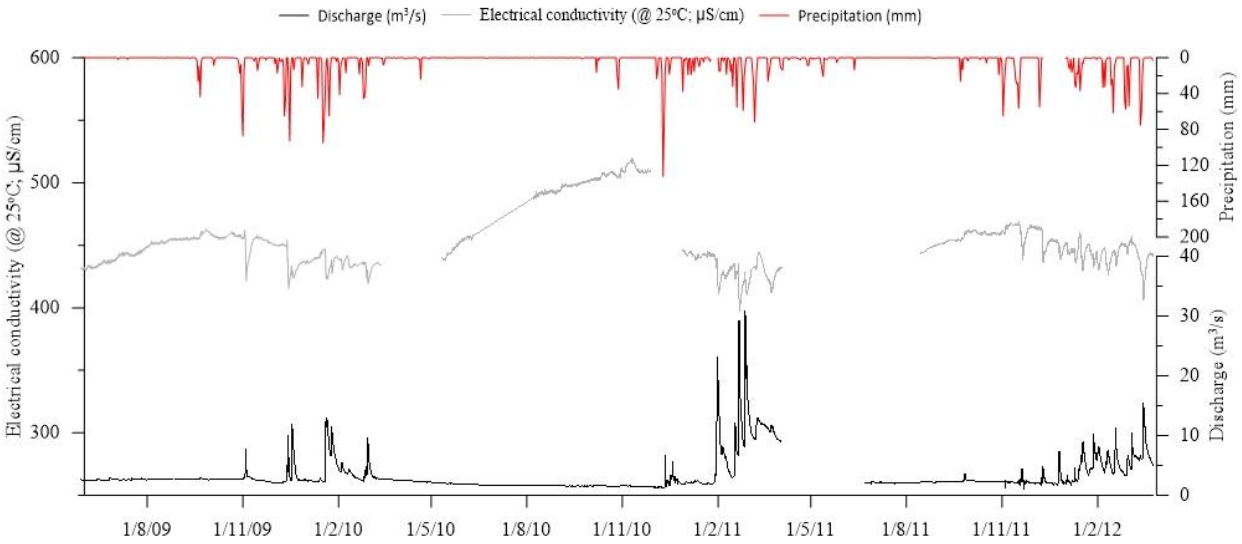

Fig. 22. Precipitation event time series for Jeita spring using discharge and electric conductivity (modified from Doummar, 2012).

A direct positive correlation is observed between the proportions of newly infiltrated waters (Vn) and the total volume observed at the spring during events (Vt). Similarly a positive correlation is established between the total volume (Vt) and the volume of phreatic waters reaching the spring (Vb); (Fig. 23)

The percentage of newly infiltrated waters are correlated with the amount of phreatic waters with a linear relationship (Vn = -0.7212Vb + 75.578), as it decreases with increasing phreatic inflow (Fig. 24).

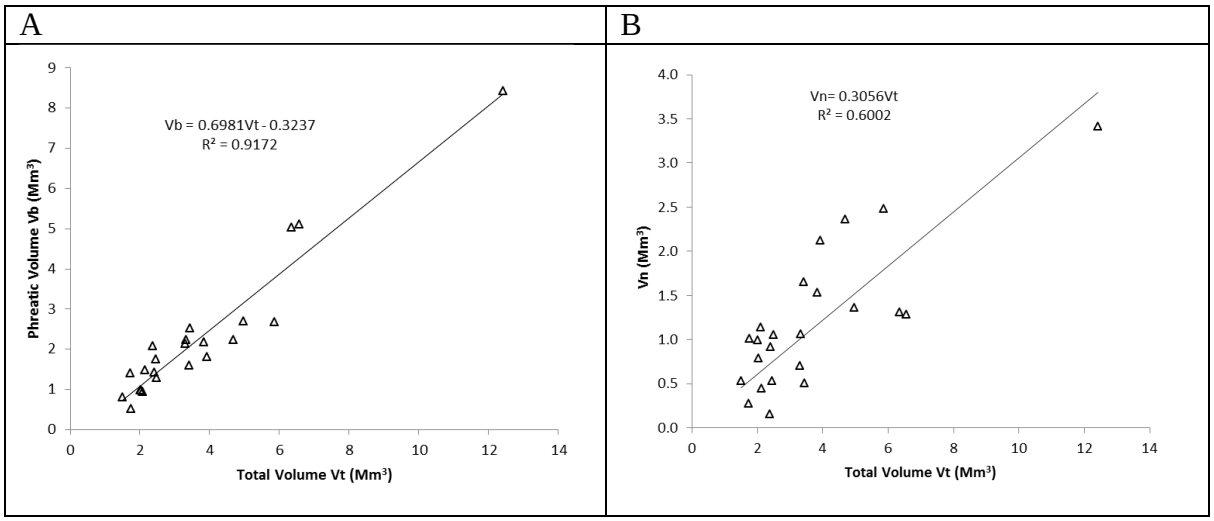

Fig. 23. (A) Correlation between the total volume of water observed at the spring during precipitation events (Vt) and the volume of phreatic waters from baseflow (Vb). (B) Correlation between the total volume of water observed at the spring during precipitation events (Vt) and the proportions of newly infiltrated waters (Vn).

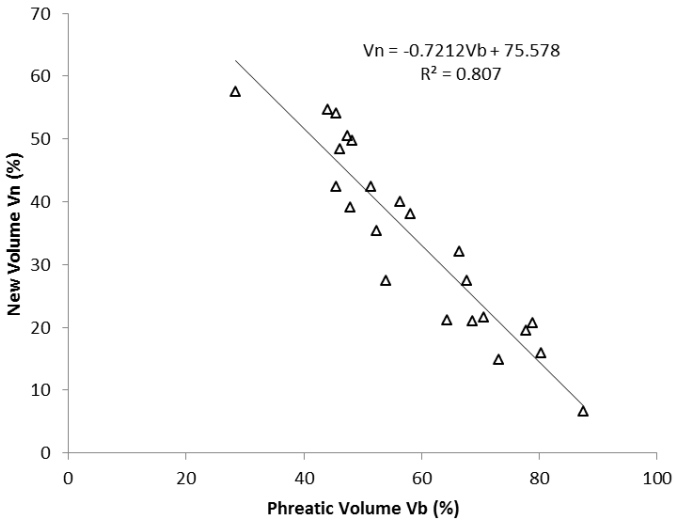

Fig. 24. Relationship between new volumes (Vn) from fast infiltrated waters and Phreatic Volume of the base flow (Vb).

The diameter of the phreatic main conduit was calculated based on the total volume of old waters reaching the spring directly after the start of the spring response. The length of the conduit was estimated to be the total length of the cave i.e., 5300 m.

$$d = \sqrt{\frac{4Vc}{\pi L}}$$

(Equation 27)

Where *d* is the diameter (m), *Vc* is the total volume expulsed from the conduit at the beginning of event (m^3), and *L* is the length of the cave (m). The diameter of the phreatic conduit ranges between 2.0 and 15 m. The phreatic volume is assumed to travel in the aquifer at a relatively higher transit time with respect to fast infiltrated waters. Thus, their percentage is reflective of slow transit time in the aquifer and storage.

6.1.2 *Single Event Analysis*

The discharge during the event varied between 7.0-18 m^3/s. The response to the event lasted for about 7 days. The measurements obtained from the analysis of the samples collected following a precipitation event were plotted as a function of time in the hydrograph and chemogaphs shown in Fig. 25.

The calculation of newly infiltrated fast waters was performed using a binary mixing model with Deuterium, heavy Oxygen and calcium. The total volume of water arriving to the spring during the event was estimated at about 7.45 Mm^3. The percentage of fast flood waters to total discharge volume before the arrival of phreatic stored waters ranged between 11.9% using heavy Oxygen and 12.5% using Deuterium, equivalent to about 0.89 and 0.94 Mm^3 respectively. Calculations using calcium yielded

17.4%, which is overestimated due to the calcium originating from the stored matrix too.

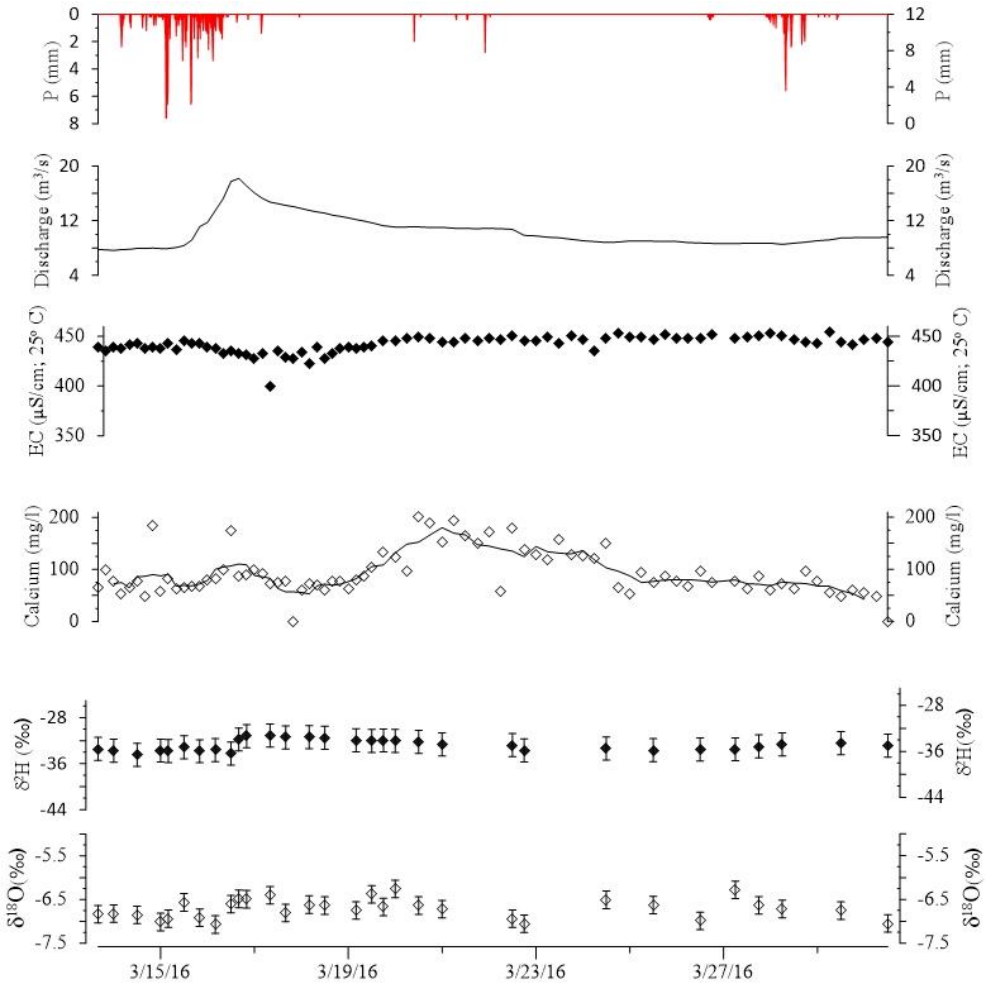

Fig. 25. Precipitation event analysis in the Jeita spring using discharge, Electric conductivity, Calcium, δ^2H, and $\delta\ ^{18}O$.

6.2 Hydrochemistry

6.2.1 *Major Ions*

The chemical analyses of water samples taken from the eleven sites are summarized in Table 3. The sites are of different elevations ranging between 64 m (the

lowest) and 1237 m above sea level (the highest). Three parameters were measured during sampling: temperature, electric conductivity (EC), and pH. The temperature showed a linear correlation with elevation in most sites, i.e. wells found at higher elevation were characterized by lower temperatures, which indicates that the variation of temperature with depth cannot be defined from the temperature data. The electric conductivity varied between 371.0 and 1666 μS/cm as to reflect the chemical composition of the sampled water; the higher the electric conductivity, the higher the ionic activity of the major ions in the sample. However, most of the values fall within the freshwater standards except for Aintoura (AN) well. The pH did not vary significantly between the different samples as it ranged between 7.09 and 7.82 indicating neutral to slightly basic type of water.

The cation and anion concentrations showed a great variation among the samples. Calcium, sodium, potassium, chloride, and sulfate were among the highest reported concentrations in Aintoura (AN) site reflecting the relatively pronounced salinity of the water well, possibly due to sea water intrusion. Moreover, the ionic concentration of the Harissa (HR) well reflects a higher salinity.

Plotting the ionic concentrations of the sampled wells in a piper-plot (Fig. 26) provides a percentage distribution of the cations and anions within each sample. The cations and anions are plotted together in a diamond shaped piper diagram and separately in single ternary diagram.

Table 3. Major cations and anions composition of the sampled wells.

						Cations (mg/l)				Anions (mg/l)							
Site	**Date**	**Elevation (m)**	**EC (µS/cm)**	**T (˚C)**	**pH**	**Ca^{2+}**	**Mg^{2+}**	**Na^{+}**	**K^{+}**	**HCO_3^-**	**CO_3^{2-}**	**Cl^-**	**SO_4^{2-}**	**F**	**NO_3^-**	**SI***	**Ionic Balance**
AD	25/10/2014	1083	380	12.5	7.82	53.90	12.70	4.50	0.50	220	0.72	6.50	7.00	0.00	5.70	2.22	-0.53
AN	25/10/2014	79	1666	19.6	7.24	103.10	23.90	77.70	2.30	317	0.27	144	37.00	0.00	9.10	1.21	3.78
AR	26/10/2014	280	506	16	7.70	71.30	15.40	10.10	0.70	268	0.65	12.50	9.00	0.00	8.50	2.48	2.49
HL	25/10/2014	1237	414	11.4	7.75	66.50	9.00	7.00	0.70	220	0.61	8.00	8.00	0.00	6.30	2.27	6.28
HR	26/10/2014	499	786	18.7	7.25	92.50	34.20	14.90	0.80	384	0.34	23.50	12.00	0.00	22.30	1.43	3.20
JC	26/10/2014	90	483	15.3	7.52	72.30	13.30	10.50	0.70	244	0.40	10.00	19.00	0.00	9.70	1.55	5.13
OJ	25/10/2014	1082	371	13.1	7.76	48.90	13.70	6.10	0.50	201	0.57	7.50	5.00	0.00	10.10	1.63	0.70
QQ	7/5/2016	64	599	19.2	7.69	81.3	18.9	10.4	0.9	323	0.78	18	32	0.00	7.7	3.18	-1.32
KZ	10/5/2016	1127	449	14.5	7.09	74.60	4.40	8.00	1.40	268.00	0.16	10.00	9.00	0.00	8.10	0.66	-5.06
JN	7/5/2016	95	550	14.8	7.60	76.00	12.80	8.80	0.90	298.00	0.63	16.00	10.00	0.00	7.20	2.50	-8.69
CL	4/4/2016	1005	509	16.1	7.60	65.30	25.20	6.30	0.30	299.00	0.59	11.50	8.00	0.00	4.80	1.99	1.87

*SI: Solubility index $\mathrm{SI} = \frac{\log IAP}{K_{eq}}$

Where IAP is the actual ion activity product with respect to the equilibrium constant at the same temperature and Keq is the K solubility constant at the measured temperature of $CaCO_3$

if SI= 1→ solution is at equilibrium

SI> 1→ IAP of solution is greater than the equilibrium constant→ supersaturated solution

SI< 1→ IAP is less that Keq→ under saturated solution

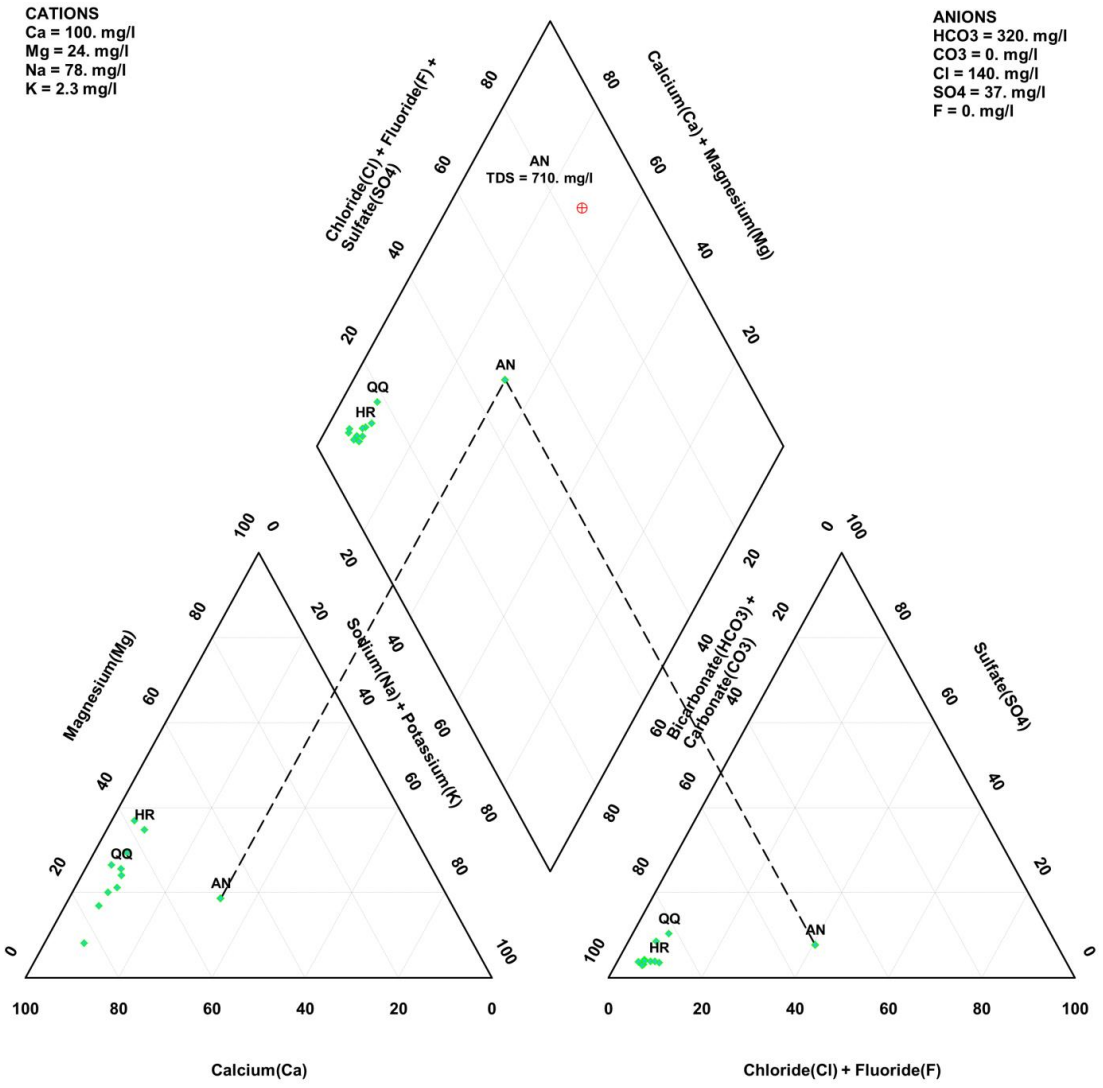

Fig. 26. Piper-plot showing the percentage distribution of the cations and anions in each collected groundwater sample.

6.2.2 *Water Types*

According to the Piper diagram (Fig. 26), the sampled wells can be classified as Ca-HCO_3 type waters. The samples cluster approximately around the same ionic distribution; for anions, 10-15% (Cl-F-SO_4) and 85-90% carbonate + bicarbonate (HCO_3-CO_3), and for cations 5-10% sodium + potassium (Na-K) and 90-95% calcium + magnesium (Ca-Mg). Aintoura (AN) well is characterized by higher percentages of

sodium + potassium (up to 30%) and higher chloride + fluoride + sulfate (up to 50%), indicating a contamination by saline intrusion. The anion piper diagram shows also clustering at the carbonate + bicarbonate higher end with the least chloride + fluoride percentages. The cation piper diagram shows no clusters; on the contrary, it reveals some variation in calcium to magnesium concentrations with approximately invariant K-Na concentrations. The Harissa (HR) well shows higher magnesium to calcium percentages; but it also displays a slightly higher chloride + fluoride and sodium + potassium percentages with respect to other wells related to the aforementioned salt water intrusion to this well. It is worth noting that the Harissa (HR) well is tapping a Formation of the Upper Jurassic adjacent to the main Formation of the Jeita Catchment and Aintoura (AN) well is tapping the lower Cretaceous (Chouf sandstone Formation). These wells were sampled for comparison purposes.

The Chahtoul (CL) and Outa el Joz (OJ) wells show higher magnesium to calcium percentages with normal chloride + fluoride and sulfate percentages. This higher magnesium content is mainly due to the dissolution of dolomites as these wells are tapping the aquifer mainly made up of dolomitic limestone as it is located close to a major fault where basaltic intrusions have occurred and hydrothermal dolomitization has taken place along fissures (refer to section 3.3.1) leaving behind dolostones and dolomitized bedrocks.

The Quachqouch (QQ) well has a slightly different chemistry than other wells; it is slightly richer in magnesium, owing to the chemical composition of the Jurassic rock Formation. The relatively higher chloride/ sulfate concentrations might indicate that other sources of surface or groundwater water contribute to the Quachqouch (QQ) well. The higher magnesium content in the Quachqouch (QQ) well suggest that this

well is tapping a lower aquifer that is greatly made up of dolomtized limestone of the Jurassic lower member that underlies the major aquifer where the Jeita spring is originating.

The ionic activity of the ions was calculated given the measured pH at the real measured temperature. The product of ionic activities of both calcium and carbonates was calculated and contrasted with the equilibrium constant (K_{eq}) of calcite at the measured temperature of each sample to calculate the solubility index and the saturation of the solutions with respect to calcite. The latter indicate that all water samples are supersaturated solutions with one exception, the Kfar Zebian (KZ) sample, which consists of an undersaturated solution. The samples being supersaturated is normal in a carbonate aquifer especially that the water coming from precipitation and infiltration is highly corrosive or aggressive (highly undersaturated with respect to calcite and enriched with carbon dioxide) passing through the vadose zone for a period of time and reaching the water table and being stored in the bedrock matrix will enhance dissolution of the adjacent carbonetic rocks making the groundwater supersaturated with calcium (SI>1), hence precipitation of calcite can take place such as stalactites and stalagmites seen in the Jeita cave (Verheyden et al., 2008). Concerning the Kfar zebian (KZ) undersaturation with calcium this is mainly due to sampling problems and difficulties in bailing the sampled well, and it is assumed that the sampled groundwater had some proportions of stagnant water coming from precipitation or flooded stagnant waters.

6.2.3 *Oxygen-18 ($\delta^{18}O$) and Deuterium ($\delta^{2}H$) Isotopes*

Based on a previous study (Königer and Margane, 2014), the local meteoric isotopic line (Oxygen and Deuterium) was estimated based on samples collected from

rain over the Jeita catchment at varying altitudes. This Meteoric line, along with the East Mediterranean meteoric lines will be used to assess the isotopic signatures of the sampled wells.

In this current study, the analyzed water samples revealed isotopic ratios that ranged between -6.34‰ to -7.65‰ for $\delta^{18}O$ while $\delta^{2}H$ ratio varied between -33.93‰ to -41.00‰ as shown in Table 4, reflecting depleted heavy isotopic signature.

Table 4. Mean stable isotope ($\delta^{18}O$ and $\delta^{2}H$) values of groundwater samples.

Well/Spring	**Symbol**	**Altitude**	**Well Depth (BG)**	**Water Level**	**Temperature**	**$\delta^{18}O$ vs V-SMOW**	**$\delta^{2}H$ vs V-SMOW**
		(m)	**(m)**	**(m)**	**(˚C)**	**(‰)**	**(‰)**
Ain delbeh	**(AD)**	1083	-	783	13.6	-7.65	-39.62
Ouata el Joz	**(OJ)**	1082	650	482	16.9	-7.62	-38.53
Hrajel	**(HL)**	1237	-	-	14.3	-7.34	-41
Ain errihane	**(AR)**	383	450	288	18.7	-6.5	-35.99
Jeita new cave	**(JN)**	95	-	-	19	-6.53	-35.35
Kfar zebian	**(KZ)**	1127	-	-	14.5	-7.39	-39.45
Quachqouch	**(QQ)**	60	240	-160	19.2	-6.34	-36.4
Chahtoul	**(CL)**	1005	375	-	16.1	-7.08	-33.93

6.2.3.1 Comparison with Local Meteoric lines

The groundwater isotopic results were compared to the East Mediterranean Meteoric Water Line (EMWL) and Local Meteoric Water Line (LMWL) obtained from Jeita local precipitation (Aouad-Rizk et al., 2005 and Königer and Margane, 2014). The relation between $\delta\ ^{18}O$ and $\delta\ ^{2}H$ in samples is characterized by a linear correlation with a slope of 3.14 and a coefficient of correlation R^2 of 0.45 (Fig. 27). This line deviates from both the East Mediterranean Meteoric Water Line (EMWL) and the Local Meteoric water Line (LMWL) as shown in Fig. 27. The obtained correlation line plots below the Eastern Mediterranean meteoric water line along a line that intersects the EMWL at the location of the original un-evaporated composition of the water (Al-Ameri et al., 2014).

Chahtoul (CL), Ouata el Joz (OJ), and Ain delbeh (AD) samples plot along the east Mediterranean line (EMWL) whereas the samples of Kfar zebian (KZ), Hrajel (HL), Jeita new cave (JN), Ain errihane (AN), and Quachqouch (QQ) samples deviate from it. None of the samples plots along the Local Meteoric Water Line (LMWL) as shown in Fig. 27. However the extension of LMWL may lead to the plot of Ouata el Joz (OJ) and Ain delbeh (AD) samples on this line. These samples show high depletion of $\delta\ ^{18}O$ and $\delta\ ^{2}H$ ratios. This isotopic depletion is due to the presence of water coming from higher altitudes, indicating infiltration of isotopic depleted snow melt into the Jeita groundwater system (Königer and Margane, 2014).

The samples of Jeita new cave (JN), Ain errihane (AN), and Quachqouch (QQ) deviate from both water lines, EMWL and LMWL and they show enrichment of ^{18}O with respect to ^{2}H. This could be attributed to older groundwater occurrence. This deviation is caused by natural processes for instance water that has evaporated in the

unsaturated zone before recharge or has mixed with old evaporated water (Al-Ameri et al., 2014). This may lead to isotopic ratios different than the East Mediterranean meteoric line and Local Meteoric water Line (LMWL; Fig. 27).

In addition, the degree of mixing of new precipitated water and snow melt and fractionated old stored water tend to produce a new isotopic ratio that differs from the Jeita meteoric signature (Fig. 27).

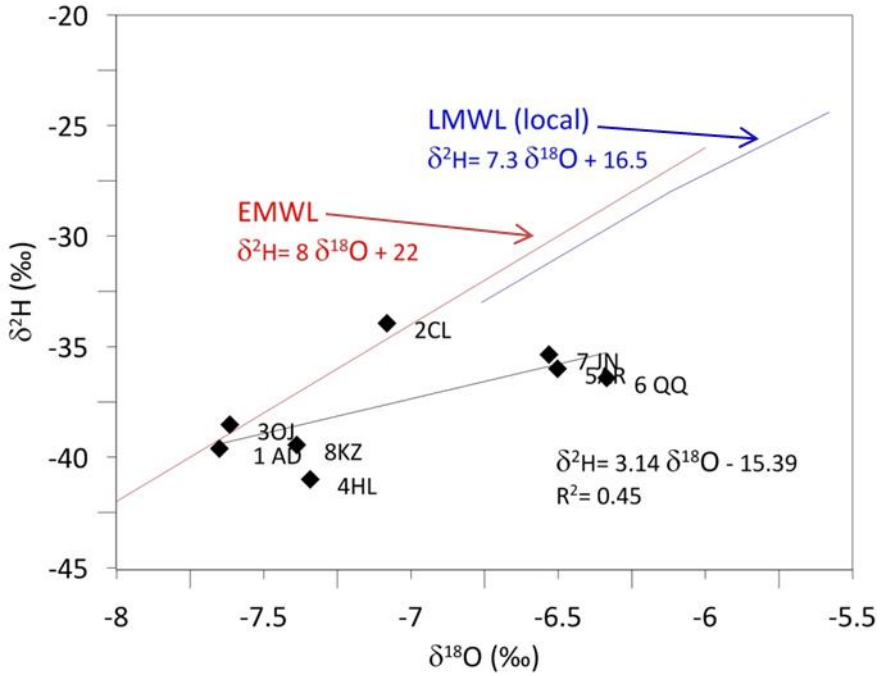

Fig. 27. ($\delta^{18}O$) plotted against ($\delta^{2}H$) for the groundwater samples along with Local Meteoric Water Line (LMWL); (Königer and Margane, 2014) and East Mediterranean Meteoric water Line (EMWL); (Dotsika et al., 2010).

The temperature of the sampled water is plotted against the altitude of the well head (Fig. 28). It shows that the latter relationship is linear implying that water temperature decreases by 0.56 degrees for an increase in elevation of 100 m. Any

deviation from this line towards higher temperature indicates a deeper circulation of water and a limited snow melt component.

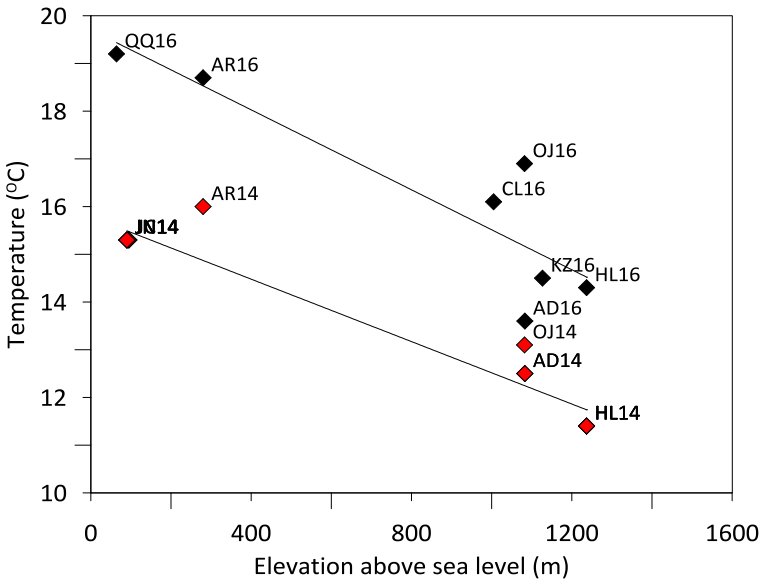

Fig. 28. Correlation between the sample temperature against altitude of well head. The suffixes (14) and (16) refer to the year of sampling.

6.2.3.2 Altitude and Temperature Effect

The isotopic ratio in the study area is clearly affected by the altitude effect as Hrajel (HL), Ain delbeh (AD), and Ouata el Joz (OJ) wells that are located at higher elevations show a higher depletion of $\delta\ ^{2}H$ and $\delta\ ^{18}O$ ratios than Ain errihanne (AR), Jeita new cave (JN), and Kfar zebian (KZ) located at lower altitudes as shown in Fig. 29 A and Fig. 29 B. The altitude adopted is the altitude of the well head, especially where information about well depth is missing. Chahtoul (CL) well appears to deviate from this general trend; and this might be the result of an artefact or of relatively less influence from snowmelt recharge.

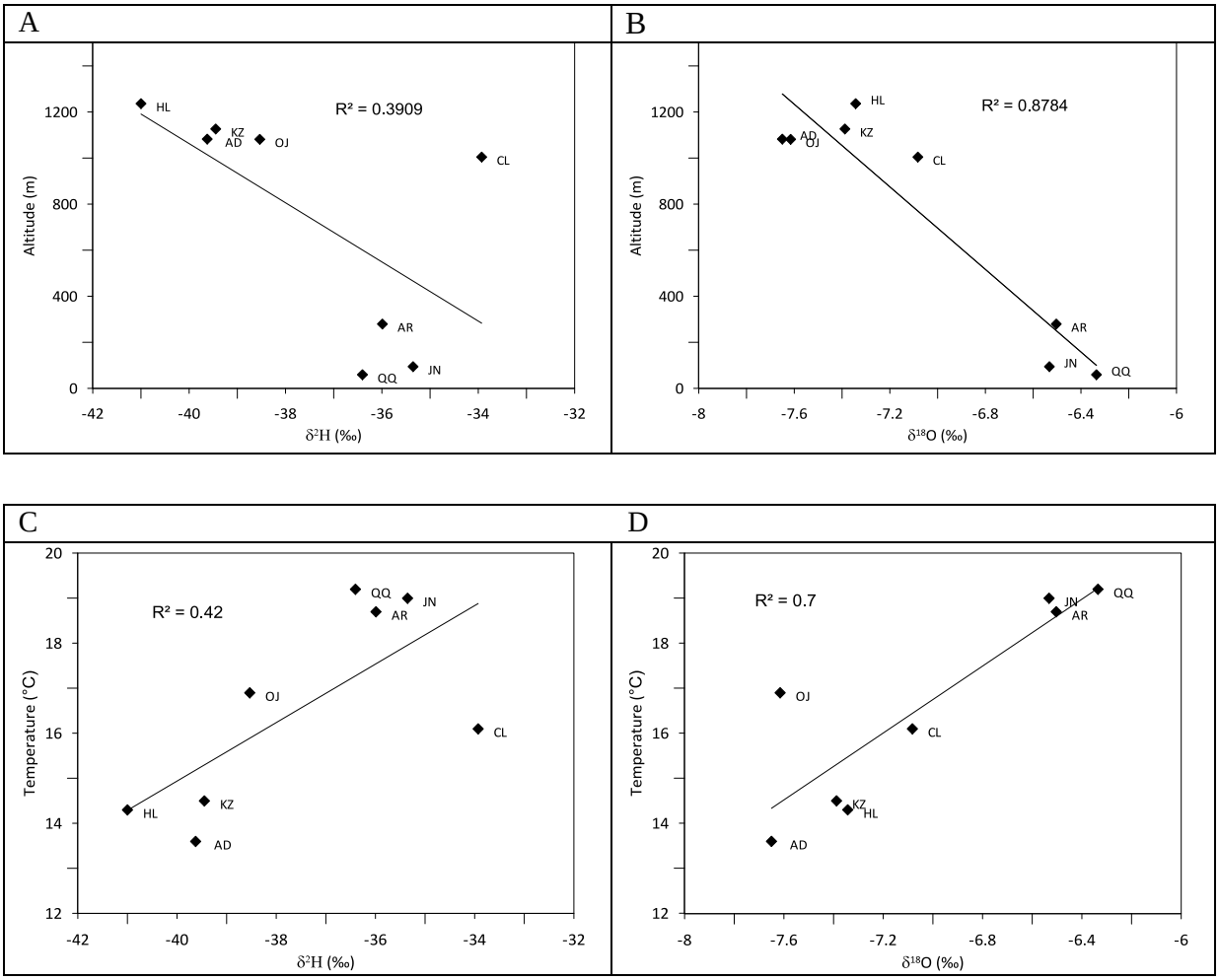

Fig. 29. Correlations between (A) δ^2H and altitude, (B) $\delta^{18}O$ and altitude, (C) δ^2H and Temperature, and (D) $\delta^{18}O$ and Temperature.

Similarly the temperature effect has a great influence on the isotopic ratio, colder water tends to be more depleted in heavier isotopes than warmer ones as shown Fig. 29 C and Fig. 29 D, with one exception the Ouata el Joz well (OJ) sample that showed a high depletion of $\delta\ ^{18}O$ although it is characterized by a higher temperature with respect to the other water samples. This might be due to the limited contribution of snowmelt water into this well or deeper groundwater circulation in this well.

6.3 Environmental Tracers

6.3.1 *Tritium-Helium (^{3}H-^{3}He)*

This section presents the results of both sampling campaigns undertaken in 2014 and 2016. The residual Tritium in the groundwater samples varied between 2.26 and 2.97 TU. The Tritium measured in precipitation water in 2016 at 600 and 900 meters above sea level revealed to vary between 1.5 and 2.0 TU. Most of the Helium in the sample is found under the form of Helium-4 and ranges between 4.34 $E10^{-5}$ 4.34 $E10^{-5}$ and 1.08$E10^{-4}$ccSTP/kg.

Neon measured in the samples ranges between 1.85E 10^{-4} and 4.20$E10^{-44}$ccSTP/kg. Excess air was calculated based on the ratio of Neon concentration in air. Excess air is present in all groundwater with respect to air in equilibrium as denoted by high percentages of ΔNe, and it ranges variably between 10 % and 154%. Some samples portrayed relatively significant excess air exceeding 90% and reaching 140%, such as samples of Ain delbeh (AD), Ouata el Joz (OJ), and Harissa (HR) in the first sampling campaign (Fig. 30), Ain delbeh (AD), Hrajel (HL), Ain errihane (AR), and Ouata el Joz (OJ) in the second campaign (Fig. 30), while samples likes Jeita New Cave (JN) and Chahtoul (CL) displayed much lower ranges of 30 %.

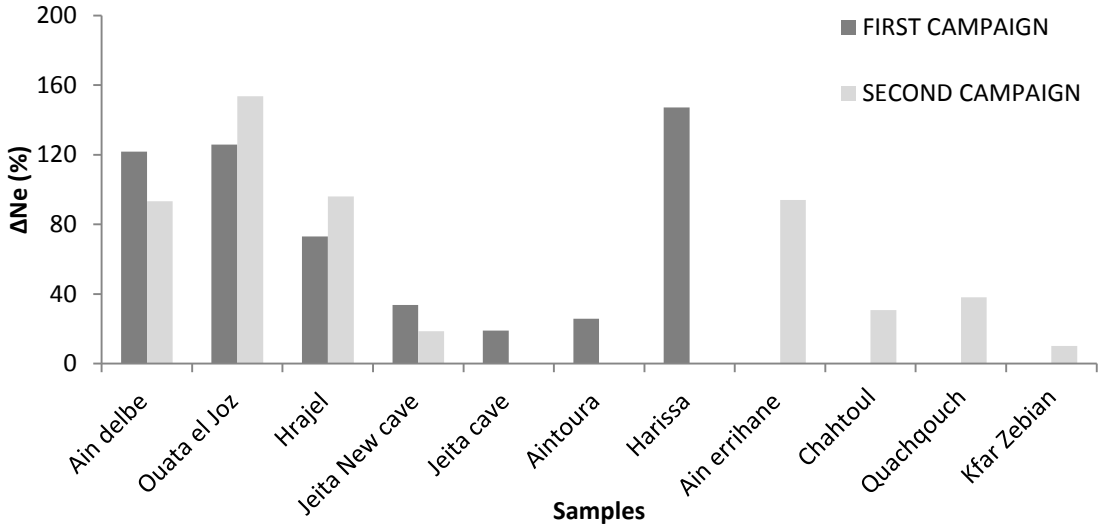

Fig. 30. Percentages of excess air (ΔNe) for the groundwater samples of the first campaign and second campaign.

The measured concentrations of Helium-3, Helium-4, and Neon concentrations were used to calculate the tritiogenic and radiogenic Helium if present in the groundwater samples (refer to Section 5.2.1). The total concentration of Tritium is the sum of tritiogenic Helium and Tritium measured in the sample. The stable Tritium levels (^3H sample and $^3He_{trit}$) in the collected water samples from both campaigns range between 2.56 and 10.2 TU (Fig. 31 and Fig. 32). These numbers fit with certain uncertainty to the modern Tritium concentration in precipitation for the northern hemisphere through the last 30 years (refer to chapter 5). Based on Equation 5 in Section 5.1.1, the average recharge year was calculated. Each sample yielded a different average groundwater age ranging between 1.0 and 23 years as shown in Table 5. Some samples showed some radiogenic Helium indicative of a proportion (~10%) of groundwater older than 50 years. These samples are Jeita new cave (JN), Aintoura (AN), Ain errihane (AR), and Quachqouch (QQ). It is worth noting that the

concentration of gas such as Neon and Helium in the atmosphere and the equilibrium constant were considered at STP conditions, i.e., Pressure of 1 atm and temperature of 0 °C. The recharge temperature was considered to be 10 °C as a mean annual temperature for the recharge area to standardize the results (other authors have adopted the same assumptions, such as Price et al., 2003 and Delbart et.al. 2014). The highest average age is characteristic of samples located in the upstream parts of the catchment such as Ouata el Joz and Ain delbeh, while younger ages are attributed to samples closer to the coast (Fig. 33).

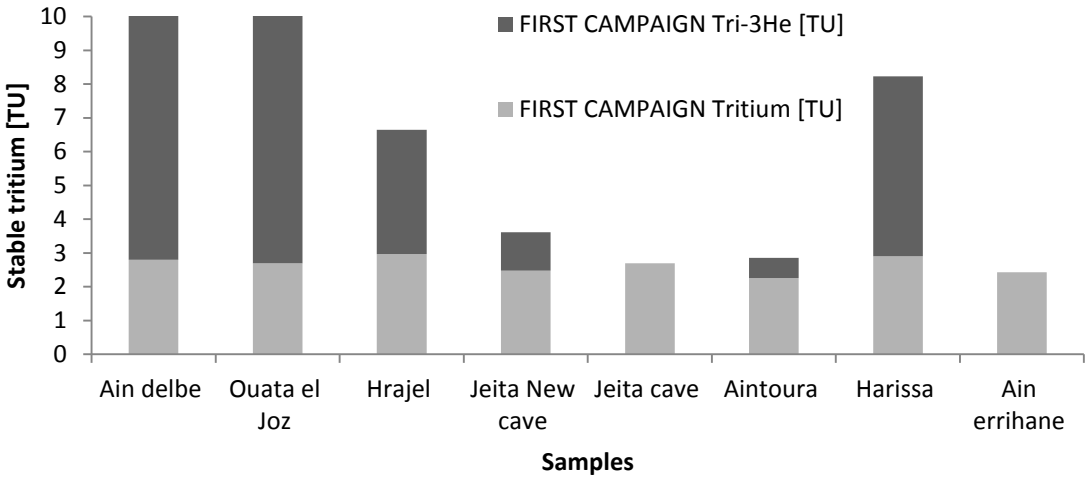

Fig. 31. Tritium and tritiogenic Helium concentration in collected water samples of the First campaign. Stable Tritium is the sum of Tritium and tritiogenic Helium. Note that the absence of He_{trit} in Ain Errihane is due to unsuccessful sampling.

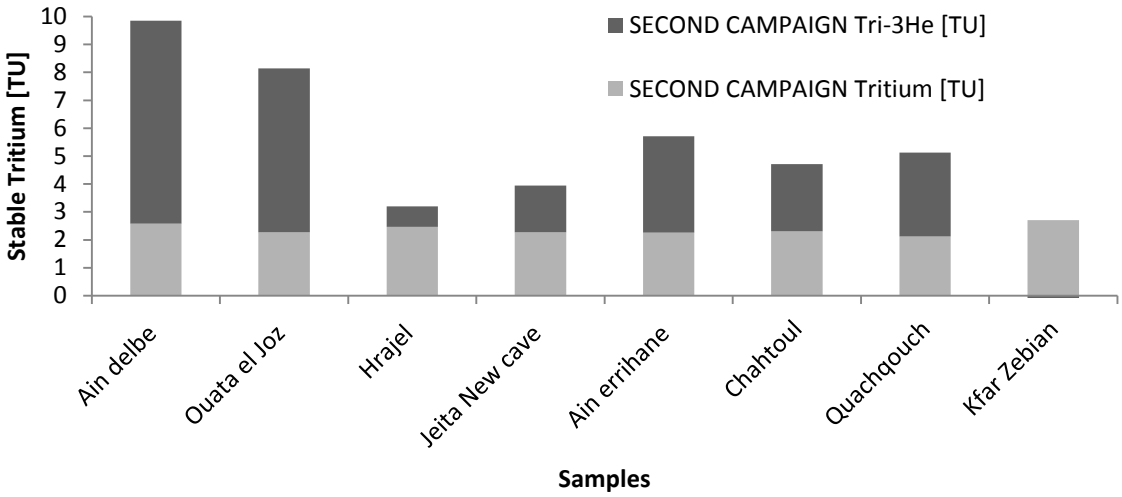

Fig. 32. Tritium and tritiogenic Helium concentration in collected water samples of the second campaign. Stable Tritium is the sum of Tritium and Tritiogenic Helium. Note that the absence of He_{trit} in Kfar zebian is due to unsuccessful sampling.

Table 5 Mean groundwater ages for the collected samples from the two campaigns.

	Well	Date	Sal	Z	^{3}H	Error	T	^{3}He	^{4}He	Ne	$^{3}He/^{4}He$	Ne/He	$\Delta^{3}He$	ΔHe	ΔNe	$^{4}He_{rad}$	$^{3}He_{trit}$	Tritium	Age	Av. Recharge Year
			[g/kg]	[m; asl]	[TU]	[TU]	[°C]	[ccSTP*/kg]					[%]			[ccSTP/kg]	[TU]	[TU]	[Years]	
FIRST CAMPAIGN	AD	25/10/14	0.3	1300	2.80	0.10	12.5	1.5E-10	9.4E-05	3.7E-04	1.6E-06	4.0	13.2	141	122	0.E+00	7.4	10.19	23	1992
	OJ	25/10/14	0.3	1300	2.69	0.09	13.1	1.5E-10	9.6E-05	3.8E-04	1.6E-06	3.9	13.0	147	126	0.E+00	7.5	10.16	24	1991
	HL	25/10/14	0.3	1300	2.97	0.10	11.4	1.1E-10	7.2E-05	2.9E-04	1.5E-06	4.1	8.1	84	73	0.E+00	3.68	6.65	14	2000
	JN	29/10/14	0.34	1000	2.48	0.09	15.3	8.0E-11	5.7E-05	2.3E-04	1.4E-06	3.9	0.7	43	34	9.E-07	1.14	3.61	7	2008
	JC	26/10/14	0.3	1000	2.68	0.09	15.3	6.5E-11	4.8E-05	2.0E-04	1.4E-06	4.2	-1.9	19	19	0.E+00	0.01	2.69	0	2015
	AN	25/10/14	1.2	800	2.26	0.11	19.6	7.3E-11	5.7E-05	2.1E-04	1.3E-06	3.7	-7.4	42	26	5.E-06	0.60	2.86	4	2011
	HR	26/10/14	0.5	1100	2.91	0.10	18.7	1.5E-10	1.0E-04	4.0E-04	1.5E-06	3.9	8.5	163	147	0.E+00	5.32	8.23	19	1996
	AR	26/10/14	0.4	1000	2.43	0.09	16.0	-	-	-	-	-	-	-	-	-	-	-		-
SECOND CAMPAIGN	AD	4/4/2016	0.2	1084	2.59	0.11	13.6	1.3E-10	8.3E-05	3.3E-04	1.6E-06	4.0	15	107	93	0.0E+00	7.27	9.86	24	1993
	OJ	8/4/2016	0.3	1083	2.27	0.10	16.9	1.6E-10	1.1E-04	4.2E-04	1.5E-06	3.9	9	173	154	0.0E+00	5.87	8.14	23	1994
	HL	8/4/2016	0.4	1237	2.47	0.11	14.3	1.1E-10	8.2E-05	3.3E-04	1.4E-06	4.0	1	109	96	0.0E+00	0.73	3.20	5	2012
	JN	7/5/2016	0.3	95	2.27	0.10	14.8	7.9E-11	5.7E-05	2.3E-04	1.4E-06	4.0	1	27	19	1.8E-06	1.67	3.94	10	2007
	AR	8/4/2016	0.3	280	2.25	0.10	18.7	1.4E-10	9.8E-05	3.5E-04	1.4E-06	3.6	0	126	94	5.6E-06	3.45	5.71	17	2000
	CL	4/4/2016	0.3	1006	2.30	0.10	16.1	7.8E-11	5.3E-05	2.2E-04	1.5E-06	4.2	7	32	31	0.0E+00	2.41	4.71	13	2004
	QQ	7/5/2016	0.3	64	2.12	0.09	19.2	9.7E-11	7.4E-05	2.6E-04	1.3E-06	3.4	-6	67	38	9.4E-06	3.01	5.15	16	2001
	KZ	10/5/2016	0.3	1128	2.71	0.11	14.5	5.9E-11	4.3E-05	1.9E-04	1.4E-06	4.3	-2	10	10	0.0E+00	-0.16	2.56	-1	2018

*CCSTP: 0˚C and 1 atm
*Sal: Salinity
*T: Temperature
*Error of the calculated mean age is ±1 year.

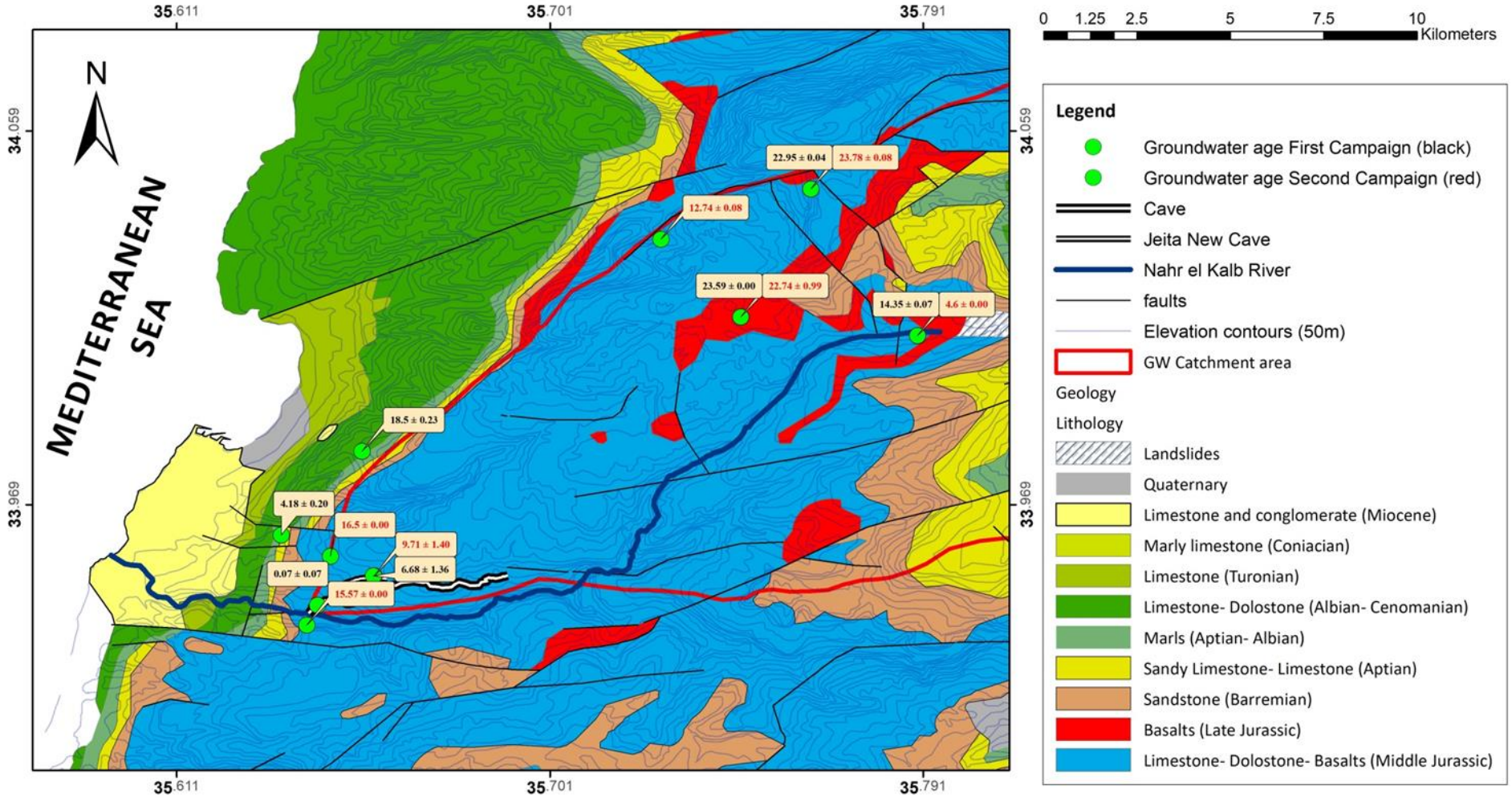

Fig. 33. Characterization of Jeita Spring Catchment Area showing the groundwater ages for the selected wells and springs. Age in years computed in first sampling campaign is reported in black, while that of second campaign is reported in red.

Groundwater age distribution on the Jeita catchment is quite complex varying according to the karst compartments. Samples of Ain delbe (AD) and Ouata el Joz (OJ) score the highest mean ages in both campaigns with 23 and 24 years respectively in the first campaign, and 24 and 23 years respectively in the second campaign. These highest ages samples have showed the highest levels of stable Tritium with 10.19 and 10.16 TU respectively in the first campaign and 9.85 and 8.14 TU respectively in the second campaign (Fig. 31 and Fig. 32). By comparing these stable Tritium values with the Tritium in precipitation values in northern hemisphere throughout the years they fit approximately in the same year of infiltration for these two samples as revealed by Tritium-Helium method (Fig. 31and Fig. 32). Moreover, these two wells show high excess air in both campaigns (Fig. 30). Sampling in these wells was conducted according to standard operating procedure, thus avoiding excess air to the maximum. The excess air can be in that case due to high fluctuation of the water table typical of karst aquifers and the trapping of air bubbles in the fluctuation zone.

The Hrajel sample showed in the first campaign a mean age 14 years, while in the second campaign it revealed a mean age of 5 years. Moreover if we compare the Tritium in the samples of both campaigns they are very close to each other 2.97 TU in the first campaign (Fig. 31) and 2.47 TU in the second one (Fig. 32). However the calculated tritiogenic Helium for both campaigns is relatively dissimilar, 6.65 TU and 3.20 TU respectively (Fig. 31 and Fig. 32), hence the difference in the two ages is caused by the difference in tritiogenic Helium. It is to be noted that this discrepancy in the measured age is attributed to the sampling time, while the first campaign was undertaken during low flow periods in November 2014 before considerable rain events; and the second campaign was undertaken during snowmelt. Therefore a mixing of the

water with relatively new water might result in the decrease of the relative apparent age of the water.

The Jeita spring new branch (JN) showed a mean age of 7 years in the first campaign and a mean age of 10 years in the second campaign. The ages in both campaigns are close and they reveal a relatively young groundwater, that is not only affected by fast flow components. Moreover some radiogenic Helium was detected in both sampling campaign in the Jeita new branch samples along with little lower Tritium, this indicate some pre 1963 water.

Some other samples also such as Aintoura (AN) in the first campaign, Ain errihane (AR), and Quachqouch (QQ) in the second campaign contained some pre 1963 groundwater as they showed radiogenic Helium along with slight lower Tritium concentrations. The other groundwater samples are mostly recent waters (post 1963). The Aintoura (AN) revealed a mean age of 4 years (very young water) with very low $^{3}He_{trit}$ and some radiogenic ^{4}He ($4.6E10^{-6}$ ccSTP/kg) and which is consistent with a little lower Tritium (2.26 TU); (Fig. 31). Hence this well is characterized by a mixing of very old water older than 50 years (about 10%; Geyer, 2008) with either very young water coming from the sea water as this well is affected by sea water intrusion or groundwater has been re-equilibrated with the air in the unsaturated zone or during sampling. The mean age for Ain errihane (AR) in the first campaign was difficult to detect as air bubbles were highly present during sampling, however in the second campaign, a more efficient sampling procedure was adopted to minimize air bubbles, to overcome the difficulties faced due to the diameter of rising pipe at the well head. Therefore, air bubbles were avoided to the maximum extent possible. The second campaign revealed a mean age of 17 years along with some radiogenic Helium (5.64E10-^{6} ccSTP/Kg) and

little lower Tritium concentration (2.25 TU) indicating the presence of very old groundwater greater than 50 years mixed with more recent groundwater giving a mean age of 17 years. Hence, Ain errirahne (AR) is tapping part of the aquifer characterized by water infiltrating through fissured matrix or a relatively longer transit time and a larger catchment area. The Quachqouch (QQ) well lies outside the Jeita catchment area and is tapping this same Jurassic aquifer south to the no-flow boundary condition (Nahr el Kalb River). The well is artesian and goes to about -160 m above sea level; it is tapping a confined part of the aquifer at the same level of Ain Rihane, and it is used as buffer well for comparison reasons. In that case groundwater in Quachqouch (QQ) is revealed to have an average age of 16 years, indicative of a rather significant transit time. The flow in this aquifer is assumed to occur under confined condition over a certain portion of the aquifer, with an indirect recharge area located farther from the well head.

The Harissa well (HR) that taps middle Jurassic Formations also lies outside the Jeita catchment area. It revealed a mean age of 19 years lying in the same range with respect to the wells tapping the Jeita aquifer. The Chahtoul (CL) well was sampled in the second campaign and revealed a young mean age of 13 years. The Jeita cave (JC) sampled in the first campaign showed a very low tritiogenic Helium reflecting a mean age of 0.07 along with low excess air (ΔNe= 19%; Fig. 30). Such a result is expected since the Jeita cave water is in direct contact with the ambient air in the cave. Therefore re-equilibration with the local ambient air has taken place. A similar result was obtained during the sampling campaign undertaken in two locations inside the cave (Geyer and Doummar 2013). Sampling of springs in France (Delbart et al., 2014) yielded similar results. The Jeita new cave, however, is a confined conduit feeding the Jeita cave where

sampling has been performed under pressure inside the fully saturated conduit, thus inhibiting degassing and equilibration with the local ambient air. Finally, the Kfar zebian (KZ) showed negative values of tritiogenic Helium and mean ages which are mainly due sampling problems mentioned in a previous section.

6.3.2 *Chlorofluorocarbons (CFCs) and Sulfur Hexafluoride (SF_6)*

Chlorofluorocarbon-12 (CFC-12) was measured in the eight groundwater samples. The results are reported in pmol/kg of water (Table 6). They ranged between 1.70 and 4.66 pmol/kg. These measured values of CFC-12 were corrected by a correction factor based on the amount of excess air present in each sample (Darling et al., 2012). The correction of excess air is required as this excess air contains excess CFC-12 that was not present during infiltration and doesn't reflect the true age of the sample. As mentioned previously, excess air was calculated based on Neon concentration in each sample. In order to obtain the atmospheric concentration of CFC-12 that was present during infiltration, the solubility at two different temperatures was calculated at T1 (representing the measured temperature during sampling) and T2 (representing a mean annual temperature of 10˚C; mean annual temperature adopted in various studies specifically in areas of deep unsaturated zones such as Mazor, 1972; Busenberg and Plummer, 1992; Price et al., 2003; Delbart et al., 2014, especially that the direct recharge zone of each well is poorly delineated. Comparing the CFCs atmospheric concentrations at T1 and T2, reveals that much more elevated atmospheric concentrations are present at T1 than at T2, since solubility of CFCs increase with lower temperatures. Additionally T2 concentrations yielded more realistic air concentrations as they coincide along with the atmospheric histories of CFCs (1765-2015) (Bullister,

2015). Moreover, the sensitivity of temperature was calculated and it was found that the CFC-12 concentration in air increases by 15 to 42 pptv for every increase by 1˚C depending on the concentration of CFC-12 in the sample (Fig. 34). The higher the amount of CFC-12 in the sample the higher the effects of 1˚C change in temperature. Therefore, the latter indicates the sensitivity of the temperature in the calculation of input values of CFC-12.

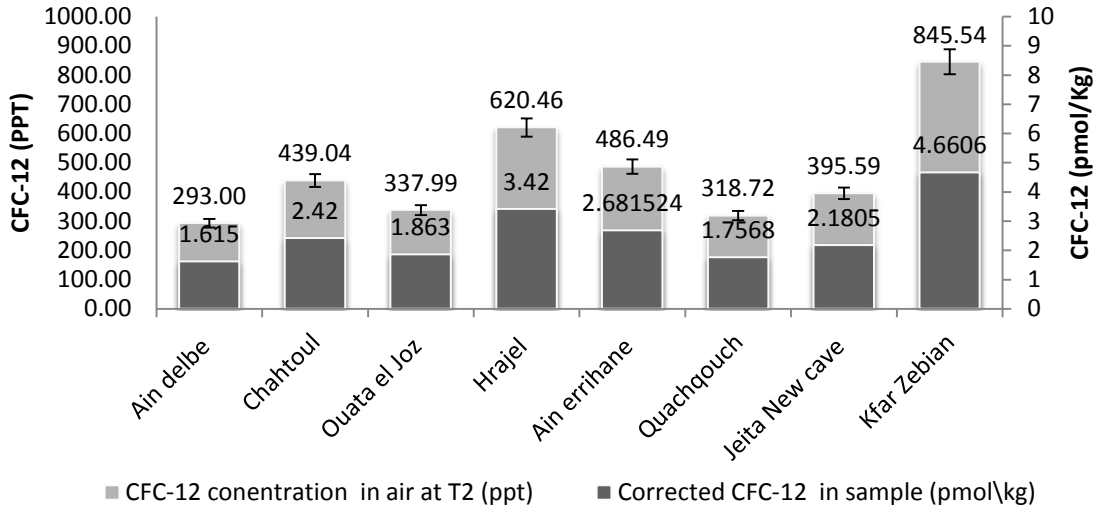

Fig. 34. Atmospheric concentration of CFC-12 in samples and air.

Table 6. Summary of CFC-12 results.

Well	CFC-12 in sample	Error CFC-12	Excess air	Correction factor CFC	Corrected CFC-12 in sample	Kcfc-12 at T1	Kcfc-12 at T2	CFC-12 concentration in air at T1	CFC-12 concentration in air at T2	CFC-12 concentration in air at T1	CFC-12 concentration in air at T2	(+/-) CFC-12 for 1˚c
	(pmol\kg)	(pmol\kg)			(pmol\kg)			(mol/kg)	(mol/kg)	(ppt)	(ppt)	(ppt)
AD	1.70	0.10	7.05	0.95	1.62	4.6E-03	5.5E-03	3.50E-10	2.93E-10	350	293	15
CL	2.42	0.03	1.26	1.00	2.42	4.1E-03	5.5E-03	5.89E-10	4.39E-10	589	439	22
OJ	2.07	0.03	12.33	0.90	1.86	4.0E-03	5.5E-03	4.70E-10	3.38E-10	470	338	17
HL	3.60	0.05	6.92	0.95	3.42	4.5E-03	5.5E-03	7.67E-10	6.20E-10	767	620	31
AR	2.91	0.03	8.63	0.92	2.68	3.7E-03	5.5E-03	7.30E-10	4.86E-10	730	486	24
QQ	1.83	0.03	3.47	0.96	1.76	3.6E-03	5.5E-03	4.88E-10	3.19E-10	488	319	16
JN	2.18	0.03	0.00	1.00	2.18	4.1E-03	5.5E-03	5.29E-10	3.96E-10	529	396	20
KZ	4.66	0.05	-	1.00	4.66	4.4E-03	5.5E-03	1.05E-09	8.46E-10	1055	846	42

Sulfur Hexafluoride (SF_6) was measured in the collected groundwater samples and reported in fmol/kg of water (Table 7). Values ranged between 2.05 and and 6.39 fmol/kg (Fig. 35), and similar to CFCs they have been corrected using a calculated correction for SF_6 due to the presence of excess air (Darling et al., 2012). Also atmospheric concentrations of SF_6 were calculated at T1 and T2 as in CFCs. But here at both temperatures, four samples showed SF_6 values exceeding the atmospheric historical values of SF_6, three samples have showed atmospheric concentration coinciding with atmospheric history of SF_6 at (1765-2015); (Bullister, 2015); (Fig. 35). Also temperature sensitivity was done for SF_6 concentration similar to CFC-12; the greater the concentration of SF_6 in the sample the greater the effect of ±1˚C (Fig. 35). The results of Kfar zebian well for both CFC-12 and SF_6 were very poor and they showed unrealistic values due to sampling problems. High SF_6 values could be attributed to local contamination by anthropogenic activities. However, this seemingly higher trend portrayed by all the samples might imply that atmospheric SF_6 values are higher in air in the area of study due to regional anthropogenic activities. Therefore, a correction factor of 1.65 was adopted to increase the SF_6 input in air (Delbart et al., 2014). However a correct estimation of the SF_6 input function and of the correction factor should be performed based on SF_6 concentrations in the soil, which was not conducted for the purpose of the study.

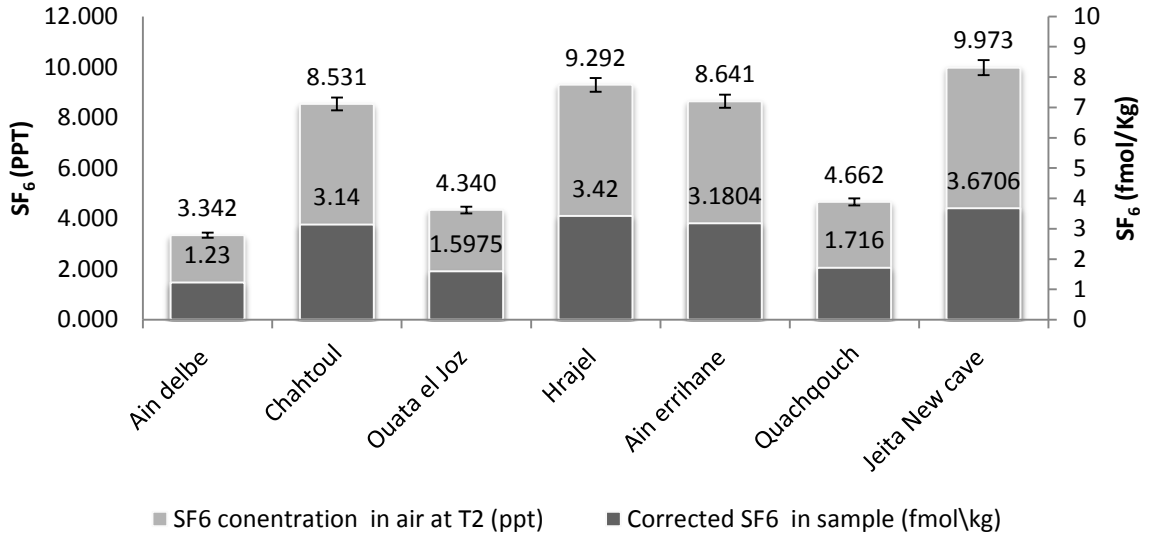

Fig. 35. Atmospheric concentration of SF_6 in samples and air.

Table 7. Summary of SF_6 results.

Well	SF_6 in sample	Error SF_6	Excess air	Correction factor SF_6	Corrected SF_6 in sample	KSF_6-12 at T1	KSF_6-12 at T2	SF_6 concentration in air at T1	SF_6 concentration in air at T2	SF_6 concentration in air at T1	SF_6 concentration in air at T2	(+/-) SF_6 for 1˚c
	[fmol/kg]				(fmol\kg)			(fmol/kg)	(fmol/kg)	(ppt)	(ppt)	(ppt)
AD	2.05	0.1	7.05	0.6	1.23	3.31E-04	3.68E-04	3720	3342	3.72	3.34	0.10
CL	3.14	0.05	1.26	1.0	3.14	3.07E-04	3.68E-04	10212	8531	10.21	8.53	0.25
OJ	3.55	0.05	12.33	0.5	1.60	3.01E-04	3.68E-04	5316	4340	5.32	4.34	0.13
HL	5.70	0.1	6.92	0.6	3.42	3.24E-04	3.68E-04	10557	9292	10.56	9.29	0.28
AR	6.36	0.05	8.63	0.5	3.18	2.86E-04	3.68E-04	11137	8641	11.14	8.64	0.26
QQ	2.20	0.05	3.47	0.8	1.72	2.82E-04	3.68E-04	6094	4662	6.09	4.66	0.14
JN	3.67	0.05	0.00	1.0	3.67	3.08E-04	3.68E-04	11903	9973	11.90	9.97	0.30
KZ	6.40	0.1	-	1.0	6.40	3.22E-04	3.68E-04	19861	17380	-	-	-

Plotting the CFC-12 against SF_6 concentrations in groundwater samples reveal a positive linear relationship between both tracers with a slope of 1.29 and a good fit (R^2 = 0.8407) (Fig. 36). A similar correlation was done by Darling et al (2012) between CFC-12 and SF_6 in order to determine groundwater ages of the samples based on different water flow methods.

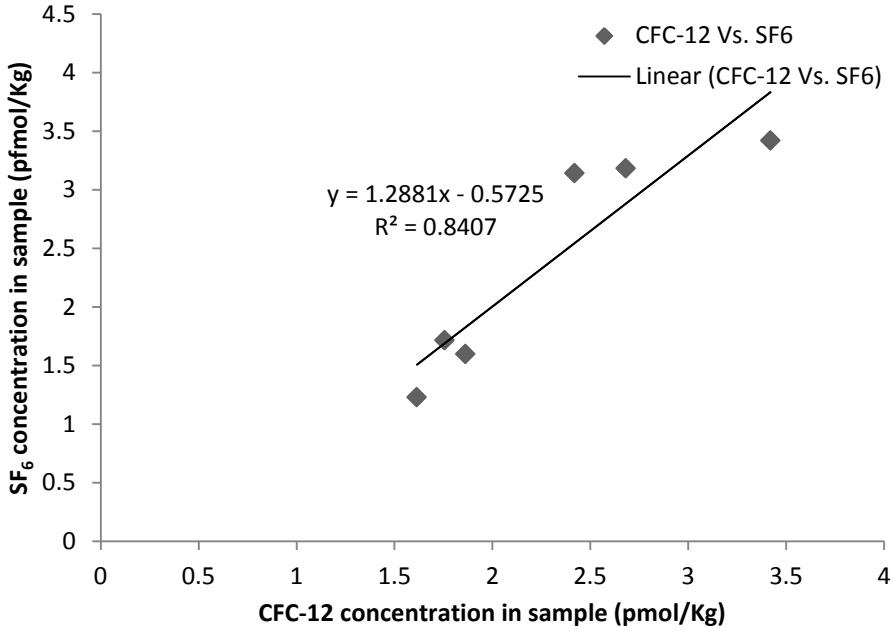

Fig. 36. CFC-12 concentration vs. SF_6 concentration in groundwater samples.

The concentration of CFCs and SF_6 in water allow to backtrack the concentration in air at given temperature and pressure conditions. Theoretically, the age of the samples corresponds to times during which calculated concentration in air matches each of CFCs and SF_6 atmospheric concentration. After applying a piston flow model to the obtained atmospheric concentration of CFCs and SF_6, the following recharge years for each of the samples are shown in Fig. 37 and Fig. 38 respectively. As

noted previously, a correction factor of 1.65 was adopted to increase the SF_6 input in air (Delbart et al., 2014).

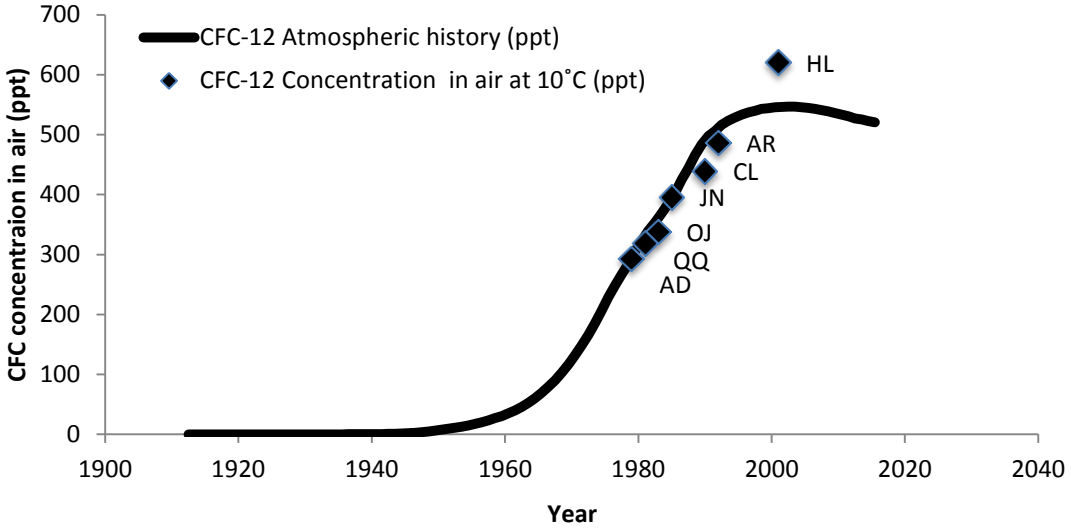

Fig. 37. CFC-112 atmospheric input curve and the corresponding infiltration year for the groundwater samples.

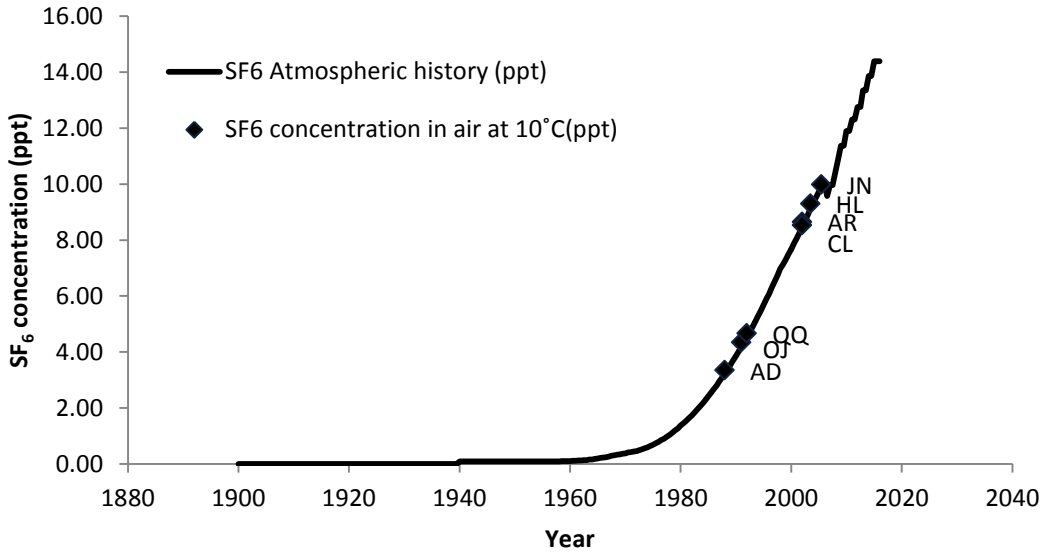

Fig. 38. SF_6 atmospheric input curve and the corresponding infiltration year for the groundwater samples.

CHAPTER 7

DISCUSSION

7.1 Recharge and Water Type

The isotopic ratio results of Deuterium and Oxygen-18 show that wells of Ouata el Joz (OJ) and Ain delbe (AD) fit on the local meteoric water line. This indicate that mixing and fractionation in these two wells is minimal, moreover these wells showed more depletion in the two stable isotopes than other groundwater sampled wells. This can reveal that the recharge zone to these wells are from higher altitudes characterized by depleted heavy isotopic rainfall signature (Königer and Margane, 2014). The Hrajel (HL) well isotopic composition deviates slightly from the local meteoric line with low isotopic signature. This deviation indicates the presence of fractionation occurring in the recharge zone of Hrajel (HL) well where slight enrichment of Oxygen-18 has occurred (Horst, 2007). The Ain errihane (AR) sample shows major deviation from the local meteoric line with isotopic enrichment with respect to other wells. This indicates the presence of high fractionation effect in this site due to a thick saturated zone where significant evaporation of the Oxygen-16 has occurred (Horst, 2007). The Jeita new cave (JN) sample shows also a major deviation from the local meteoric line with isotopic enrichment of Oxygen-18. This is due to the high mixing of fractionated groundwater. This fractionated water is most likely the old water component (10%) that was previously indicated due to the presence of radiogenic Helium in the sample. The Chahtoul (CL) isotopic result deviates from the other wells

as it showed lower depletion of Deuterium than other wells while Oxygen-18 lies within expected ranges, so the Chahtoul (CL) isotopic results might not be reliable.

7.2 Age Estimation

7.2.1 *Tritium-Helium (^{3}H-^{3}He)*

The calculated mean groundwater age from the Tritium-Helium is based on the assumption of piston flow conditions, considering that all water particles arriving at the sampling well, follow the same path similar to flow through a pipe (Bethke and Johnson, 2008). The calculated ages can be considered reliable as they reflect an average time for the decay of Tritium to tritiogrenic Helium. The mean ages of sampled water are well distributed along the Jeita catchment area. Wells located at higher altitude to the North east end of the catchment showed higher mean ages such as Ain delbe (AD) and Ouata el Joz (OJ). This higher age range is attributed to the geology of the infiltration area and the potential lack of large conduits in the subsurface, inhibiting therefore a higher extent of binary mixing. Precipitated water reaches these wells through fissured matrix and small fractures from higher altitudes areas as revealed by isotopic signatures. The absence of dolines or sinkholes in the infiltration vicinity of these two wells ensure a slower water transit time. Moving down toward the coast, the geology of the catchment area changes, important clusters of dolines (Fig. 9) are observed in the middle of the catchment area; here the wells show lower mean ages, such as Hrajel (HL) and Chahtoul (CL) located at high altitudes. Aintoura (AN) and Ain errihane (AR) at lower altitudes are characterized by a higher age range, the latter could

be due to the infiltration in the area of recharge that occurs diffusively (very few dolines i.e., fast flow pathways can be detected) whereas Chahtoul (CL) and Aintoura (AN) wells are located downstream to a doline field that enhances fast infiltration to these wells, especially in the case of Chahtoul (CL) located on the major northeast-southwest Chahtoul fault (Refer to section 3.4). Moreover, the Hrajel well (HL) showed different ages in the two sampling campaigns, as mentioned in a previous section, because of the age variation under varying flow conditions: the high contribution of recent water from snow melt or precipitation through fast pathways could be the cause for mixing new with older water and yielding a younger mean age in the second campaign. Hence, the aquifer here is recharged by water flowing through fissured matrix along with rapid flow along larger fractures (Delbart et al., 2014). The young age, variance in the ages between samples, and presence of some water older than 50 years in the Jeita new branch (JN) samples all indicate the high mixing effect in the Jeita new branch. Hence, the Jeita new branch (JN) is characterized by mixing of stored old conduit water, phreatic water in fissured matrix mixed with fast water coming directly from precipitation through large solution conduits to the Jeita new branch (JN). As a matter of fact, the isotopic signature of Jeita new cave confirms the high mixing effect and fractionation.

The high positive values of ΔNe, is mainly due to the presence of high excess air in most samples indicating the entrapment of gases in thick unsaturated zones along with complete dissolution of small air bubbles possibly caused by water table fluctuation in the recharge area (Heaton and Vogel, 1981).

In order to assess the reliability of the Tritium method in the current study, the curve of concentration of Tritium in samples was constructed based on the decay of

Tritium to Helium-3 from the year of infiltration to the years of sampling 2014 and 2016. A plot for the decay curve along with measured Tritium (^{3}H) in collected samples after calculating their ages based on total Tritium for the two campaigns (2014 and 2016) are shown in Fig. 39 and Fig. 40 respectively.

None of the measured ^{3}H in samples of 2014 and 2016 plot on their respective curve they all plot below their respective curve, except for Jeita cave sample (2014) and Hrajel sample (2016) plot above the curve, indicating the uncertainty in the Tritium concentration in precipitation. Furthermore, the constructed decay curve is highly fluctuating with low variations in the last 30 years and extremely minimal variations in the late 14 years, as Tritium concentration in precipitation is minimal in the last 30 years, putting the Tritium method to its end (Visser et al., 2013).

It is worth to note here that the Jeita cave (JC) sample (2014) showed approximately zero (0) years groundwater age with a Tritium concentration value of 2.68 TU which is slightly higher than the Tritium concentration in precipitation (2.3 TU) for the respective calculated infiltration year 2014. This assure the high uncertainty in the Tritium concentration in precipitation in addition to the stability of Tritium with very slight variation in precipitation in the last 30 years making the Tritium method not reliable.

Moreover, the Jeita new cave sample (2014) showed a zero age along with the lowest excess air ($\Delta Ne = 19\%$) and with the lowest tritiogenic Helium (0.01 TU) this indicate the degassing and partial re-equilibration of the noble gases (Ne, ^{3}He, and ^{4}He) in the water prior of sampling with the atmosphere inside the cave (Visser et al., 2013), which is typical in cave and spring samples due to the sensitivity of light noble gas to the atmosphere (Kluge et al., 2010; Delbart et al., 2014).

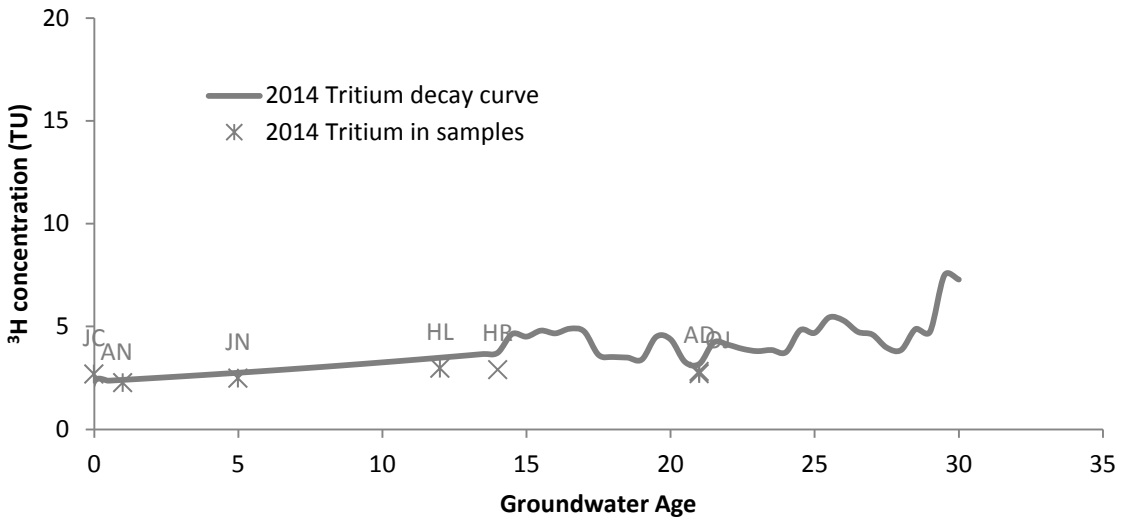

Fig. 39. Comparison between measured Tritium (^{3}H) in samples of 2014 campaign and constructed Tritium decay curve for water recharge in 2014 (The age is determined from the total Tritium).

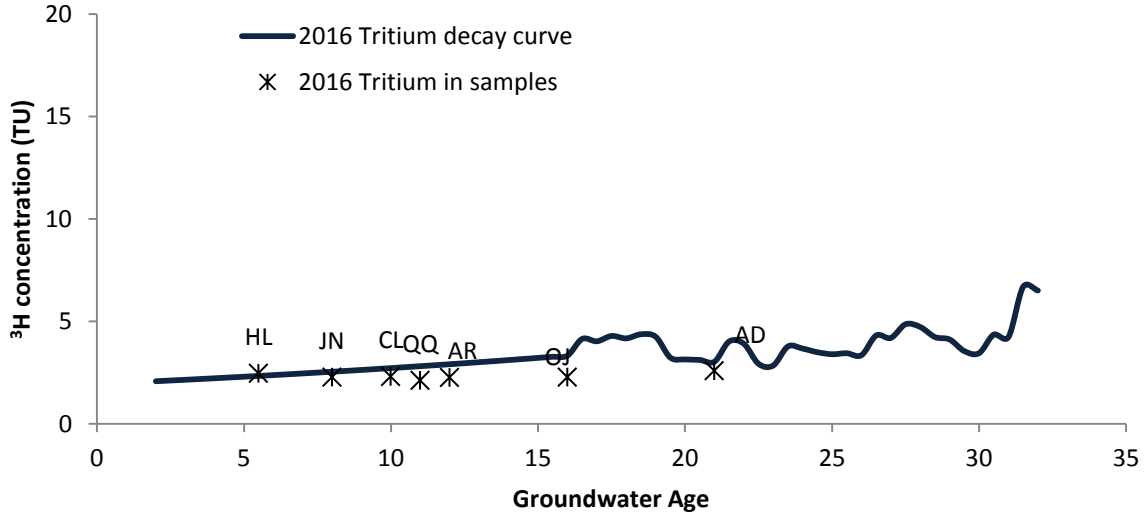

Fig. 40. Comparison between measured Tritium (^{3}H) in samples of 2016 campaign and constructed Tritium decay curve for water recharge in 2016 (The age is determined from the total Tritium).

7.2.2 *Chlorofluorocarbons (CFC) and Sulfur Hexafluoride (SF_6)*

Given the high uncertainty observed in the input gas concentrations especially in the last 20 years for CFC's and the anthropogenic effect on SF_6 , applying piston flow conditions to determine the ages using CFC and SF_6 separately with each method is not reliable here, (Fig. 37 and Fig. 38). Hrajel (HL) sample didn't lie on the input atmospheric line of CFC-12, this could indicate that the CFC-12 input function is not precise to our study site (local contamination). Similarly the case with SF_6 input function most of the samples did not fit to the atmospheric history of SF_6 due to local contamination by anthropogenic activities. So, a correction factor of 1.65 was adopted (Delbart et al., 2014). After applying this correction factor to the atmospheric input function, the samples fit to the SF_6 input function (Fig. 38). In addition, the computed groundwater ages or the recharge year using these two methods were not compatible to each other. Therefore, groundwater ages for these two methods can be determined by using other flow models that relate concentration of CFC to SF_6 in the atmosphere.

7.2.3 *Comparison of Methods*

Correlations between SF_6, CFC-12, and Tritium concentration in the atmosphere and samples are made and shown in Fig. 41 and Fig. 42. The correlations reveal that all samples do not correlate with atmospheric input functions except for Ain errihane (AR).

Ain errihane (AR) sample shows good correlation between SF_6 and Tritium concentration in sample to the input curve and a close correlation between SF_6 and CFC-12 concentration in sample to the input curve. This indicates that a piston flow model can be used in the case of Ain errihane (AR) (Darling et al., 2012). With a piston

flow model, the estimated age of Ain errihane (AR) using SF_6 is 14 years and using Tritium-Helium method is 17 years and using CFC-12 method it is 24 years. The variation in ages between SF_6 and Tritium Helium is mainly due to the cumulative errors in calculation and in the input curve for each tracer. Concerning the higher variation in age using CFC-12 this is mainly due to the high uncertainty in the atmospheric input function of CFC-12 since local contamination might be present and since the CFC-12 atmospheric values are very slightly changing in the past 20 years making a piston flow model for Ain errihane (AR) less reliable.

For the remaining water samples piston flow models are not applicable since the samples do not fall on the piston flow curve for CFCs-SF_6 and Tritium (Darling et al., 2012). In addition to the uncertainty in the CFC-11 and SF_6 concentration in atmosphere, these three tracers tend to diffuse and mix differently if dispersion effect is pronounced within the aquifer (Szabo et al., 1996; Darling et al., 2012).

Hence, another flow model conditions should be adopted in order to obtain true groundwater ages. Binary mixing flow model or more complicated lumped parameter flow conditions such as the exponential mixing model, exponential piston flow models and dispersion model are needed to determine true groundwater ages for each sample (Darling et al., 2012).

Therefore, based on the preceding correlations we can deduce that Tritium-Helium appears to be a suitable and reliable method for the estimation of an absolute average age to the contrary of CFC-11 and SF_6 methods which didn't provide neither true ages nor reliable mean ages due to highly possible local contamination.

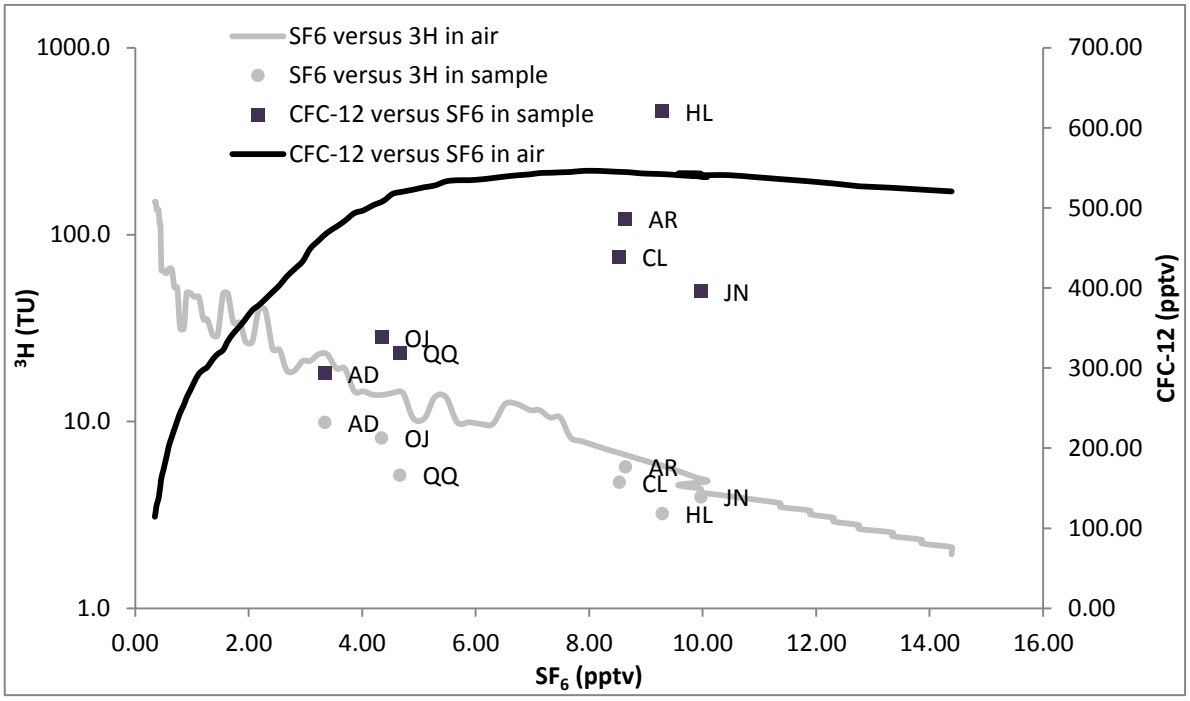

Fig. 41. Correlations between SF_6 and ^3H concentrations in samples and air and between CFC-12 and SF_6 concentrations in sample and air throughout the years.

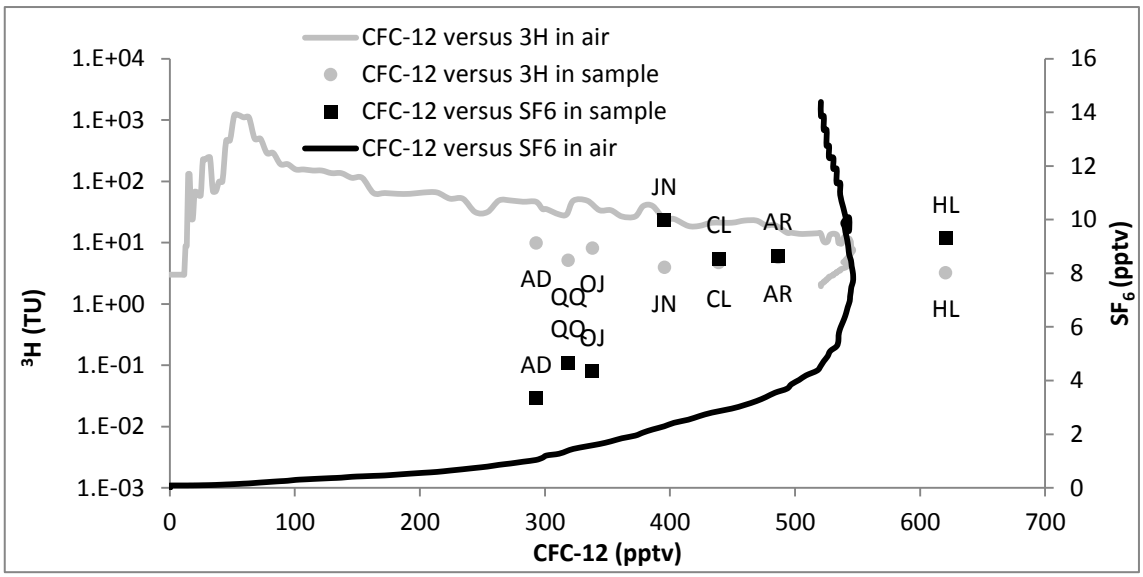

Fig. 42. Correlations between SF_6 and ^3H concentrations in samples and air and between CFC-12 and SF_6 concentrations in sample and air throughout the years.

A binary mixing model is developed by constructing two input functions using the atmospheric concentration of CFC-12 to SF_6 and CFC-12 based on different proportions of mixing assumptions between young and old groundwater (Darling et al., 2012). The concentrations of different samples were plotted, as shown in Fig. 43.

In the first binary mixing model, zero age and 34 years water age (1982 infiltration year of water) were assumed. As shown in Fig. 43, in this mixing model assumption only Chahtoul well (CL) plot perfectly on the constructed binary mixing curve, indicating that a mixing model conditions is suitable for the Chahtoul (CL) groundwater with new water component reaching 54%.

The second model assumes a zero age groundwater mixed with a groundwater of an age of 47 years (1969 infiltration year of water) in this binary mixing assumption only Jeita new cave (JN) sample plot perfectly on the constructed curve, indicating that a mixing model conditions is suitable for the Jeita new cave (JN) groundwater with new water component reaching 69% (Fig. 43).

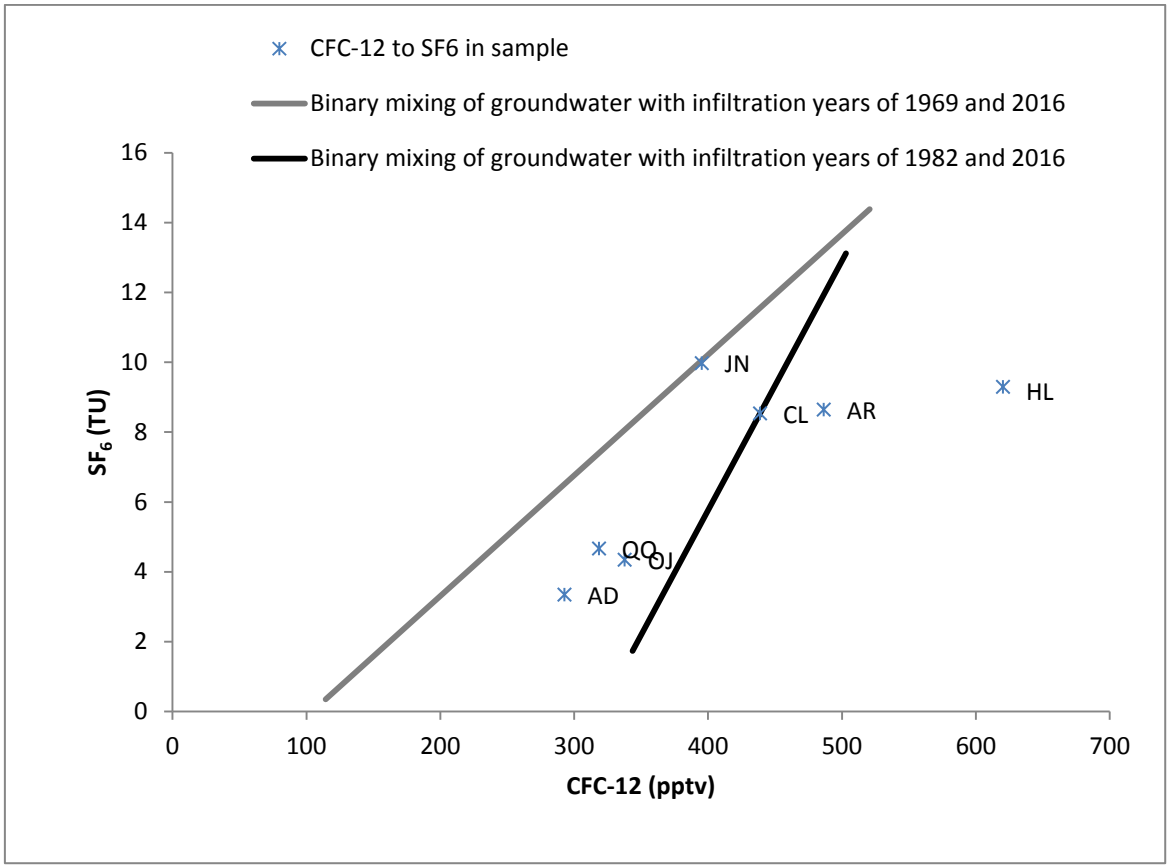

Fig. 43. Binary mixing model using CFC-12 to SF_6 input curves with a mixing of two age water assemblages, 0 with 34 (1982 infiltration year) years and 0 with 47 years (1969 infiltration year).

7.3 Limitations and Sensitivity Analysis

The environmental tracers used for groundwater age dating possess limitations that was documented (e.g. Busenberg and Plummer, 2000; Cook and Herczeg, 2000; Kazemi et al., 2006). The major uncertainties are environmental in nature, others are analytical ones. The sensitive parameters for different method are summarized in Table 8.

The Tritium- Helium method limitations are concerned in the mixing and fractionation of Helium isotopes in water, in addition to the Helium degassing and

excess air entrapment in groundwater. The noble gases (Helium and Neon) are frequently prone to degassing or re-equilibration with air, due to the presence of unsaturated zone. So, the produced tritiogenic Helium in the unsaturated zone will eventually escape to the atmosphere, only the ones produced in the saturated zone will be preserved, this will yield to an underestimated groundwater age. And in the case of a thick unsaturated zone and long water transit tine in the unsaturated zone, the degassing of noble gases would be significant and reach high levels.

Moreover some uncertainties reveal from the corrections for ^{3}He derived from radiogenic sources; also the Tritium-Helium method will be impossible if mantle and nucleogenic sources are considered to be in significant amounts. Furthermore uncertainties in estimation of recharge altitude, recharge temperature, and excess air are to be corrected for. For instance inaccurate recharge temperatures assumed for gas exchange with the atmosphere may lead to a time resolution of about 1.0 year (Sültenfuß et al., 2011).

The Limitations for CFC method are also mainly due to the nature of the CFC molecule, as CFC may undergo dispersion, diffusion, mixing at sampling points, sorption, and CFCs are prone to microbial degradation. Moreover, inside the aquifer anthropogenic CFC contamination might be present, or contamination may occur during sampling, and local atmospheric anomalies in CFC concentrations could be found, hence CFC method may possess uncertainties in the estimation of atmospheric input function that could highly underestimate or overestimate the groundwater ages. Furthermore, the CFC input curves are undergoing flattening and overturning in the 1990s and early 2000s, and uncertainties in estimation of recharge altitude, recharge

temperature, and excess air, for instance air contamination during sampling can lead to a high groundwater age underestimation (International Atomic Energy Agency, 1992).

The SF_6 possess similar limitations as CFC due to the nature of the SF_6 molecule, inside the aquifer SF_6 contamination might be present, SF_6 contamination during sampling, and spatially variable atmospheric SF_6 concentrations and local anthropogenic atmospheric contamination. Moreover SF_6 are prone to mixing, natural subsurface production, and degassing in the aquifer or during sampling due to the low solubility of SF_6, in addition to the uncertainties in estimation of recharge altitude, recharge temperature, and excess air (Kazemi et al., 2006).

Table 8. Sensitivity parameters for each groundwater age dating method.

Method	**Sensitivity parameters**							
	Excess air	**Degassing**	**Recharge Temperature**	**Recharge Altitude**	**Diffusion**	**Dispersion**	**Sorption**	**Degradation**
Tritium-Helium	Calculation of $^{3}He_{trit}$ concentration in sample	Underestimation of groundwater age	^{3}He and ^{4}He concentration at equilibrium	^{3}He and ^{4}He concentration at equilibrium (slightly sensitive)	-	-	-	-
CFC	Overestimation of CFC in sample	-	CFC solubility	CFC solubility (slightly sensitive)	Underestimation of CFC in sample	Underestimation of CFC in sample	Underestimation of CFC in sample	Underestimation of CFC in sample
SF_6	Overestimation of SF_6 in sample	Underestimation of SF_6 in sample	SF_6 solubility	SF_6 solubility (slightly sensitive)	Underestimation of SF_6 in sample	Underestimation of SF_6 in sample	-	-

7.4 Vulnerability Assessment of the Jeita Aquifer System

The assessment of risk factors and vulnerability of aquifers to natural pollution and human impacts on land such as agriculture, industry, waste disposal, urbanization, etc...(Leibundgut, 1998) requires the integration of several parameters making it a difficult task to assess (Leibundgut, 1998). These parameters include the type of aquifer (unconsolidated, fractured, or karst aquifer), the protection cover (soil cover or overlying impermeable layers), and topography (Christoph et al., 2008). These general parameters are not the only ones playing the role in the vulnerability of aquifer to contamination. A detailed study of the aquifer and the catchment area is needed along with flow and transport parameters that play a crucial role in aquifer vulnerability (Christoph et al., 2008).

Several methods has been developed and applied to assess aquifer vulnerability namely GLA, PI, DRASTIC, and EPIK (Christoph et al., 2008). Most of the methods take into account the distribution and weight of the parameters affecting vulnerability, such as geology, karstification, soil cover, precipitation, and many others. Therefore the proposed methods to date evaluate the qualitative aspect of vulnerability of a system.

The **GLA method** is based on the estimation of **transit time** of the infiltrated water to reach the water table by identifying the thickness and permeability of the unsaturated and saturated zone along with the amount of infiltrated water (Christoph et al., 2008).

Protective cover and infiltration condition (**PI**) method is similar to GLA; however it takes into consideration the karst-specific behavior in terms of infiltration conditions. The P factor is concerned with the estimation of the **thickness and permeability** of each layer in the unsaturated zone (protective cover) and the I factor is

for the assessment of the degree of **bypassing of the protective cover** by surface and near surface flow (sinking streams; Christoph et al., 2008).

The **DRASTIC** vulnerability index developed in the U.S. environmental protection agency, which is probably the most widely applied vulnerability index globally make use of seven parameters in the vulnerability assessment including the **depth to water, topography, net recharge, aquifer media, soil media, the impact of the unsaturated zone media and hydraulic conductivity** of the aquifer (Christoph et al., 2008). Recently, the DRASTIC method has been modified to account for the fast preferred pathways for percolation through large fissures and sinkholes highly affecting the vulnerability of aquifers (Weatherington-Rice et al., 2006).

The **EPIK** method focuses greatly on the karst-specific behavior by studying the development of the **epikarst and karst networks, effectiveness of the protective cover, and infiltration** conditions.

As mentioned in previous sections, karst systems possess high variability due to their heterogeneity and complex flow regimes initiating high mixing effect of new and old water in the groundwater system (Einsiedl, 2005). This mixing is owed to their duality of recharge originating from the karst catchment area (autogenic recharge) or from adjacent non-karstic areas (allogenic recharge), in addition to that, karst systems exhibit differential pathways for infiltration (duality of infiltration; Goldscheider and Drew, 2007). It is believed that the water stored in the rock matrix, conduits, and in the epikarst below the soil layer all contribute to this heterogeneity and variability in karst system (Williams, 2008).

Furthermore, vulnerability is divided into intrinsic and specific vulnerability (Leibundgut, 1998), adding to it the different contamination scenarios for a better and complete assessment of vulnerability (Perrin et al., 2004).

The intrinsic vulnerability is defined by the properties of the karst system including several key factors that play a role in the assessment of the degree of vulnerability (Leibundgut, 1998). These parameters include the presence or absence of a soil and debris cover or an impermeable protective layer and the thickness of this protective cover, the presence and intensity of epikarst, the degree of karst development and karstic features, and infiltration processes either diffuse, spatial infiltration through a covered karst (fissured matrix) having a low vulnerability, or a concentrated point infiltration leading to high vulnerability. However, a key factor in karst system is important to tackle and can have a great impact on vulnerability, which is the degree and type of mixing between these different groundwater flow regimes (Christoph et al., 2008). The type of flow regime, transport mechanisms, and mixing in karst systems, i.e., the physical processes governing a system cannot be determined through one single method, an integration of several methods is more appropriate to ensure a better conceptualization of the groundwater flow and transport mechanisms to be able to have an appropriate vulnerability assessment (Christoph et al., 2008).

Precisely, in the case of the Jeita system, one should address the vulnerability of each of sampled well or point, and then look at their interaction with the Jeita spring. (Perrin et al., 2004) From this point of view, this study was conducted in order to have an insight into in the underground system of Jeita spring catchment area and the ratio between fast and slow base flow components.

The previous 26 artificial tests conducted in the Jeita spring catchment area in the period from April 2010 to December 2011 (Doummar, 2012) provided an assessment of transport and flow characteristics in the Jeita spring subsurface system for the short transit times ranging between 3 and 300 hours (12 days; Doummar, 2012).

The tracer injections that were performed directly in the Jeita subsurface conduit (from Daraya to Jeita spring) under different flow conditions yielded the shortest transit times 3 to 19 hours (Doummar, 2012). Other artificial tracers were also injected in two sinkholes, in an artificial pit hole, and in a borehole in order to acquire transport parameters in different media (Doummar, 2102). For unsaturated rock matrix overlying the subsurface channel and fissured saturated matrix (borehole) resulted in a wider range of relatively longer transit times (69 to 292 hours; Doummar, 2012). A tracer experiment in a sinkhole, leading directly to the subsurface channel (phreatic cave) yielded short to moderate transit times ranging between 25 and 90 hours under different flow conditions (Doummar, 2012). The variation in transit time in different flow conditions gives an insight on the importance of discharge and dilution and their effect on transport and flow velocities of contaminations (Doummar, 2102). As shown in Fig. 44, discharge play a double role; on the one hand, the increase of discharge results in the increase in groundwater velocities (shorter transit times) so, contamination will be transported and reach the outlet in shorter periods of time with a high concentration peak recorded on the breakthrough curve (BC) and less dispersion yielding a high vulnerability on the outlet water source. On the other hand, an increase in discharge means an increase in water volume influencing higher dilution of contamination takes place, thus decreasing the risk of contamination (Doummar, 2012). However, the type and the mass of contaminants play another role in the risk analysis,

not all contaminations are soluble in water so they are considered as solute loaded water, and dilution will have no effect on them so as discharge increase vulnerability to these contamination is absolutely high (Doummar, 2012). Hence it's very essential to have a knowledge of the pollution sources surrounding our groundwater resources (well/spring) in order to identify the contaminant type and mass (specific vulnerability; Leibundgut, 1998). So, a water resource with a short transit time and high contamination concentration is considered to be extremely vulnerable and a rapid response (shut down of water resource for a certain period of time) during a high discharge periods is highly recommended.

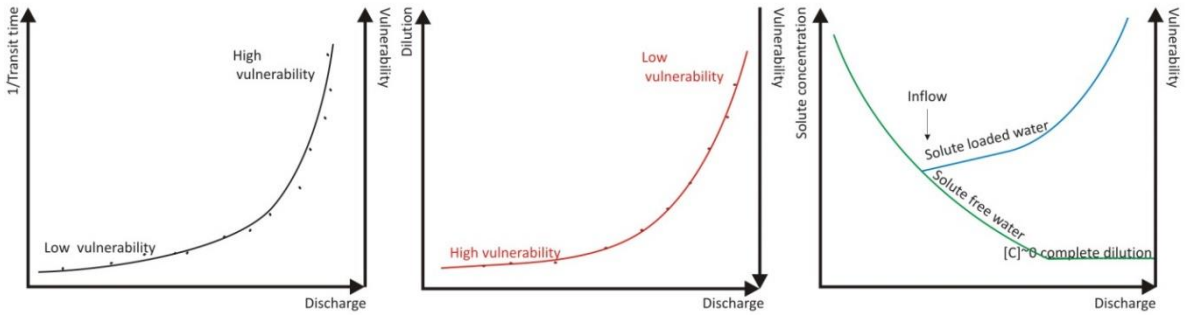

Fig. 44. Relationship between discharge and transit time, dilution and solute concentration in a system and their relevance to vulnerability (Doummar, 2012).

On the other hand in the case of a more diffusive infiltration, with a longer transit time other scenarios are expected, usually longer transit time and slow flow regimes provide natural filtration of the groundwater and give more time for the decay of many contaminants (Leibundgut, 1998). However, dilution is minimal here as discharge is considerably low so, rapid flushing of contaminated water is not applicable here as in high discharge conditions, for that reason contamination is expected to be

more persistent if it ever reaches the saturated zone (Leibundgut, 1998). So, protective measures and protective zones are highly recommended in these situations to prevent threats to these groundwater resources (Refer to Section 1.1).

This study aimed at combining several methods for a better conceptualization of the transport and transit time in the Jeita spring catchment area. The analysis of the Jeita spring response (hydrograph and chemograph) following a precipitation event based on the electric conductivity, Deuterium, Oxygen-18, and calcium provided an estimate of the different percentages of phreatic stored matric water old conduit water and new conduit water that ranged between a minimum of 6% and maximum of 73%. This variation in the percentage of new conduit water and phreatic stored water makes the Jeita spring water more vulnerable. For that reason, it is crucial to estimate a range for the age of phreatic stored matrix water (base flow) of the Jeita Spring. The relatively high mean ages that were calculated using Titium-Helium method (7 to 24 years) and the high mixing that is occurring in the Jeita new cave (branch of the Jeita spring system) along with the detected very old water component (~10%). The variability of ages indicates a larger catchment area, longer residence time, and a predominant older base flow. The degree of mixing within the baseflow is still to be assessed.

In order to evaluate the vulnerability of other water resources (sampled water wells) several factors should be studied including the presence/absence of a natural protection cover, the type, thickness, permeability of soil, development of epikarst, thickness of unsaturated zone, groundwater residence time, and type of infiltration. Further investigation of all these parameters using numerical simulation along representative conceptual hydrogeological model of the karst area in Jeita can generate a vulnerability map to the Jeita catchment area.

Based on the data collected in this study a preliminary vulnerability for the water point sources can be accomplished and summarized in Table 9.

An aquifer can be classified as well protected if the percolation time through the unsaturated covering layers exceeds 10 years (Hölting et al., 1995). Aquifer Vulnerability Index (AVI) is a method that quantifies vulnerability by hydraulic resistance to vertical flow of water through the protective layers (Stempvoort et al., 1993). Hydraulic resistance c is defined by

$$c = \sum_i \frac{d_i}{k_i}$$

(Equation 28)

Where d_i is the thickness of layer and $k_i$is the hydraulic conductivity of each protective layer.

The absence of a protective layer above the Jurassic Jeita aquifer system makes the entire aquifer more vulnerable to contamination with a medium to high vulnerability depending on the thickness of soil cover and unsaturated zone. Using stable isotopes (Deuterium and Oxygen-18) and the presence of excess air a thick unsaturated zone in the Jeita catchment area was deduced. Hence, this thick unsaturated zone provides some protection to the Jeita Spring aquifer. For that reason it was important to determine the mean residence time of different wells distributed along the Jeita catchment area using several environmental tracer age dating methods (Tritium-Helium, CFC, and SF_6). After the comparison and correlating these different dating methods together and with artificial tracer tests and event analysis, the dominant flow process and the type of infiltration (diffuse or concentrated) for different water resources are clearer. For Jeita cave (JC), Jeita new cave (JN), and Chahtoul (CL) high mixing of recently recharged

and old water indicates their high vulnerability. On the other hand, the Ain errihane (AR) revealed to be characterized by a piston flow with relatively older transit times, making it slightly less vulnerable to recent contamination. For the other water resources Ain delbe and Ouata el Joz a diffusive infiltration of water from a higher altitude infiltration area though fissured matrix is more likely consistent with its derived groundwater age and isotopic ratios. The Hrajel (HL) well showed two different ages in the two sampling campaigns, groundwater ages calculated were 14 and 5 years respectively. This high difference in ages can be attributed to the effect of sampling campaigns taken at dry and wet flow conditions respectively, this indicate that some more younger water is reaching the Hrajel (HL) well at faster rate during the wet flow condition. This might be due to the presence of some larger fractures in the vicinity of Hrajel (HL) well.

Table 9. Preliminary vulnerability assessment of the water resources in the Jeita catchment area based on unsaturated zone, mean residence time, and type of infiltration parameters.

Well/Spring	Unsaturated Zone	Mean Residence Time (Years)	Type of Infiltration	Vulnerability
Jeita New cave (JN)	Thick	7 to 10	Concentrated and Diffuse	Extreme
Ain-Rihane (AR)	Thick	17	Diffuse	Medium
Ouata El Joz(OJ)	Thick	23 to 24	Diffuse	Medium
Ain Delbe (AD)	Thick	23 to 24	Diffuse	Medium
Hrajel (HL)	Thick	5 to 14	Diffuse with Large Fractures	High
Chahtoul (CL)	Thick	13	Diffuse and Concentrated	Extreme

CHAPTER 8

CONCLUSION

The Jeita spring is characterized by baseflow and newly infiltrated water. Analysis of 26 Jeita spring responses with time revealed that between 6% and 73% of the Jeita discharge is composed of newly infiltrated water reaching the spring through fast flow pathways. Thus, the baseflow is assumed to have an age of one hydrological year or more.

Therefore, there is a need not only to estimate transit times of fast waters, but also of the base flow. In the latter case tracer tests conducted (Doummar, 2012) revealed a maximum fast transit time of 12 days.

In this study, environmental tracers (Tritium, Helium, Neon, CFC, and SF_6) were used to determine the mean transit time in wells tapping the Jeita aquifer in two sampling campaigns in low and high flow periods. The results were complemented by the characterization of the water and the estimation of the recharge area of each of the wells. The Tritium-Helium method has given absolute mean residence times that ranged from 7 to 24 years except for the Jeita cave sample where zero age was determined due the high large interfaces with the cave air, explaining the re-equilibration and degassing of light noble gas with the atmosphere. In addition the presence of radiogenic Helium in some samples (JN, AR, QQ, and AN) indicate the presence of very old groundwater (pre 1963) component (~10%). Despite the high sensitivity of the recharge temperature and excess air in the calculation of tritiogenic Helium, the computed ages using Tritium-Helium method were absolute and reliable ages as the uncertainty and stability

of the Tritium input curve in precipitation in the last 20 years has no effect on Tritium-Helium method age results as this method is based on the decay of Tritium to Helium only. Furthermore, the groundwater ages showed well distribution through the catchment area as the longer mean residence times were localized away from the clustering of dolines, shafts or faults that can transport infiltrated water at shorter transit times to the subsurface. However, the Tritium-Helium method alone provides average ages without giving insights into the flow dynamics in the Jeita system. The combined use of the CFC and SF_6 methods with Tritium-Helium allowed specifying which lumped model to use in the interpretation. The CFC and SF_6 method rely to a great extent on the CFC and SF_6 atmospheric input curve in order to determine the year of infiltration of sampled groundwater while assuming a piston flow model. As such, correlations between CFC, SF_6 and Tritium were made to validate the results, these correlations showed that none of the samples fits to a piston flow model except for Ain errihane (AR) well that showed some good fit to a piston flow model, however the slight variation and stability in the Tritium and CFCs input curves for the last 20 years in addition to uncertainties in CFCs and SF_6 atmospheric input curve due to a local anthropogenic contamination making this outcome less reliable, hence refinement of the atmospheric input curve for CFC and SF_6 is highly recommended in the future through CFC and SF_6 measurements in collected local soil samples for a better interpretation of the obtained results. In addition, a Binary mixing model was developed with two different water assemblages, one with zero age water (recently infiltrated water) and a water age of 34 years, the second one is with zero age water (recently infiltrated water) and a water age of 47 years, Chahtoul (CL) well and Jeita New cave (JN) fit respectively on these mixing curves. The high mixing in Jeita new cave is compatible

with stable isotopes (Oxygen-18 and Deuterium) results that showed high mixing of fractionated water in Jeita new cave sample. The remaining wells are believed to follow an exponential mixing or exponential piston models that were not included in the scope of this thesis. Furthermore, the stable isotopes results for Ain delbe (AD) and Ouata el Joz (OJ) showed very minimal mixing of fractionated water with greater depletion of stable isotopes indicating higher altitude of infiltration for these wells. All the integrated results of the several methods along with previous results of artificial tracer test in the Jeita catchment area (Doummar, 2012) provide further insights into the vulnerability of the Jeita spring and aquifer. The absence of protective cover above the Jeita Kesrouane aquifer make it highly vulnerable to contamination, however the relatively thick unsaturated zone is believed to play as a buffer. The Ain delbe (AD) and Ouata el Joz (OJ) infiltration area is localized at higher altitudes from the wells location and are characterized by diffusive infiltration due to their longer mean residence time (23 to 24 years) yielding a medium vulnerability to these wells. Similarly, the infiltration in Ain errihane (AR) is considered to be diffusive due to its relatively high residence time (17 years) yielding a medium vulnerability to the well. The Hrajel well (HL) has showed high variation in mean ages during two different flow periods, indicating high possibilityto the presence of large fractures in the vicinity of this well, providing newly fast infiltrated water at great volumes during wet periods to Hrajel well (HL), making this well highly vulnerable to contaminations. The Jeita new cave results all indicate the occurrence of high mixing in this branch of the Jeita cave. The precipitation event analysis in the Jeita cave using Deuterium, heavy Oxygen, and calcium was estimated to be between 12 % and 17%. The new infiltrated water to the Jeita cave is transported through the long subsurface conduit (5300 m) and is directly connected to the above

surface through sinkholes and pitholes; and furthermore up gradient to the Ain delbe (AD) borehole as discovered by the artificial tracer test previously done in the area (Doummar, 2012) indicating extreme vulnerability of the Jeita cave and its new branch to contamination. Based on the preceding obtained results a vulnerability map for the area can be generated. However complementary data is highly needed such as delineation of the extent, thickness, and infiltration rate in the soil cover, epikarst, and unsaturated zone, in addition to the integration of recharge numerical simulation along based with a conceptual hydrogeological model of the karst Jeita catchment.

REFERENCES

Abi Rizk, J., & Margane. A., (BGR) (2011). Mapping of Surface Karst Features in the Jeita Spring Catchment. *Protection of Jeita Spring special report, NO. 7.*

Al-ameri, A., Schneider, M., Abo-Lohom, N., & Janetz, S. (2014). Characteristics of stable isotopes of oxygen-18 and deuterium of groundwater in the Sana'a basin aquifer systems, yemen. *Arabian Journal for Science and Engineering, 39*(7), 5625-5636. doi:10.1007/s13369-014-1130-7

Aouad-Rizk, A., Job, J.L., Najem, W., Travi, Y., Blavoux, B. & Gourcy, L. (2005). Oxygen-18 and Deuterium contents over Mount Lebanon related to mass trajectories and local parameters. *IAEA Technical documents* 1453, 75-82.

Bethke, C. M., & Johnson, T. M. (2008). Groundwater age and groundwater age dating.*Annual Review of Earth and Planetary Sciences, 36*(1), 121-152. doi:10.1146/annurev.earth.36.031207.124210

Boronina, A., Renard, P., Balderer, W., & Stichler, W. (2005). Application of Tritium in precipitation and in groundwater of the Kouris catchment (Cyprus) for description of the regional groundwater flow. *Applied Geochemistry, 20*(7), 1292-1308. doi:10.1016/j.apgeochem.2005.03.007

Bou Jawdeh, I. Y., & American University of Beirut. Faculty of Arts and Sciences. Department of Geology. (1999). *Evidence for the tectonic evolution of central-north lebanon from structural and geomorphological data*

Breidenich, C., Magraw, D., Rowley, A., & Rubin, J. W. (1998). The kyoto protocol to the united nations framework convention on climate change. *The American Journal of International Law, 92*(2), 315-331.

Bullister, J.L. (2015). Atmospheric Histories (1765-2015) for CFC-11, CFC-12, CFC-113, CCl4, SF_6 and N2O. *Carbon Dioxide Information Analysis Center, Oak Ridge National Laboratory, US Department of Energy, Oak Ridge, Tennessee*. doi:10.3334/CDIAC/otg.CFC_ATM_Hist_2015

Busenberg, E., & Plummer, L. N. (1992). Use of chlorofluorocarbons (CCl3F and CCl2F2) as hydrologic tracers and age-dating tools: The alluvium and terrace system of central oklahoma. *Water Resources Research, 28*(9), 2257-2283. doi:10.1029/92WR01263

Busenberg, E., & Plummer, L. N. (2000). Dating young groundwater with sulfur hexafluoride: Natural and anthropogenic sources of sulfur hexafluoride. *Water Resources Research, 36*(10), 3011-3030. doi:10.1029/2000WR900151

Carey, M., Hayes, O., & Renner, A. (2009). Groundwater Source Protection Zones – Review of Methods. *Environment Agency*. Integrated catchment science programme Science report: SC070004/SR1

Caron, F. (2014). Isotope methods for dating old groundwater. *Journal of Environmental Radioactivity, 134*, 75. doi:10.1016/j.jenvrad.2014.03.002

Christoph, N., Heinz, H., & Thomas, H. (2008). Validation of vulnerability mapping methods by field investigations and numerical modelling. *Hydrogeology Journal*, *16*(4), 641-658.

Clark, I. (2015). *Groundwater geochemistry and isotopes* (1st ed.). Baton Rouge: CRC Press.

Clark, Ian D. (Ian Douglas), & Fritz, P. (1997). *Environmental isotopes in hydrogeology*. Boca Raton: Lewis Publishers

Cook, Peter G. (Peter Gordon), & Herczeg, A. L. (2000). *Environmental tracers in subsurface hydrology*. Dordrecht, NL: Kluwer Academic Publishers.

Cornaton, F. J. (2011). Transient water age distributions in environmental flow systems: The time-marching laplace transform solution technique. doi:10.1029/2011WR010606

Cornaton, F., & Perrochet, P. (2006). Groundwater age, life expectancy and transit time distributions in advective–dispersive systems; 2. reservoir theory for sub-drainage basins.*Advances in Water Resources*, *29*(9), 1292-1305. doi:10.1016/j.advwatres.2005.10.010

Craig, H. (1961). Isotopic Variations in Meteoric Waters. *Science*, 133, 1702-1703. doi.10.1126/science.133.3465.1702.

Darling, W., Gooddy, D., MacDonald, A., & Morris, B. (2012). The practicalities of using CFCs and SF_6 for groundwater dating and tracing. *Applied Geochemistry*, *27*(9), 1688-1697. doi:10.1016/j.apgeochem.2012.02.005

Davis, S. N., Fabryka-Martin, J., Wolfsberg, L., Moysey, S., Shaver, R., Alexander, E. C., & Krothe, N. (2000). Chlorine-36 in ground water containing low chloride concentrations.*Ground Water, 38*(6), 912-921. doi:10.1111/j.1745-6584.2000.tb00691.x

Delbart, C., Barbecot, F., Valdes, D., Tognelli, A., Fourre, E., Purtschert, R., & Jean-Baptiste, P. (2014). Investigation of young water inflow in karst aquifers using SF6–CFC–3H/He–85Kr–39Ar and stable isotope components. *Applied Geochemistry*, 50164-176. doi:10.1016/j.apgeochem.2014.01.011

Dotsika, E., Lykoudis, S., & Poutoukis, D. (2010). Spatial distribution of the isotopic composition of precipitation and spring water in Greece. *Global & Planetary Change*, *71*(3/4), 141-149. doi:10.1016/j.gloplacha.2009.10.007

Doummar, J. (2012). *Identification of quantitative parameters for vulnerability assessment in karst aquifers. Ph.D., Georg-August-Universität Göttingen, GZG*.

Doummar, J., Geyer, T., Baierl, M., Nödler, K., Licha, T., & Sauter, M. (2014). `Carbamazepine breakthrough as indicator for specific vulnerability of karst springs: Application on the Jeita spring, Lebanon. *Applied Geochemistry, 47*150-156. doi:10.1016/j.apgeochem.2014.06.004

Doummar, J., Sauter, M., & Geyer, T. (2012). Simulation of flow processes in a large scale karst system with an integrated catchment model (Mike She) – Identification of relevant parameters influencing spring discharge. *Journal Of Hydrology, 426-427*112-123. doi:10.1016/j.jhydrol.2012.01.021

Dubertret, L. (1955). *Carte Geologique du Liban, scale 1: 200 000, with explanatory notes*. Beyrouth: Ministe`re des Travaux Publics de la Republique Libanaise.

Edgell, H. S. (1997). Karst and hydrogeology of lebanon. *Carbonates and Evaporites, 12*(2), 220-235. doi:10.1007/BF03175419

Einsiedl, F. (2005). Flow system dynamics and water storage of a fissured-porous karst aquifer characterized by artificial and environmental tracers. *Journal Of Hydrology, 312*(1-4), 312-321. doi:10.1016/j.jhydrol.2005.03.031

Fetter, C. W. (. W. (2001). *Applied hydrogeology* (4th ed.). Upper Saddle River, N.J: Prentice Hall.

Fienen, M. N., Luo, J., & Kitanidis, P. K. (2006). A bayesian geostatistical transfer function approach to tracer test analysis. *Water Resources Research, 42*(7), W07426. 10.1029/2005WR004576

Fontes, J. (1983) Dating of Groundwater. *In Guidebook to Nuclear Techniques in Geology. IAEA, Vienna, Tech. Rept. Series No. 91*.

Gedeon, M. A., & American University of Beirut. Faculty of Arts and Sciences. Department of Geology. (1999). *Structural analysis of latitudinal faults in the mount lebanon north of beirut: Their kinematics and their role in the tectonic evolution of Lebanon*

Geyer, T. (2008) *Process-based characterisation of flow and transport in karst aquifers at catchment scale.*

Geyer, T., & Doummar, J. (2013). Protection of the Jeita Spring: Bestimmung der mittleren Verweilzeit des Grundwassers im Einzugsgebiet der Jeita Quelle-Libanon. Special report. Protection of the Jeita Spring. *Applied Geosciences*. Georg August University, Göttingen.

Geyer, T., Birk, S., Licha, T., Liedl, R., & Sauter, M. (2007). Multitracer test approach to characterize reactive transport in karst aquifers. *Ground Water, 45*(1), 36-45. doi:10.1111/j.1745-6584.2006.00261.x

Goldscheider, N., Drew, D. (. P., & International Association of Hydrogeologists. (2007). *Methods in karst hydrogeology*. London: Taylor & Francis.

Hahne, K., (BGR) (2011). Geological Map, Tectonics and Karstification in the Groundwater Contribution Zone of Jeita Spring supported by Remote Sensing. *Protection of Jeita Spring special report, NO. 4*

Han, D. M., Song, X. F., Currell, M. J., & Tsujimura, M. (2012). Using chlorofluorocarbons (CFCs) and Tritium to improve conceptual model of groundwater flow in the south coast aquifers of laizhou bay, china. *Hydrological Processes, 26*(23), 3614-3629. doi:10.1002/hyp.8450

Han, Z., Tang, C., Piao, J., Li, X., Cao, Y., Matsumaru, T., & Zhang, C. (2014). Application of chlorofluorocarbons (CFCs) to estimate the groundwater age at a headwater wetland in ichikawa city, chiba prefecture, japan. *Applied Water Science, 4*(3), 291-302. doi:10.1007/s13201-013-0145-7

Harmon, R. S. (Russell S.), Wicks, C. M., Ford, D. (. C.)., & White, William B. (William Blaine). (2006). *Perspectives on karst geomorphology, hydrology, and geochemistry: A tribute volume to derek C. ford and william B. white*. Boulder, Colo: Geological Society of America.

Harvey, J. W., Newlin, J. T., & Krupa, S. L. (2006). Modeling decadal timescale interactions between surface water and ground water in the central everglades, florida, USA. *Journal of Hydrology, 320*(3), 400-420. doi:10.1016/j.jhydrol.2005.07.024

Heaton, T.H.E., & Vogel, J.C. (1981) Excess Air in Groundwater. *Journal of Hydrology*, 50 201-216.

Hölting, B., Härtlé, T., Hohberger, K.H., Nachtigall, K.H., Villinger, E., Weinzierl, W., & Wrobel, J-P. (1995). Konzept zur Ermittlung der Schutzfunktion der Grundwasserüberdeckung. *Geol. Jb*. C 63, 5–24.

Homberg, C., Barrier, E., Mroueh, M., Hamdan, W., & Higazi, F. (2009). Basin tectonics during the Early Cretaceous in the Levant margin, Lebanon. *Journal Of Geodynamics, 47*(4), 218-223. doi:10.1016/j.jog.2008.09.002

Horst, A., Mahlknecht, J., & Merkel, B. J. (2007). Estimating groundwater mixing and origin in an overexploited aquifer in Guanajuato, Mexico, using stable isotopes (strontium-87, carbon-13, deuterium and oxygen-18). *Isotopes In Environmental & Health Studies, 43*(4), 323-338. doi:10.1080/10256010701701756

https://esrl.noaa.gov/gmd/hats/graphs/

https://water.usgs.gov/lab/

http://www.rsmas.miami.edu

https://www.thermofisher.com

HYDROISOTOP GMBH. (2005). *Use of Deuterium and Oxygen-18 as natural environmental isotopes and as artificial tracer.*

International Atomic Energy Agency. (1992). *Statistical treatment of data on environmental isotopes in precipitation.* Vienna: International Atomic Energy Agency.

Jurgens, B.C., Böhlke, J.K., & Eberts, S.M. (2012). TracerLPM (Version 1): An Excel® workbook for interpreting groundwater age distributions from environmental tracer data: *U.S. Geological Survey Techniques and Methods Report 4-F3*.

Kaufman, A., Bar-Matthews, M., Ayalon, A., & Carmi, I. (2003). The vadose flow above soreq cave, israel: A tritium study of the cave waters. *Journal of Hydrology, 273*(1), 155-163. 10.1016/S0022-1694(02)00394-3

Kazemi, G. A., Lehr, J. H., & Perrochet, P. (2006). *Groundwater age*. Hoboken, N.J: Wiley-Interscience.

Kendall, C., & McDonnell, J. J. (1998). *Isotope tracers in catchment hydrology*. Amsterdam;New York;: Elsevier.

Kluge, T., Wieser, M., & Aeschbach-Hertig, W. (2010). Assessing the use of 3H-3He dating to determine the subsurface transit time of cave drip waters. *Isotopes In Environmental & Health Studies, 46*(3), 299-311. doi:10.1080/10256016.2010.503893

Königer, P., & Margane. A., (BGR) (2014). Stable Isotope Investigations in the Jeita Spring catchment. *Protection of Jeita Spring special report , NO. 12*

Kurwadkar, S. (2017). Groundwater Pollution and Vulnerability Assessment. *Water Environment Research (10614303), 89*(10), 1561-1579. doi:10.2175/106143017X15023776270584

Leibundgut, C., (1998). Vulnerability of karst aquifers, Karst Hydrology, Proceedings of Workshop W2 held at Rabat, Morocco, April-May 1997, IAHS, Publ. no. 247, 45 Geyer

Leibundgut, C., Maloszewski, P., & Külls, C. (2009). Tracers in hydrology. doi:10.1002/9780470747148

Lo Russo, S., & Taddia, G. (2012). Aquifer vulnerability assessment and wellhead protection areas to prevent groundwater contamination in agricultural areas: An integrated approach.*Journal of Water Resource and Protection, 4*(8), 674-685. doi:10.4236/jwarp.2012.48078

Mazor, E. (1972). Paleotemperatures and other hydrological parameters deduced from noble gases dissolved in groundwaters; jordan rift valley, israel. *Geochimica Et Cosmochimica Acta, 36*(12), 1321-1336. 10.1016/0016-7037(72)90065-8

Mazor, E. (1997). *Chemical and isotopic groundwater hydrology: The applied approach*. United States:

McCallum, J. L., Cook, P. G., & Simmons, C. T. (2015). Limitations of the Use of Environmental Tracers to Infer Groundwater Age. *Ground Water, 53*56-70. doi:10.1111/gwat.12237

McGuire, K. J., & McDonnell, J. J. (2006). A review and evaluation of catchment transit time modeling. *Journal Of Hydrology*, *330*(3/4), 543-563. doi:10.1016/j.jhydrol.2006.04.020

Mull, R. (1981). Ground-water protection zones. *Geojournal, 5*(5), 473-481. doi:10.1007/BF02484719

Newman, B. D., Osenbrück, K., Aeschbach-Hertig, W., Solomon, D. K., Cook, P., Różański, K., & Kipfer, R. (2010). Dating of 'young' groundwaters using environmental tracers: advantages, applications, and research needs. *Isotopes In Environmental & Health Studies*, *46*(3), 259-278. doi:10.1080/10256016.2010.514339

Peltekian, A. & American University of Beirut. Faculty of Arts and Sciences. Department of Geology. (1980). *Groundwater quality in Greater Beirut in relation to geological structure and the extent of seawater intrusion*.

Perrin, J., Pochon, A., Jeannin, P. -., & Zwahlen, F. (2004). Vulnerability assessment in karstic areas: Validation by field experiments. *Environmental Geology*, *46*(2), 237-245. 10.1007/s00254-004-0986-3

Phillips, F. M., & Castro, M. C. (2003). Groundwater dating and residence-time measurements. (pp. 451-497) Elsevier Ltd. doi:10.1016/B0-08-043751-6/05136-7

Plummer. L.N., & Friedman. L.C. (1999). *Tracing and Dating Young Ground Water. USGS,* fact sheet.134-99.

Polemio, M., Dragone, V., & Limoni, P. P. (2009). Monitoring and methods to analyse the groundwater quality degradation risk in coastal karstic aquifers (apulia, southern italy).*Environmental Geology, 58*(2), 299-312. 10.1007/s00254-008-1582-8

Price, R. M., Top, Z., Happell, J. D., & Swart, P. K. (2003). Use of tritium and helium to define groundwater flow conditions in everglades national park. *Water Resources Research, 39*(9), 1267. 10.1029/2002WR001929

Schlosser, P., Stute, M., Dörr, H., Sonntag, C., & Münnich, K. O. (1988). Tritium/ 3He dating of shallow groundwater. *Earth and Planetary Science Letters, 89*(3), 353-362. 10.1016/0012-821X(88)90122-7

Stute, M., & Schlosser, P. (2001). *Environmental tracers in subsurface hydrology*, Dordrecht, NL: Kluwer Academic Publishers.

Sültenfuß, J., Purtschert, R., & Führböter, J. F. (2011). Age structure and recharge conditions of a coastal aquifer (northern Germany) investigated with Ar, C, H, He isotopes and Ne. *Hydrogeology Journal*, *19*(1), 221-236. doi:10.1007/s10040-010-0663-4

Szabo, Z., Rice, D. E., Plummer, L. N., Busenberg, E., Drenkard, S., & Schlosser, P. (1996). Age dating of shallow groundwater with chlorofluorocarbons, Tritium/Helium: 3, and flow path analysis, southern new jersey coastal plain. *Water Resources Research,* 32(4), 1023-1038. doi:10.1029/96WR00068

Tolstikhin, I. N., & Kamensky, I. L. (1969). Determination of groundwater age by the T-^{3}He method. *Geochemistry International*, 52(6), 810-811.

Turnadge, C., & Smerdon, B. D. (2014). A review of methods for modelling environmental tracers in groundwater: Advantages of tracer concentration simulation. *Journal Of Hydrology*, *519*3674-3689. doi:10.1016/j.jhydrol.2014.10.056

United Nations Development Program (UNDP). (1970*). Liban Etude Des Eaux Souterraines. (Beirut: Government of Lebanon).*

United Nations Development Program (UNDP). (2014). *National Groundwater Resources Assessment of Lebanon.*

Stempvoort, D. V., Ewert, L., & Wassenaar, L. (1993). aquifer vulnerability index: A gis - compatible method for groundwater vulnerability mapping. *Canadian Water Resources Journal, 18*(1), 25-37. doi:10.4296/cwrj1801025

Verheyden, S., Nader, F. H., Cheng, H. J., Edwards, L. R., & Swennen, R. (2008). Paleoclimate reconstruction in the levant region from the geochemistry of a holocene stalagmite from the jeita cave, lebanon. *Quaternary Research, 70*(3), 368-381. doi:10.1016/j.yqres.2008.05.004

Visser, A., Broers, H. P., Purtschert, R., Sültenfuß, J., & Jonge, M. (2013). Groundwater age distributions at a public drinking water supply well field derived from multiple age tracers (85Kr, 3H/3He, and 39Ar). *Water Resources Research, 49*(11), 7778-7796. doi: 10.1002/2013WR014012

Walley, C. D. (1988). A braided strike-slip model for the northern continuation of the dead sea fault and its implications for levantine tectonics. *Tectonophysics, 145*(1), 63-72. doi:10.1016/0040-1951(88)90316-2

Walley, C.D. (1997). The lithostratigraphy of Lebanon: a Review. *Lebanese Scientific Bulletin*, 10, 81-108.

Walley, C. D. (1998). Some outstanding issues in the geology of lebanon and their importance in the tectonic evolution of the levantine region. *Tectonophysics, 298*(1), 37-62. doi:10.1016/S0040-1951(98)00177-2

Weatherington-Rice, J., Christy, A. D., Angle, M. P., Gehring, R., & Aller, L. (2006). DRASTIC hydrogeologic settings modified for fractured till: Part 2. field observations. *The Ohio Journal of Science, 106*(2), 51.

Weiss, R. F. (1971). Solubility of helium and neon in water and seawater. *Journal of Chemical & Engineering Data, 16*(2), 235-241. doi: 10.1021/je60049a019

White, William B. (William Blaine). (1988). *Geomorphology and hydrology of karst terrains*. New York: Oxford University Press.

Williams, P. W. (2008). The role of the epikarst in karst and cave hydrogeology: a review. *International Journal Of Speleology, 37*(1), 1-10.

Zuber, A., Różański, K., Kania, J., & Purtschert, R. (2011). On some methodological problems in the use of environmental tracers to estimate hydrogeologic parameters and to calibrate flow and transport models. *Hydrogeology Journal, 19*(1), 53-69. doi:10.1007/s10040-010-0655-4